

# **Orientability of the Moving Platform in Planar Cable Robots**

A Thesis

Submitted for the Degree of

**Master of Technology (Research)**  
in the **Faculty of Engineering**

by

**Madhirala Vikranth Kumar Reddy**



Mechanical Engineering  
Indian Institute of Science  
Bengaluru – 560012 (INDIA)

AUGUST 2019



© Madhivala Vikranth Kumar Reddy  
AUGUST 2019  
All rights reserved



DEDICATED TO

*My Parents*

*and*

*My Great Nation*



# Acknowledgements

“Whatever you do, make it an offering to me—the food you eat, the sacrifices you make, the help you give, even your suffering.”

“Your right is only to perform your duty. You do not have right to expect any consequences there of. You should neither be motivated by the fruits of your action, nor should they encourage you to be inactive.”

—The Bhagavad Gita

First and foremost, praises and thanks to God, the omnipotent and benevolent, for His showers of blessings throughout my life. I thank Him for the gift of the wonderful people I have met along this journey. Some of them inspired me, challenged me, stretched me, loved me, hated me, and encouraged me. My life has become meaningful and beautiful because of them.

I am thankful to the Indian Institute of Science (IISc), Bengaluru for providing a wonderful and conducive environment for research. The vibrant and verdant IISc campus made me feel ebullient and vivacious during my three years of stay in it. It has provided me the real education. I also thank the Ministry of Human Resource and Development (MHRD), Government of India, for their monetary support.

In my journey towards this degree, I have found an inspiring teacher, a compassionate friend, and a pillar of support in my adviser, Prof. Gondi Kondaiah Ananthasuresh. I am deeply grateful to him for introducing me to cable robots and for the freedom and independence that was provided to me during my work here. He pushed me beyond my limits, in pursuing research in cable robots, without compromising anywhere. He taught me the importance of technical writing, presentation skills, and independent thinking. I consider myself extremely fortunate to be one of his Master’s students.

## Acknowledgements

I thank Prof. C.S. Jog, Prof. V.R. Sonti, Prof. Ramsharan Rangarajan, Prof. R. Narasimhan, Prof. A. Ghosal, Prof. J.H. Arakeri, Prof. Satish Vasu Kailas, Prof. K.R.Y. Simha, and Prof. B. Gurumoorthy for their inspiring lectures. The knowledge that I assimilated by attending their lectures has not only helped me in my research work but also in my personal life. My special thanks to Prof. C.S. Jog for motivating and encouraging me during my M.Tech (Research) interview at IISc, which was pivotal for my decision to pursue higher education.

The M2D2, Multi-Disciplinary and Multi-scale Devices and Design, Lab has always been my second home for the last three years. I am proud to be a part of it. I thank my labmates P. Anoocha, H. Shamanth, K. Somanna, R. Harisankar, S. Nitish, P. Safvan, D. Akshay, G. Prasenjit, Vageesh Singh Bhagel, M. Priyabrata, B. Kishore, Dhananjay Yadav, J. Siddharth, Jose Joseph, Sudhanshu Shekhar, M. Varun B S, Geetanjali, Saketh, Ashwin, Rajesh, Rakesh, Siddhesh, Mihir, R. Ankitha, Shanthanu, Gokul, Praveen, K. Ankur, V.K. Ananya, B. Sagar, S. Jyoti Shivaji, R. Chaitra, T.C. Bharath, Rajneesh, Kedar, John sir, Ravi Kumar, and others for their constant help. I would like to specifically thank B. Sudhanva and A. Yash for proof-reading my thesis and also for their valuable suggestions while I was writing my thesis.

I thank my dearest friends M. Naveen Kumar, V.V.S.M.S Ganesh, T. Himanshu, N.C. Pra-  
neet, H. Venu Madhav, D. Surya Teja, B. Krishnakanth, Sandeep Verma, J. Satej, T. Uday  
Bhaskar, Pranay, Nilesh Bagale, P. Sanjay Rao, T. Srinivas, Suveen, and G. Rambabu for their  
constant companionship. I cannot forget the time that I have spent with these wonderful peo-  
ple. They have always showered their love on me. I owe a tremendous debt to them. My  
heartfelt thanks to Keerthana Nuti whose name I cannot miss here.

I thank Somavathi Devi, B. Chinnamma, and other staff who helped me in academic-related  
issues. My reverence to mess workers for providing delicious food to me every day on time. My  
tributes to the staff of the Health Center for taking care of me when I was admitted there.

Finally, I am grateful to the support extended by my parents. The blessings of my parents  
(M. Srinivas Reddy and M. Geetha Reddy), grandparents, V.V. Reddy, and B. Harshavardhan  
Reddy are always with me. Last, but not the least, I am grateful to the good wishes of my  
younger brother M. Vinay Kumar Reddy.

**Madhirala Vikranth Kumar Reddy**

# Abstract

This thesis deals with the orientability of the moving platform in planar cable robots. In particular, feasible orientations are obtained at any point in a space of interest, for two different cases. First, for the static equilibrium of the cable robot and, second, for the fully constrained condition. With the help of a few examples, it is shown that the nature of the load acting on the platform strongly influences the orientability of the platform in the first case. Furthermore, the influence of the number of cables and geometry of the cable robot on the orientability of the moving platform is revealed through these examples. The platform is made to trace a path for specified discrete waypoints for two cases i.e., with and without the desired orientation of the platform specified at every waypoint. To validate the mathematical model, feasible orientations of the platform obtained from simulations are compared with those obtained from experiments. For this purpose, a prototype of a three-cable robot was built.

It is observed in this study that as the number of cables increases, the orientability of the platform increases, but this enhanced range may not always cover the orientability requirements of intended applications. For this, an approach to enhance the orientability of the cable robot is presented. It involves the appendage of a spool, a translational spring, an additional cable, and a rotary actuator to the existing set-up of the three-cable robot. The relevant equations are discussed and some examples presented. Also, with a slight modification, the same set-up can be used for the application of a specific moment load on the platform. The equations governing the application of a specific moment load and the corresponding examples are discussed.



# Notation

$\beta_1$	Angle of wrap of the additional cable on the spring side
$\beta_2$	Angle of wrap of the additional cable on the orientation motor side
$\delta$	Initial elongation of the spring to maintain tension in the spring
$\phi$	Orientation of the platform w.r.t. the $y$ -axis
$\phi_1$	Orientation of the platform of the spatial cable robot w.r.t. the $x$ -axis
$\phi_2$	Orientation of the platform of the spatial cable robot w.r.t. the $y$ -axis
$\phi_3$	Orientation of the platform of the spatial cable robot w.r.t. the $z$ -axis
$\mu$	Coefficient of the sliding friction between the spool and the pin joint
$\mu'$	Coefficient of the static friction between the spool and the cable
$\theta_i$	Angle of inclination of the $i^{th}$ cable relative to the $x$ -axis
$\theta_r$	Angle of inclination of the cable, relative to the $x$ -axis, connecting the spool to the orientation motor
$\theta_s$	Angle of inclination of the cable, relative to the $x$ -axis, connecting the spool to the translational spring
$\psi$	Orientation of the spool
$\Delta s$	Elongation of the spring
$\Delta\theta_i$	Angle to be rotated by the stepper motor
$\Delta\psi$	Change in the orientation of the spool
$\alpha$	A column vector of coefficients that multiply nullspace column vectors

## Notation

$\bar{\alpha}$	Intersection point of $m$ pair of equations
$k$	Stiffness of the spring
$l_i$	Length of the $i^{th}$ cable
$m$	Number of independent columns of nullspace of $\mathbf{L}$
$n$	Number of cables
$n_w$	Number of windings of the orientation cable on the spool
$r$	Rank of the matrix $\mathbf{L}$
$r_b$	Radius of the pin joint
$r_p$	Pitch circle radius of the helical groove
$s_i$	Moment arm of the $i^{th}$ cable tension
$(x, y)$	Coordinates of the centroid of the platform of the planar cable robot
$(x, y, z)$	Coordinates of the centroid of the platform of the spatial cable robot
$(x_{fi}, y_{fi})$	Coordinates of the $i^{th}$ fixed pivot of the planar cable robot
$(x_{fi}, y_{fi}, z_{fi})$	Coordinates of the $i^{th}$ fixed pivot of the spatial cable robot
$(x_{fs}, y_{fs})$	Fixed coordinates of the translational spring
$x_l$	Lower limit of the $x$ values
$(x_{mi}, y_{mi})$	Coordinates of the $i^{th}$ moving vertex of the platform
$(x_{mi}, y_{mi}, z_{mi})$	Coordinates of the $i^{th}$ moving vertex of the platform of the spatial cable robot
$(x_r, y_r)$	Fixed coordinates of the orientation motor
$(x_s, y_s)$	Fixed coordinates of the pulley on the side of the translational spring
$x_u$	Upper limit of the $x$ values
$y_l$	Lower limit of the $y$ values
$y_u$	Upper limit of the $y$ values

## Notation

$F_x$	Load acting at the centroid of the platform along the $x$ -direction
$\hat{F}_x$	Updated load along the $x$ -direction
$F_y$	Load acting at the centroid of the platform along the $y$ -direction
$\hat{F}_y$	Updated load along the $y$ -direction
$F_z$	Load acting at the centroid of the platform along the $z$ -direction
$M$	Desired moment load at the centroid of the platform
$M_x$	Moment load acting at the centroid of the platform along the $x$ -direction
$M_y$	Moment load acting at the centroid of the platform along the $y$ -direction
$M_z$	Moment load acting at the centroid of the platform along the $z$ -direction
$\hat{M}_z$	Updated moment load acting at the centroid of the platform along the $z$ -direction
$P_{i0x}$	$x$ -coordinate of the $i^{th}$ vertex from the centroid of the platform
$P_{ix}$	$x$ -coordinate of the $i^{th}$ moving vertex from the centroid of the platform
$P_{i0y}$	$y$ -coordinate of the $i^{th}$ vertex from the centroid of the platform
$P_{iy}$	$y$ -coordinate of the $i^{th}$ moving vertex from the centroid of the platform
$P_{i0z}$	$z$ -coordinate of the $i^{th}$ vertex from the centroid of the platform
$P_{iz}$	$z$ -coordinate of the $i^{th}$ moving vertex from the centroid of the platform
$T_i$	Tension in the $i^{th}$ cable
$T_r$	Magnitude of the $\mathbf{T}_r$
$T_s$	Magnitude of the $\mathbf{T}_s$
$\mathbf{f}$	A column vector containing $F_x$ , $F_y$ , and $M_z$
$\hat{\mathbf{f}}$	A column vector containing $\hat{F}_x$ , $\hat{F}_y$ , and $\hat{M}_z$
$\hat{\mathbf{i}}$	Unit vector along the $x$ -axis
$\hat{\mathbf{j}}$	Unit vector along the $y$ -axis

## Notation

$\hat{\mathbf{k}}$	Unit vector along the $z$ -axis
$\mathbf{l}_i$	Length vector of the $i^{th}$ cable
$\mathbf{l}$	A column vector containing the lengths of the cables
$\mathbf{t}$	A column vector containing the tensions of the cables
$\mathbf{t}_{\text{aug}}$	Augmented matrix of $\mathbf{t}$ and 1
$\mathbf{L}$	A matrix pre-multiplying cable-tension column vector in the equilibrium equation
$\mathbf{L}_{\text{aug}}$	Augmented matrix of $\mathbf{L}$ and $\mathbf{f}$
$\mathbf{N}$	Nullspace or kernel matrix of $\mathbf{L}$
$\mathbf{N}_{\text{aug}}$	Nullspace or kernel matrix of $\mathbf{L}_{\text{aug}}$
$\mathbf{P}_{i0}$	Position vector of the $i^{th}$ vertex from the centroid of the platform
$\mathbf{P}_i$	Position vector of the $i^{th}$ moving vertex from the centroid of the platform
$\mathbf{R}$	Rotation matrix
$\mathbf{T}_i$	Tension vector of the $i^{th}$ cable
$\mathbf{T}_r$	Tension vector of the cable connecting the spool to the orientation motor
$\mathbf{T}_s$	Tension vector of the cable connecting the spring to the spool

# Dimensions

$\beta_1$	degrees
$\beta_2$	degrees
$\delta$	cm
$\phi$	degrees
$\phi_1$	degrees
$\phi_2$	degrees
$\phi_3$	degrees
$\theta_i$	degrees
$\theta_r$	degrees
$\theta_s$	degrees
$\psi$	degrees
$\Delta s$	cm
$\Delta\theta_i$	degrees
$\Delta\psi$	degrees
$k$	N/cm
$l_i$	cm
$r_b$	cm
$r_p$	cm

## Dimensions

$s_i$	cm
$(x, y)$	cm
$(x, y, z)$	cm
$(x_{fi}, y_{fi})$	cm
$(x_{fi}, y_{fi}, z_{fi})$	cm
$(x_{fs}, y_{fs})$	cm
$x_l$	cm
$(x_{mi}, y_{mi})$	cm
$(x_{mi}, y_{mi}, z_{mi})$	cm
$(x_r, y_r)$	cm
$(x_s, y_s)$	cm
$x_u$	cm
$y_l$	cm
$y_u$	cm
$F_x$	N
$\hat{F}_x$	N
$F_y$	N
$\hat{F}_y$	N
$F_z$	N
$M$	N-cm
$M_x$	N-cm
$M_y$	N-cm
$M_z$	N-cm
$\hat{M}_z$	N-cm

## Dimensions

$P_{i0x}$	cm
$P_{ix}$	cm
$P_{i0y}$	cm
$P_{iy}$	cm
$P_{i0z}$	cm
$P_{iz}$	cm
$T_i$	N
$T_r$	N
$T_s$	N

# Contents

- Acknowledgements i
- Abstract iii
- Notation v
- Dimensions ix
- Contents xii
- List of Figures xv
- List of Tables xix
  
- 1 Introduction 1**
  - 1.1 Cable robots and their applications . . . . . 1
  - 1.2 Classification of cable robots . . . . . 6
  - 1.3 Feasible orientations of the platform . . . . . 10
  - 1.4 Motivation . . . . . 11
  - 1.5 Objectives of the present study . . . . . 12
  - 1.6 Organization of the thesis . . . . . 12
  
- 2 Literature Review 14**
  - 2.1 Introduction to parallel mechanisms . . . . . 14
  - 2.2 Static analysis of cable robots . . . . . 15
    - 2.2.1 Modeling of the planar cable robot . . . . . 15
    - 2.2.2 Modeling of the spatial cable robot . . . . . 18
    - 2.2.3 Workspace . . . . . 21
    - 2.2.4 Tension vector . . . . . 23

## CONTENTS

2.2.5	The determinant approach . . . . .	26
2.2.6	Force capabilities . . . . .	27
2.2.7	Determination of a static pose . . . . .	28
2.3	Dynamics and control . . . . .	29
2.3.1	Fully constrained cable robots . . . . .	29
2.3.2	Cable-suspended robots . . . . .	31
2.3.3	Calibration . . . . .	32
<b>3</b>	<b>Orientability of the Moving Platform</b>	<b>34</b>
3.1	Feasibility of the orientation of the moving platform . . . . .	34
3.2	Feasible orientations of the moving platform at a point . . . . .	41
3.3	Feasible orientations of the platform at multiple points . . . . .	43
3.4	Feasible orientations that fully constrain the moving platform . . . . .	56
3.4.1	Fully constrained configuration . . . . .	56
3.4.2	Feasible orientations that fully constrain the moving platform at multiple points . . . . .	57
3.5	Platform tracing a prescribed trajectory . . . . .	62
3.5.1	Trajectory tracing with an optimal orientation at every waypoint . . . . .	62
3.5.2	Trajectory tracing with specified orientation at every waypoint . . . . .	65
<b>4</b>	<b>Enhanced Orientability of the Cable Robot</b>	<b>70</b>
4.1	Limited orientability of the moving platform . . . . .	70
4.2	Modification of the set-up to achieve an additional rotary degree of freedom . . . . .	70
4.3	Working of the set-up . . . . .	73
4.4	Platform tracing a prescribed trajectory with desired orientation of the spool . . . . .	82
<b>5</b>	<b>Moment Load on the Moving Platform</b>	<b>88</b>
5.1	Modification of the set-up for the application of moment load . . . . .	88
5.2	Working of the set-up . . . . .	88
5.3	Platform tracing a prescribed trajectory with a specified moment load on it . . . . .	94
<b>6</b>	<b>Prototyping</b>	<b>100</b>
6.1	Prototype of the three-cable robot . . . . .	100
6.2	Experimenting on the prototype . . . . .	102
6.3	Prototype with additional rotary DoF . . . . .	105

## CONTENTS

<b>7 Closure and Future perspectives</b>	<b>108</b>
7.1 Summary of the work done . . . . .	108
7.2 Contributions . . . . .	110
7.3 Future perspectives . . . . .	110
<b>Appendix</b>	<b>111</b>
<b>Bibliography</b>	<b>113</b>

# List of Figures

1.1	Spatial cable robot (Kinematics and Robot Design Group, IRI, Barcelona) . . . .	2
1.2	The NIST ROBOCRANE . . . . .	3
1.3	Prototype of IPAnema-1, an eight-cable robot with 6-degrees-of-freedom for material handling developed at the Fraunhofer Institute (Andreas Pott, Fraunhofer IPA) . . . . .	3
1.4	Skycam at work during a Washington Huskies football game at Husky Stadium in Seattle, Washington (Despeaux~commonswiki) . . . . .	4
1.5	China's Five-hundred-meter Aperture Spherical Radio Telescope (FAST) in southwest china's Guizhou province (china.org.cn) . . . . .	4
1.6	Prototype of CAREX, a cable-driven arm exoskeleton for neural rehabilitation developed at Columbia University (S.K. Agrawal, ROAR LAB, Columbia University) . . . . .	5
1.7	A subject walking on a treadmill while wearing the Tethered Pelvic Assist Device (S.K. Agrawal, ROAR LAB, Columbia University) . . . . .	6
1.8	Planar cable robot with a triangular platform (this work) . . . . .	8
1.9	Cable robot configurations: (a), (d) under-constrained (b), (c), and (e) fully constrained . . . . .	9
1.10	Cable robots with actuation redundancy . . . . .	9
2.1	Planar cable robot consisting of a platform supported by $n$ cables whose lengths are to be changed by winding rotary actuators to translate and rotate the platform	16
2.2	Spatial cable robot consisting of a platform supported by $n$ cables whose lengths are to be changed by winding rotary actuators to translate and rotate the platform	19
2.3	The trivial case of a planar one-cable robot . . . . .	24
2.4	A planar two-cable robot . . . . .	25

## LIST OF FIGURES

3.1	Two different configurations of a three-cable robot. Pink arrow indicates the direction of the external load acting at the centroid of the platform. . . . .	36
3.2	Two different planar cable robots i.e., four and five-cable robots . . . . .	40
3.3	Black sectors represent feasible orientations of the platform at (2,-1) . . . . .	41
3.4	Feasible orientations of the platform of the planar three-cable robot at (2,-1) . . . . .	42
3.5	Non-negative cable forces for the feasible orientations. Cable forces for non-feasible orientations are shown with the values of zero. . . . .	42
3.6	Platform is in static equilibrium at (4,3) for the load vector $\{0 \ 1 \ 0\}^T$ . Orientation of the platform is $75^\circ$ . Range of the feasible orientations is from $64^\circ$ to $102^\circ$ . . . . .	43
3.7	Feasible orientations of the triangular platform for two different load vectors (i.e., along the $y$ -axis) with same magnitude but in opposite directions. Tiny red circles indicate the fixed pivots of the three-cable robot. The boundary of the workspace is indicated with a red curve. . . . .	44
3.8	Feasible orientations of the triangular platform for two different load vectors (i.e., along the $x$ -axis) with same magnitude but in opposite directions. The boundary of the workspace is indicated with a red curve. . . . .	45
3.9	Feasible orientations of the triangular platform for two different load vectors (i.e., about the $z$ -axis) with same magnitude but in opposite directions. The boundary of the workspace is indicated with a red curve. . . . .	46
3.10	Feasible orientations of two different platforms for the same fixed pivots of the four-cable robot . . . . .	48
3.11	Feasible orientations of two different platforms for the same fixed pivots of the four-cable robot for the load vector $\{0 \ 1 \ 0\}^T$ . . . . .	50
3.12	Feasible orientations of two different platforms for the same fixed pivots of the four-cable robot for the load vector $\{1 \ 0 \ 0\}^T$ . . . . .	51
3.13	Feasible orientations of two different platforms for the same fixed pivots of the four-cable robot for the load vector $\{0 \ 0 \ 1\}^T$ . . . . .	52
3.14	Feasible orientations of two different platforms for the same fixed pivots of the four-cable robot for the load vector $\{0 \ 1 \ 0\}^T$ . . . . .	53
3.15	Feasible orientations of two different platforms for the same fixed pivots of the four-cable robot for the load vector $\{1 \ 0 \ 0\}^T$ . . . . .	54
3.16	Feasible orientations of two different platforms for the same fixed pivots of the four-cable robot for the load vector $\{0 \ 0 \ 1\}^T$ . . . . .	55
3.17	Feasible orientations that fully constrain the rectangular platform . . . . .	58
3.18	Feasible orientations that fully constrain the square platform . . . . .	59

## LIST OF FIGURES

3.19	Feasible orientations of two different platforms at (0,0) for the same fixed pivots of the five-cable robot for the load vector $\{0 \ 1 \ 0\}^T$ . . . . .	60
3.20	Feasible orientations that fully constrain the two different platforms for the same fixed pivots of the five-cable robot . . . . .	61
3.21	Horizontal path traced by the moving platform of the five-cable robot . . . . .	63
3.22	Fourth and fifth cables support the platform for the entire path as the net external force is in the direction of the positive $x$ -axis . . . . .	64
3.23	Lengths of the cables at every waypoint . . . . .	64
3.24	Orientation chosen at every waypoint, by the algorithm, for minimum $\ \mathbf{t}\ $ . . . . .	65
3.25	Optimal $\alpha$ corresponding to the optimal orientation at every waypoint . . . . .	65
3.26	Vertical path traced by the moving platform of the six-cable robot. Curved pink arrow indicates that a positive moment load is acting on the platform. . . . .	67
3.27	Tensions in the cables for maximum $\ \mathbf{t}\ $ . . . . .	67
3.28	Lengths of the cables at every waypoint . . . . .	68
3.29	Optimal $\alpha$ chosen at every waypoint for maximum $\ \mathbf{t}\ $ within the bounds provided . . . . .	68
4.1	2D model of the three-cable robot with an additional rotary degree of freedom . . . . .	71
4.2	3D Solidworks model of the three-cable robot with a spool attached to the moving triangular platform . . . . .	72
4.3	Angles of wrap of the fourth cable on either side of the spool . . . . .	74
4.4	Orientation of the spool is $30^\circ$ . . . . .	80
4.5	Orientation of the spool is $40^\circ$ . . . . .	80
4.6	Orientation of the spool is $50^\circ$ . . . . .	81
4.7	Orientation of the spool is $60^\circ$ . . . . .	81
4.8	Tensions in the cables at every increment in the orientation of the spool . . . . .	82
4.9	Updated load vector $\hat{\mathbf{f}}$ at every increment in the orientation of the spool . . . . .	82
4.10	Orientation of the spool at (-5,-5) is $-20^\circ$ . . . . .	84
4.11	Orientation of the spool at (-5,-2) is $-50^\circ$ . . . . .	84
4.12	Orientation of the spool at (-5,1) is $80^\circ$ . . . . .	85
4.13	Orientation of the spool at (-5,5) is $11^\circ$ . . . . .	85
4.14	Minimum tensions (i.e., $\ \mathbf{t}\ $ ) in the cables at every waypoint . . . . .	86
4.15	Updated load vector $\hat{\mathbf{f}}$ at every waypoint . . . . .	86
4.16	Optimal orientation of the platform, chosen by the algorithm, for the minimum tensions (i.e., $\ \mathbf{t}\ $ ) in the cables . . . . .	87
5.1	Platform's centroid is located at (0,0) and its orientation is $0^\circ$ . . . . .	89

## LIST OF FIGURES

5.2	Platform's centroid is located at (-5,-5) . . . . .	96
5.3	Platform's centroid is located at (-1.43,-5) . . . . .	97
5.4	Platform's centroid is located at (1.43,-5) . . . . .	97
5.5	Platform's centroid is located at (5,-5) . . . . .	98
5.6	Minimum tensions in the cables . . . . .	98
5.7	Updated load vector $\hat{\mathbf{f}}$ at every waypoint . . . . .	99
5.8	Optimal orientation of the platform for the minimum $\ \mathbf{t}\ $ at every waypoint . . . . .	99
6.1	Prototype of the three-cable robot built at M2D2 Lab . . . . .	102
6.2	Procedure for obtaining the number of steps of the stepper motors for incrementing the orientation of the platform by $1^\circ$ . . . . .	103
6.3	Schematic of the experimental set-up . . . . .	104
6.4	Prototype of the three-cable robot with additional rotary degree of freedom . . . . .	106
6.5	Procedure for obtaining the number of steps of the stepper motor for incrementing the orientation of the spool by $1^\circ$ . . . . .	107

# List of Tables

3.1	Cable forces for two different configurations of the three-cable robot whose $\mathbf{L}$ matrix has full rank. Cable forces of Configuration 2 are not all non-negative. . . . .	35
3.2	Data for two different configurations of the planar cable robots i.e., for $n = 4$ and $5$	37
3.3	Parameters of the three-cable robot . . . . .	41
3.4	Parameters of the three-cable robot . . . . .	43
3.5	Parameters of the four-cable robot. Columns 3 and 4 indicate the initial vertices of the rectangular and square platforms respectively. . . . .	49
3.6	Parameters of the four-cable robot . . . . .	57
3.7	Parameters of the five-cable robot . . . . .	60
3.8	Parameters of the five-cable robot . . . . .	63
3.9	Parameters of the six-cable robot . . . . .	66
4.1	Three different cases of $\beta_1$ and $\beta_2$ . . . . .	74
4.2	Cable forces of the three-cable robot for the two different orientations of the spool	75
4.3	Parameters used for the three-cable robot . . . . .	78
4.4	Desired orientation of the spool at every waypoint . . . . .	83
5.1	Cable forces of the three-cable robot when there is no moment load on the platform	90
5.2	Cable forces of the robot when a moment load is applied on the platform . . . . .	92
5.3	Parameters of the cable robot used for simulation . . . . .	95
6.1	Parameters of the three-cable robot . . . . .	101
6.2	Components used for building the prototype . . . . .	101
6.3	Comparison of the experimental orientability limits with the corresponding limits obtained from simulations at three different points . . . . .	104
6.4	Parameters of the three-cable robot . . . . .	105
6.5	Orientability limits from the experiments and simulations . . . . .	105

# Chapter 1

## Introduction

### Summary

This chapter contains background to cable robots (i.e., cable-driven robots) and their applications. It also contains a classification of cable robots, basics of the work undertaken, motivation and objectives of the study, and the organization of the thesis.

### 1.1 Cable robots and their applications

Cable robots are parallel mechanisms with a single moving platform that is moved around by cables. The moving platform is connected to a set of cables that are actuated by motors, usually rotary motors. The robotic platform can then be moved around by increasing or decreasing the lengths of the cables in concert. Cable robots are structurally similar to parallel robots but with the fundamental difference that cables can only pull the moving platform, i.e., they can only sustain tension but not compression [1, 2]. This property makes planning, design, and control of cable robots relatively complicated in comparison to their counterparts, i.e., parallel robots. A prototype of a cable robot can be seen in Fig. 1.1.

There are several advantages to using cable robots over conventional robots because they have relatively large workspace for their size; low weight; superior stiffness under external disturbances; low noise; low energy consumption; easier portability; and low cost ([3]–[6]). Because of the inherent flexibility of the cables, they provide a natural protection in the case of external disturbances [7]. These attributes are important for applications that require the robot to be brought to the worksite (e.g., a construction site).

Cable robots can be used when heavy loads have to be moved with precision (e.g., shipbuild-

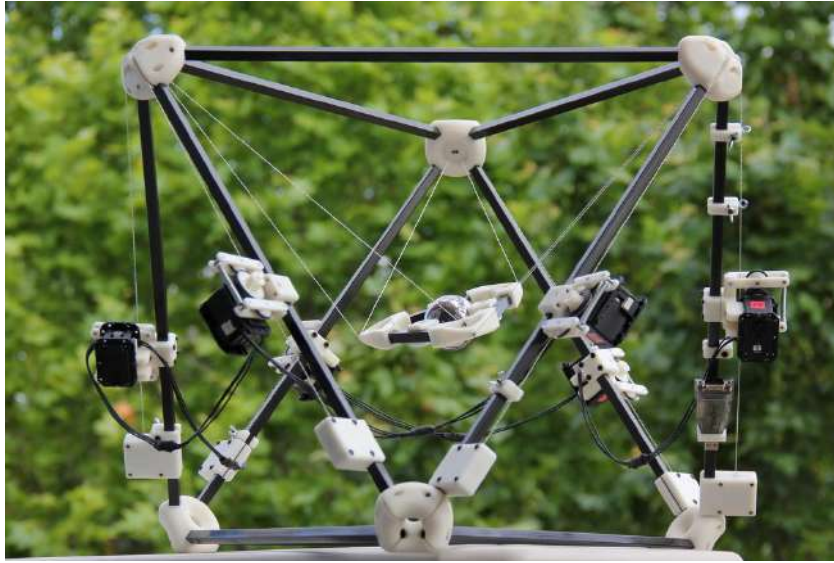


Figure 1.1: Spatial cable robot (Kinematics and Robot Design Group, IRI, Barcelona)

ing [7]) or when lighter loads have to be moved with high acceleration [8]. They are implemented in construction applications, which are labor-intensive and expensive, typically requiring cranes and scaffolding ([9]–[11]). Tasks such as spray painting, window cleaning, and visual inspections have been accomplished with cable robots. ROBOCRANE [12, 13] technology is applied for cleaning up of nuclear and toxic waste. It can also be implemented for cutting, excavating and grading, shaping, finishing, lifting, positioning, flexible-fixturing, and transporting manipulators. A modification of the ROBOCRANE device was used to fight oil-well fires that were set in Kuwait during the Persian Gulf War. An image of the NIST ROBOCRANE Mobile 2m prototype is shown in Fig. 1.2. Space-related and non-space-related applications (for example, virtual reality interface, an aerial robotic camera system, and material processing and handling systems) have been explored ([14]–[18]). A cable robot used for material processing and handling systems is shown in Fig. 1.3. Skycam is an aerial robotic camera system used for moving cameras above stadium fields for filming sports events or other performances which is shown in Fig. 1.4. Installation of a Skycam on the stadium field does not perturb the visibility of the event to the audience as the cables are thin and barely visible.

Cable-suspended robots are used in the development of very large radio-telescopes. One such example, shown in Fig. 1.5, is that of a five-hundred-meter aperture spherical radio telescope (FAST) currently being developed in China ([19]–[24]). Another similar project was developed in Canada, in which an aerostat was used to tension a six-cable parallel robot ([25]–[30]).



Figure 1.2: The NIST ROBOCRANE

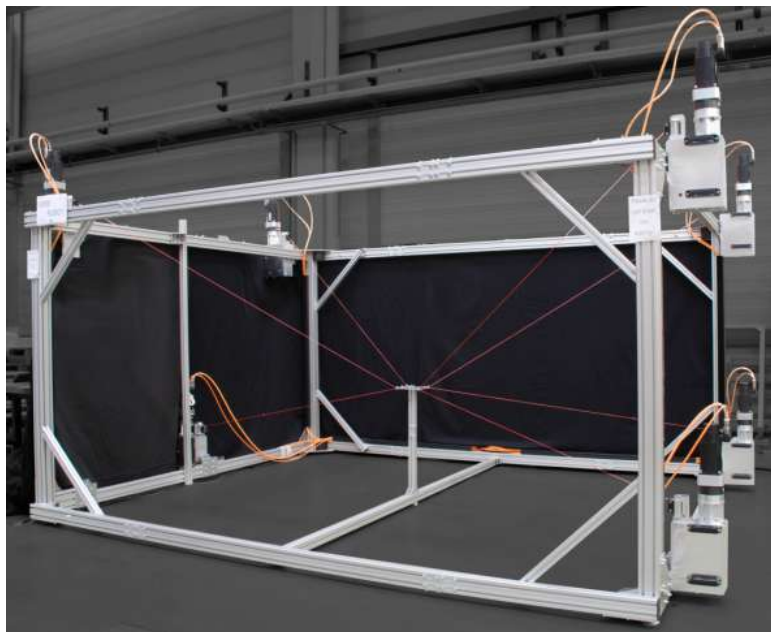


Figure 1.3: Prototype of IPAnema-1, an eight-cable robot with 6-degrees-of-freedom for material handling developed at the Fraunhofer Institute (Andreas Pott, Fraunhofer IPA)



Figure 1.4: Skycam at work during a Washington Huskies football game at Husky Stadium in Seattle, Washington (Despeaux~commonswiki)



Figure 1.5: China's Five-hundred-meter Aperture Spherical Radio Telescope (FAST) in south-west china's Guizhou province (china.org.cn)

Haptic devices are often controlled using an impedance-control scheme, in which the user can feel the inertia and friction induced by the device [31]. A key requirement in the design of haptic systems is to minimize the inertia and reduce the friction of the mechanism on which the user interaction port is mounted [32]. Haptic devices have to be stiff for the purpose of allowing high-bandwidth mechanical interactions and they must provide workspace sufficient for the immersion to be convincing. Cable robots can be utilized for the aforementioned applications because of their low inertia and high stiffness over a large workspace. Few such examples are reported in ([33]–[49]). Locomotion interface consisting of footplates supported by two eight-cable parallel robots are reported in ([50]–[52]). Applications in teleoperation have also been proposed [53]. Cable-suspended robots are implemented in rehabilitation systems and their performances are assessed in [54]. An application of a cable robot in rehabilitation is shown in Fig. 1.6.

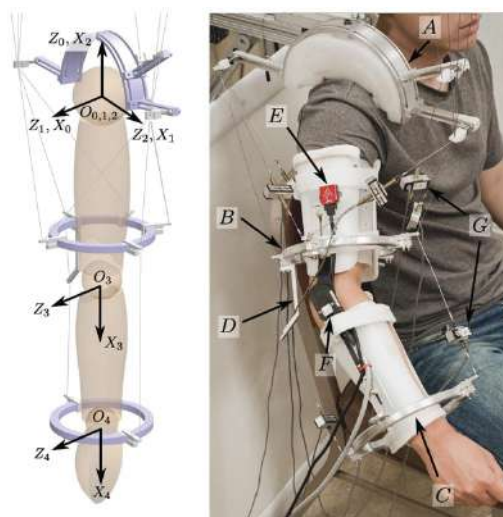


Figure 1.6: Prototype of CAREX, a cable-driven arm exoskeleton for neural rehabilitation developed at Columbia University (S.K. Agrawal, ROAR LAB, Columbia University)

A fixed-base planar cable robot was proposed for upper arm rehabilitation in [55]. Cable robot-based leg exoskeleton was introduced in [56] and a wearable upper-limb exoskeleton system based on a cable robot was developed ([57]–[59]). A cable robot is used as a gait rehabilitation tool that is used to apply controlled loads on a patient walking on a treadmill [60] as shown in Fig. 1.7. They are also used for the development of high-speed robots because of their lightweight characteristics [8, 61, 62]. Because of their large workspaces, they are used in warehouses and other similar applications ([63]–[68]). A cable system suspended on a traditional overhead bridge is proposed in [69, 70]. Cable robots are also implemented in 3D printing [71]

and for the cooperation of flying vehicles [72]. Their dynamic trajectory planning is suitable for artistic performances as discussed in [73, 74]. Cable robots are used for the mechanical teleoperation of surgical tools in magnetic resonance imaging (MRI) environments [75] and also for search and rescue operations ([76]–[80]). They have been proposed for the manipulation of models in wind tunnels ([81]–[83]) and for the scanning of artefacts for the construction of digital models [84, 85]. A very large cable robot was proposed to inspect the facade of a building and to provide active interaction between the building and its occupants [86]. Finally, cable robots are also used in motion simulators for a variety of applications ([87]–[92]). The past two decades have seen rapid growth in this area due to the rise in a variety of applications.

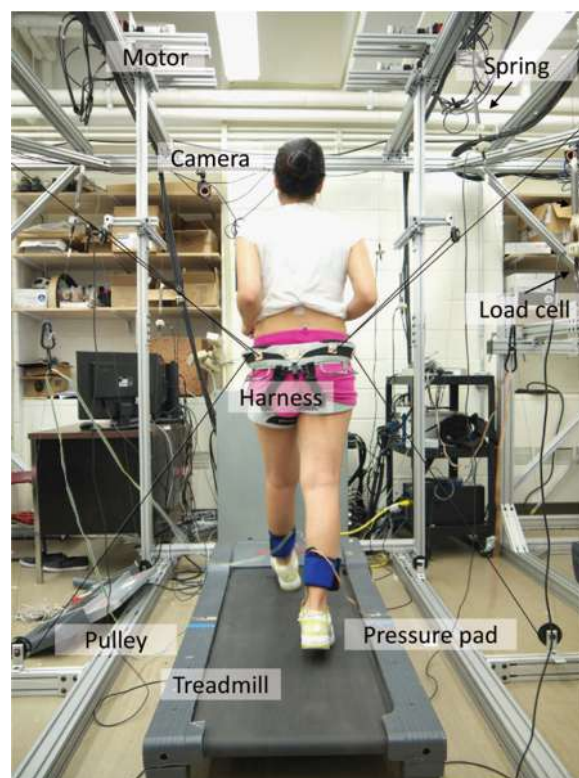


Figure 1.7: A subject walking on a treadmill while wearing the Tethered Pelvic Assist Device (S.K. Agrawal, ROAR LAB, Columbia University)

## 1.2 Classification of cable robots

Cable robots can be classified into two categories:

1. Spatial cable robot
2. Planar cable robot

A spatial cable robot is a six-degrees-of-freedom (DoF) robot, i.e., it can undergo translations and rotations about all the three axes. Fig. 1.1 depicts a spatial cable robot. This robot is similar to an upside-down six DoF Stewart platform, with six cables instead of hydraulic-cylinder legs. Gravity acts as an additional actuator ensuring that cables are always in tension in these robots. The number of cables in a spatial cable robot are not just limited to six. One such example is Charlotte [14]. It is a rectangular box driven in-parallel by eight cables, with eight tensioning motors mounted on-board (one on each corner). Spatial cable robot will become redundant if it has got more than six cables i.e., more cables than wrench-exerting DoF. Many of the cable robots are designed to have actuation redundancy in an attempt to avoid configurations where certain wrenches require an impossible compression force in one or more cables. An advantage with actuation redundancy is that the workspace can be expanded. Shiang et al. [10] chose four-cable robot over a three-cable robot in order to double the work area for the same three DoF of the robot. Another benefit of a redundant system is that additional cables increase load capacity and speed of the robot. This also reduces loads on individual cables, thereby reducing the requirement to smaller rotary actuators. Despite the provided actuation redundancy, there still exists subspaces in the potential workspace where cables can lose tension.

A planar cable robot has got three DoF, i.e., it can undergo translations about two axes and rotation about the third axis, as indicated in Fig. 1.8. A planar cable robot can be supported with as many cables as possible as long as we avoid the interference among the cables. Furthermore, cable robots can be placed into one of two categories: fully constrained or under-constrained [18, 93]. A configuration is said to be fully constrained if for a given set of cable lengths, the suspended object cannot be moved in position or orientation. A fully constrained configuration requires at least one cable length to become longer and any one other cable length to become shorter for motion of the robot [93]. Under-constrained configuration is the configuration for a given set of cable lengths, the suspended object can be moved in position or orientation. Fig. 1.1 depicts an under-constrained configuration of the six-cable spatial robot. In an under-constrained configuration, there are motions of the robot that can cause the cables to become slack. A cable robot in a pendulum-like configuration, for instance NIST ROBOCRANE shown in Fig. 1.2, is under-constrained not only because it can swing back and forth, but also because the cables can become slack when the robot is lifted by an external force [93]. However, a robot can be under-constrained but be able to manipulate all DoF of an object with the use of gravitational forces.

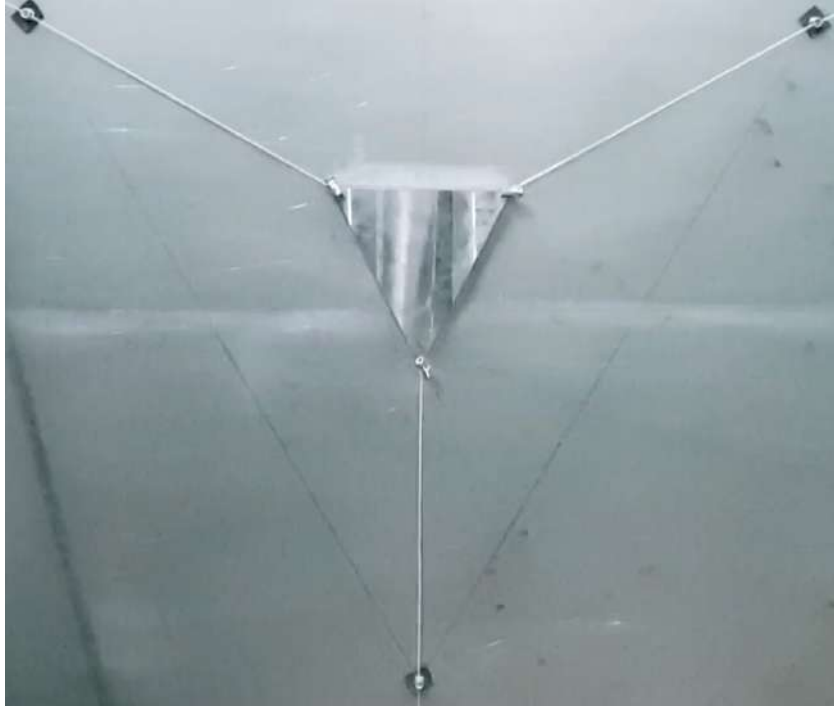


Figure 1.8: Planar cable robot with a triangular platform (this work)

Few configurations of a cable robot that operates in a plane are shown in Fig. 1.9. The two-cable configuration shown in Fig. 1.9(a) is under-constrained, since there is no cable to constrain the motion in the upward direction (i.e., along the  $y$ -axis). Figs. 1.9(b) and 1.9(c) are fully constrained. Three cables constrain them on both the axes in the plane. Rotation is not considered in the cases of Figs. 1.9(a) – 1.9(c) because all the cables are connected at a point. Another two-cable configuration that is also under-constrained, shown in Fig. 1.9(d), attempts to couple the motion of the cables to the rotation of the object. However, the three DoF of the object cannot be controlled independently since there are only two cable lengths. The three-cable configuration shown in Fig. 1.9(e) is fully constrained in that the object cannot be moved from its position and orientation. However, the orientation and position cannot be controlled independently in this configuration. In order to have a fully constrained configuration and be able to control all the three DoF independently, the robot requires more cables as shown in Fig. 1.10. A planar cable robot is said to be redundantly actuated, if it has more cables than three. Redundant robots can be either kinematically under-constrained or fully constrained. Redundancy can make a system to be fully constrained throughout the workspace. It is important to note that the use of a greater number of cables can still result in an under-constrained configuration for a specific position and orientation of the object. More details about fully constrained configuration are presented in Chapter 3.

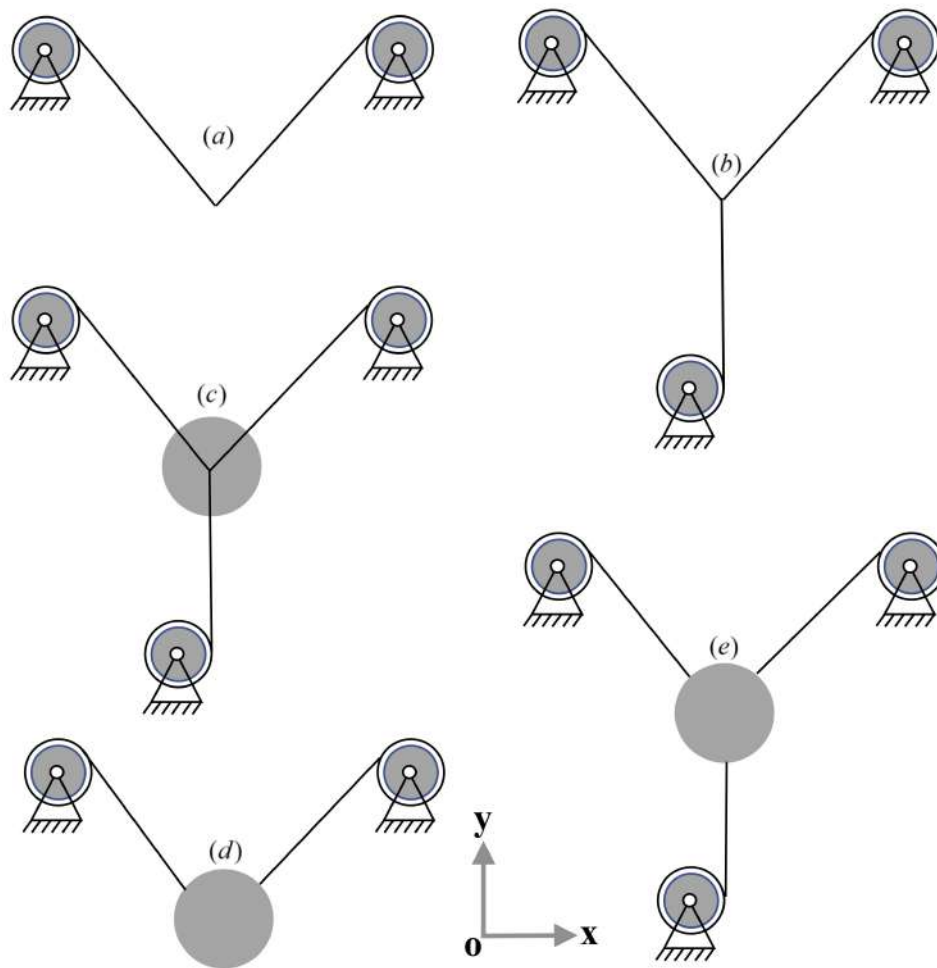


Figure 1.9: Cable robot configurations: (a), (d) under-constrained (b), (c), and (e) fully constrained

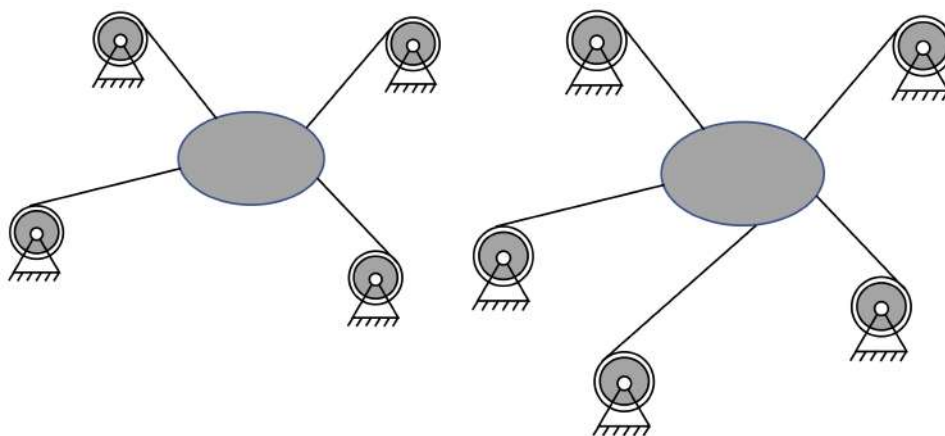


Figure 1.10: Cable robots with actuation redundancy

### 1.3 Feasible orientations of the platform

Let us consider a planar cable robot with  $n$  cables supporting the moving platform. Platform's centroid is located at  $(x, y)$  and its orientation is  $\phi$  w.r.t. the  $x$ -axis. An external load vector  $\mathbf{f} = \{F_x \ F_y \ M_z\}^T$  is acting at the centroid of the platform. Static equilibrium equations of the cable robot can be given as follows.

$$\mathbf{L}\mathbf{t} + \mathbf{f} = \mathbf{0} \tag{1.1}$$

where  $\mathbf{L}$  is a  $3 \times n$  matrix. Its elements depend on the coordinates of the centroid of the platform and its orientation, fixed pivots of the cable robot, and vertices of the moving platform. And,  $\mathbf{t}$  is the tension vector of size  $n \times 1$ . It is a column vector containing the tensions in the cables as elements. Since cables are used, the components of  $\mathbf{t}$  must not be negative. Therefore,  $\mathbf{t}$  satisfying Eq. 1.1 must contain non-negative elements for the configuration considered to be in equilibrium, i.e., orientation  $\phi$  of the platform to be feasible at  $(x, y)$ . When no such  $\mathbf{t}$  exists, then it is impossible to hold the robot in static equilibrium in that configuration. Note that the constraints for achieving static equilibrium are of the same form as the constraints found in a linear programming problem:  $\mathbf{L}\mathbf{t} = -\mathbf{f}$  with  $\mathbf{t} \succeq \mathbf{0}$ , where  $\succeq$  denotes the component-wise inequality. Eq. 1.1 and procedure to obtain the solution, i.e., tension vector  $\mathbf{t}$  with non-negative elements is discussed in Chapter 2.

At a point  $(x, y)$  that belongs to the workspace of a cable robot, there might exist a range of feasible orientations for a given external loading. All the orientations that are feasible will have a solution satisfying Eq. 1.1 with non-negative elements. To obtain these orientations,  $\phi$  is varied from  $-180^\circ$  to  $180^\circ$  with an increment of  $1^\circ$ .  $\mathbf{L}$  is obtained at every increment. Tension vector  $\mathbf{t}$  is calculated from Eq. 1.1 using the procedure discussed in Section 2.2.4. It is observed that the range of these feasible orientations will vary depending on the nature of the load acting on the platform, number of cables, and geometry of the cable robot. Feasible orientations are obtained not only at a single point but also at multiple points in a space of interest with the same procedure. For this, a grid is created in the region of interest. At every point in the grid, the aforementioned procedure is carried out to obtain feasible orientations.

As noted earlier, an orientation  $\phi$  of the platform is said to be fully constrained when its position and orientation cannot be changed without changing the cable lengths. To alter the orientation of the platform, the motion of the robot requires at least one cable length to become

longer and any one other cable length to become shorter. Mathematically, it can be expressed as follows.

$$\mathbf{N}\boldsymbol{\alpha} \succ \mathbf{0} \tag{1.2}$$

where  $\mathbf{N}$  is the nullspace or kernel matrix of  $\mathbf{L}$ . Its size is  $n \times m$  (i.e.,  $m = n - r$  where  $r$  is the rank of  $\mathbf{L}$ ). And  $\boldsymbol{\alpha}$  is a  $m \times 1$  underdetermined vector. For an orientation to fully constrain the cable robot, elements of the linear combinations of the column vectors of  $\mathbf{N}$  must be strictly positive (discussed in Section 3.4). Feasible orientations that fully constrain the cable robot are obtained at multiple points in the space of interest. It is observed that feasible orientations that fully constrain the planar cable robot belong to a subset of those for maintaining it in static equilibrium.

## 1.4 Motivation

Workspace of the cable robot can be characterized by a set of points where the center of mass of the moving platform can be positioned while all the cables have non-negative tension. At each point within the possible workspace, depending on the configuration of the cable robot, there might exist only one orientation or multiple orientations of the platform feasible for static equilibrium. It is observed in this study that the orientability of the platform for static equilibrium is limited. To fully constrain the cable robot of the same configuration, more limitations are put on the orientability of the platform.

Limited orientability is a hindrance for manipulating an object within a defined workspace where complete orientability (i.e.,  $0^\circ - 360^\circ$ ) of the platform is desired, such as in motion planning and for obstacle avoidance, etc. For example, human arm is highly dexterous because it can orient an object at any angle in its workspace. When it comes to conventional robots, they are not as dexterous as human arm in terms of orientability of the object in their workspace. These limitations in conventional robots can be attributed to joint limitations, force/torque capacities of actuators, and singularities etc. Cable robots suffer with more limitations as compared to both conventional robots and human arm because of singularities, interference between the cables, and tension constraints of the cables etc. The goal of this thesis is to enhance the orientability of planar cable robots, which is helpful in many applications. For this, a three-cable robot set-up is modified with the appendage of four components. Full details about this modified set-up and relevant analysis are provided in Chapter 4.

## 1.5 Objectives of the present study

- To obtain feasible orientations of the platform at any general point  $(x, y)$  or multiple points in the workspace of an  $n$ -cable planar robot that allow it to be in static equilibrium for a given external loading. No orientation is feasible at  $(x, y)$  indicates that the chosen point is not a part of the workspace.
- To obtain feasible orientations of the platform at multiple points in the space of interest for a  $n$ -cable planar robot that fully constrain it.
- To observe the effect of the parameters such as the number of cables, nature of the load acting on the platform, and geometry of the cable robot etc., on the behavior of feasible orientations.
- To make the platform of a cable robot trace a path for specified discrete waypoints. At every waypoint, an optimal orientation is to be obtained out of all the feasible orientations satisfying a chosen criterion.
- To note that the orientability of the platform is limited and this does not serve well for some applications.
- To conceive a design that enhances the orientability of the cable robot. This design has to be tested on a planar cable robot that has got fewer feasible orientations for a given external load acting on the platform.
- To make a provision for applying a moment load on the platform.

## 1.6 Organization of the thesis

**Chapter 2:** This chapter contains the background of the prior work carried out in the area of cable robots.

**Chapter 3:** This chapter deals with feasible orientations of the platform in the workspace of  $n$ -cable planar robots for given external loading. Concept related to fully constrained configuration is discussed in detail. By creating a grid in the space of interest, feasible orientations of the platform are obtained at every point in the grid for two different cases. First, orientations that allow the platform to be in static equilibrium, and second, orientations of the platform that fully constrain the cable robot. For discretized trajectories, we obtain the most favorable orientation at each waypoint using a criterion of either maximum or minimum of  $\|\mathbf{t}\|$ . Limited

orientability of the platform in different regions of the workspace is revealed.

**Chapter 4:** An approach to enhance the orientability of the cable robot is explored. For this, we modify the existing set-up with the appendage of a spool, a translational spring, an additional cable, and a rotary actuator.

**Chapter 5:** Arresting the free rotation of the spool w.r.t. the platform provides an opportunity for the application of moment load. The effect of this on the behavior of the cable robot is analyzed.

**Chapter 6:** Validation of the mathematical model is carried out using a prototype consisting of stepper motors, nylon gut cables, platform, and other accessories.

**Chapter 7:** This chapter gives a brief summary and contribution of the work of the thesis. It also talks about the scope of further research in this area.

**Appendix:** OneDrive links of the MATLAB scripts used for this thesis are provided. And link for the experimental videos is also provided here.

## Closure

Cable robots are parallel mechanisms in which the moving platform is actuated by cables. They are structurally similar to parallel actuated robots but with the fundamental difference that cables can only pull the moving platform but not push it. They have relatively large workspace for their size compared to conventional robots; superior stiffness under external disturbances; low noise; low energy consumption; low weight; easier portability; and low cost. These attributes make them suitable for many applications, but they have a short coming of limited orientability of the platform. We address this issue in Chapter 3 after presenting the relevant background and prior work on cable robots in Chapter 2.

# Chapter 2

## Literature Review

### Summary

This chapter begins with an introduction to parallel mechanisms. The subsequent section deals with the static analysis of cable robots. In that section, modeling of both the planar and spatial cable robots is discussed. Several definitions of the workspace such as wrench-closure workspace, wrench-feasible workspace, and dynamic workspace, etc., are introduced. Theorems and relevant tools used by various researchers for obtaining these workspaces are presented. The procedure for obtaining the tension vector for different cases of the planar cable robots is presented next. An approach to check the feasibility of the pose of the platform without obtaining a tension vector with non-negative elements is explained. Several concepts used for the determination of the force capabilities of a cable robot for given actuator limits when it is at a feasible pose are presented. Similarly, techniques used for the determination of static pose for a given geometry of the attachment points and cable lengths of under-actuated cable-suspended robots are discussed. In the following section, the dynamics and control of cable robots are considered, first for fully constrained cable robots and secondly for cable-suspended robots. Finally, calibration and identification issues are also addressed.

### 2.1 Introduction to parallel mechanisms

In the last few decades, robots are used for various applications. Parallel mechanisms play an important role in robotics. Their properties make them appropriate for tasks that require large payload to weight ratios or very demanding dynamic trajectories (e.g. high-speed robots) [94, 95]. Many of the parallel mechanisms involve some links that are subjected to only tension and compressive loads. One such example is the Gough-Stewart-Cappel platform ([96]–[98]). It involves six hydraulic cylinder legs coupled to the platform via Hooke’s joints and mounted

on spherical joints at their ends. It is used in various applications and can be considered as the archetypal parallel mechanism. Similarly, cable-driven mechanisms are parallel mechanisms that involve members loaded solely in tension. They are also called as wire-driven parallel mechanisms, tendon-driven parallel mechanisms, cable-driven parallel mechanisms (CDPMs), and cable-suspended parallel mechanisms (CSPMs) etc., [99, 100]. Cable robots (i.e., cable-driven parallel robots) are designed based on these CDPMs. Cables are flexible members and can only support the tensile load. Because of their properties, they have been employed in construction and in machines since antiquity [101]. They have a large payload to weight ratios, can provide potentially very large workspaces, and can be wound on spools. Conversely, struts and joints such as prismatic joint cannot be wound on the spool, rather they must be retracted. However, several issues arise in the analysis, design, control, and practical implementation of cable robots.

## 2.2 Static analysis of cable robots

### 2.2.1 Modeling of the planar cable robot

A planar cable robot with a moving platform suspended by  $n$  cables is shown in Fig. 2.1. Cable  $i$  (where  $i = 1, 2, \dots, n$ ) is connected to the platform at  $(x_{mi}, y_{mi})$  and is, at its other end, connected to a spool mounted on a rotary actuator fixed at  $(x_{fi}, y_{fi})$  which is used to wind or unwind the cable. By controlling the extension of the cables, the pose—position and orientation—of the platform can be controlled. The centroid of the platform located at the origin  $O$  of the  $xy$  coordinate system serves as the reference for position and orientation of the platform. The orientation of the platform, measured positive in the counter-clockwise direction, is indicated by  $\phi$  at any general point occupied by the centroid,  $(x, y)$ . Let  $\mathbf{P}_{i0} = P_{i0x}\hat{\mathbf{i}} + P_{i0y}\hat{\mathbf{j}}$  (where  $\hat{\mathbf{i}}$  and  $\hat{\mathbf{j}}$  denote the unit vectors along  $x$  and  $y$  axes, respectively) be the position vector from the centroid to the  $i^{th}$  vertex of the platform. When the centroid of the platform moves to a point  $(x, y)$  and the platform rotates by  $\phi$ , the changed coordinates of the moving platform and the changed position vector can be written as follows.

$$\begin{Bmatrix} x_{mi} \\ y_{mi} \end{Bmatrix} = \begin{Bmatrix} x \\ y \end{Bmatrix} + \mathbf{R} \begin{Bmatrix} P_{i0x} \\ P_{i0y} \end{Bmatrix} \quad (2.1)$$

$$\mathbf{P}_i = P_{ix}\hat{\mathbf{i}} + P_{iy}\hat{\mathbf{j}} = (P_{i0x} \cos \phi - P_{i0y} \sin \phi)\hat{\mathbf{i}} + (P_{i0x} \sin \phi + P_{i0y} \cos \phi)\hat{\mathbf{j}} \quad (2.2)$$

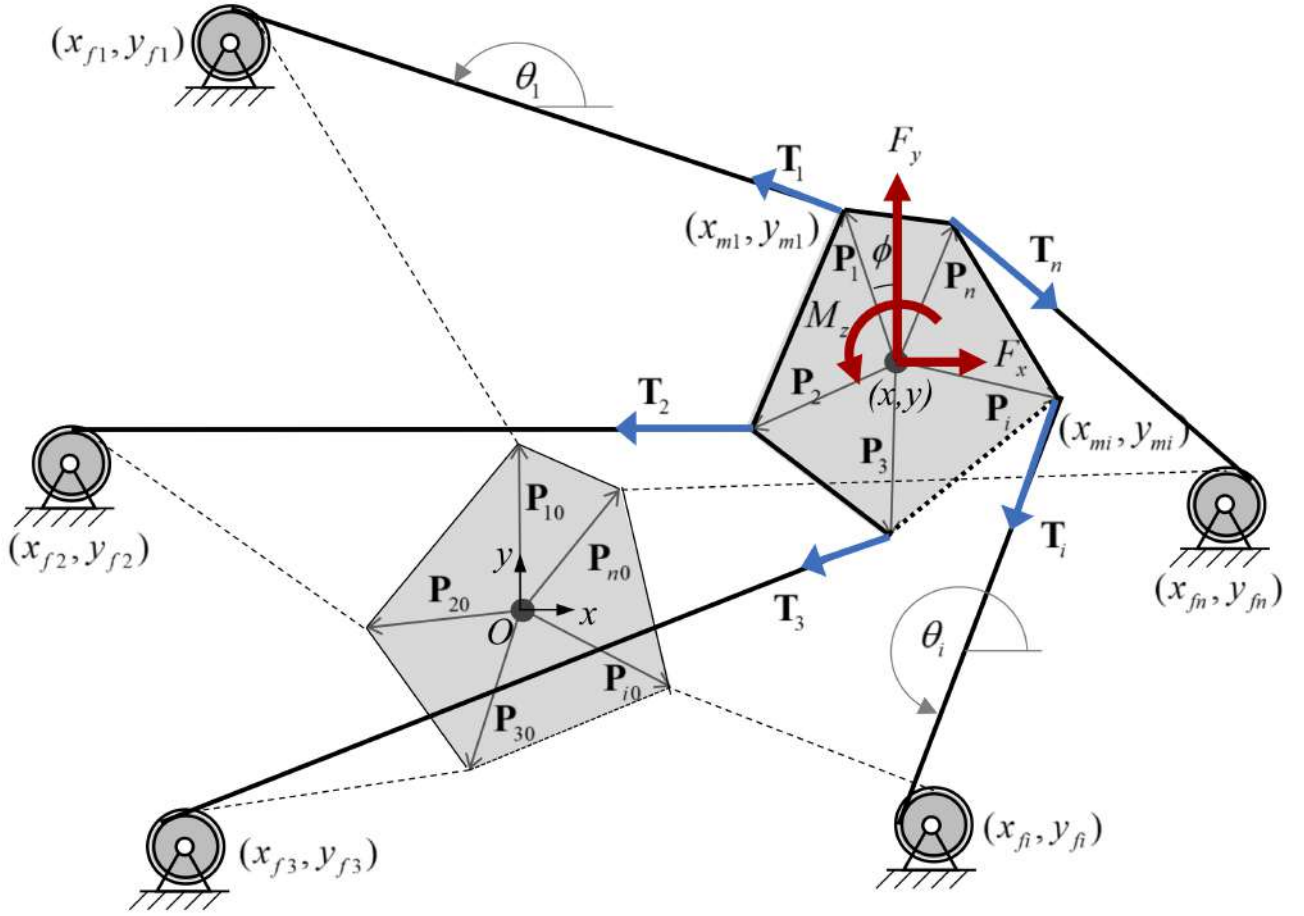


Figure 2.1: Planar cable robot consisting of a platform supported by  $n$  cables whose lengths are to be changed by winding rotary actuators to translate and rotate the platform

where  $\mathbf{R} = \begin{bmatrix} \cos \phi & -\sin \phi \\ \sin \phi & \cos \phi \end{bmatrix}$  is the rotation matrix. The cable vectors denoted by  $\mathbf{l}_i$  ( $i = 1, 2, \dots, n$ ) and directed from the moving vertex to the corresponding fixed point, are given by

$$\mathbf{l}_i = (x_{fi} - x_{mi})\hat{\mathbf{i}} + (y_{fi} - y_{mi})\hat{\mathbf{j}} \quad (2.3)$$

whose angles of inclination w.r.t. the  $x$ -axis are denoted by  $\theta_i = \tan^{-1} \left( \frac{y_{fi} - y_{mi}}{x_{fi} - x_{mi}} \right)$ . When tension is applied, cable  $i$  exerts at vertex  $\mathbf{P}_i$  a force on the mobile platform which is given as follows.

$$\mathbf{T}_i = T_i \frac{\mathbf{l}_i}{\|\mathbf{l}_i\|} = T_i \frac{\mathbf{l}_i}{l_i} \quad (2.4)$$

where  $T_i$  and  $l_i$  are the tensions and lengths of the cables, respectively. This tension force  $\mathbf{T}_i$  generates a moment  $\mathbf{P}_i \times \mathbf{T}_i$  about the centroid of the moving platform. By denoting the external load with  $(F_x \hat{\mathbf{i}} + F_y \hat{\mathbf{j}}, M_z \hat{\mathbf{k}})$ , which include forces in  $x$  and  $y$  directions and moment about the out-of-plane direction (i.e.,  $\hat{\mathbf{k}} = \hat{\mathbf{i}} \times \hat{\mathbf{j}}$ ) acting at the centroid of the platform, static equilibrium equations can be written as follows.

$$\sum_{i=1}^n \mathbf{T}_i + (F_x \hat{\mathbf{i}} + F_y \hat{\mathbf{j}}) = 0 \quad (2.5)$$

$$\sum_{i=1}^n (\mathbf{P}_i \times \mathbf{T}_i) + M_z \hat{\mathbf{k}} = 0 \quad (2.6)$$

Eqs. 2.5 and 2.6 can be represented in matrix form for convenience, as will be seen later:

$$\mathbf{L}\mathbf{t} + \mathbf{f} = \mathbf{0} \quad (2.7)$$

where

$$\mathbf{L} = \begin{bmatrix} \cos \theta_1 & \cos \theta_2 & \cdots & \cos \theta_n \\ \sin \theta_1 & \sin \theta_2 & \cdots & \sin \theta_n \\ s_1 & s_2 & \cdots & s_n \end{bmatrix} = \left\{ \mathbf{L}_1 \quad \mathbf{L}_2 \quad \cdots \quad \mathbf{L}_n \right\} \quad (2.8)$$

$$\mathbf{L}_i = \begin{bmatrix} \cos \theta_i \\ \sin \theta_i \\ s_i \end{bmatrix} = \begin{bmatrix} \left( \frac{\mathbf{l}_i}{l_i} \right)^T \\ \mathbf{P}_i \times \frac{\mathbf{l}_i}{l_i} \end{bmatrix} \quad (2.9)$$

$$s_i = P_{ix} \sin \theta_i - P_{iy} \cos \theta_i \quad (2.10)$$

$$\mathbf{t} = \begin{bmatrix} T_1 \\ T_2 \\ \vdots \\ T_n \end{bmatrix} \quad (2.11)$$

$$\mathbf{f} = \begin{Bmatrix} F_x \\ F_y \\ M_z \end{Bmatrix} \quad (2.12)$$

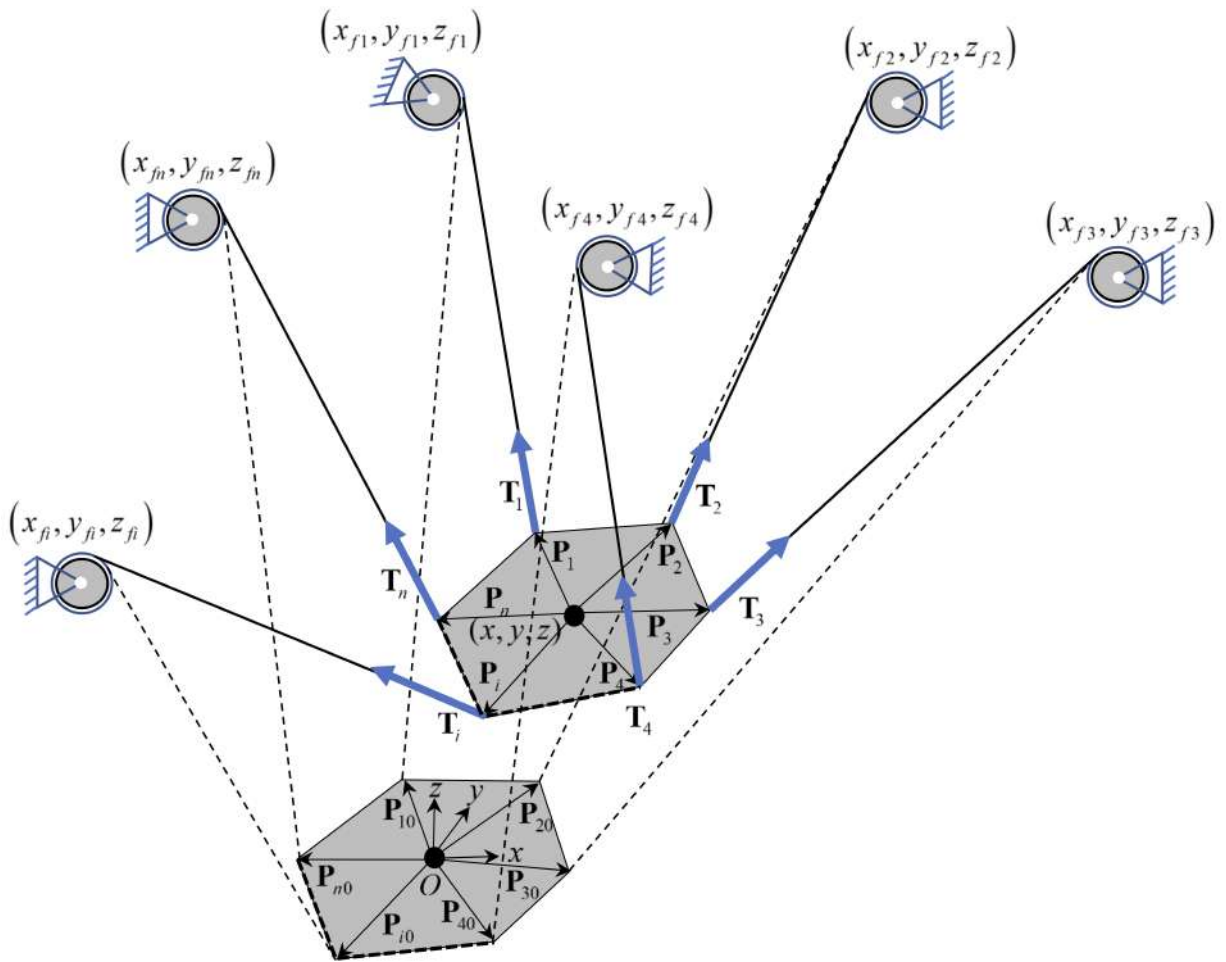
### 2.2.2 Modeling of the spatial cable robot

A spatial cable robot with a moving platform suspended by  $n$  cables is shown in Fig. 2.2. Cable  $i$  (where  $i = 1, 2, \dots, n$ ) is connected to the platform at  $(x_{mi}, y_{mi}, z_{mi})$  and is, at its other end, connected to a spool mounted on a rotary actuator fixed at  $(x_{fi}, y_{fi}, z_{fi})$  which is used to wind or unwind the cable. The centroid of the platform located at the origin  $O$  of the  $xyz$  coordinate system serves as the reference for position and orientation of the platform. The orientation of the platform measured positive in the counter-clockwise direction is  $\phi_1$ ,  $\phi_2$ , and  $\phi_3$  w.r.t. the  $x$ ,  $y$ , and  $z$  axes, respectively at any general point occupied by the centroid,  $(x, y, z)$ . Let  $\mathbf{P}_{i0} = P_{i0x}\hat{\mathbf{i}} + P_{i0y}\hat{\mathbf{j}} + P_{i0z}\hat{\mathbf{k}}$  (where  $\hat{\mathbf{i}}$ ,  $\hat{\mathbf{j}}$ , and  $\hat{\mathbf{k}}$  denote the unit vectors along  $x$ ,  $y$ , and  $z$  axes, respectively) be the position vector from the centroid to the  $i^{\text{th}}$  vertex of the platform. When the centroid of the platform moves to a point  $(x, y, z)$  and the platform rotates by  $\phi_1$ ,  $\phi_2$ , and  $\phi_3$  w.r.t. the  $x$ ,  $y$ , and  $z$  axes, respectively, the changed coordinates of the moving platform and the changed position vector can be written as follows.

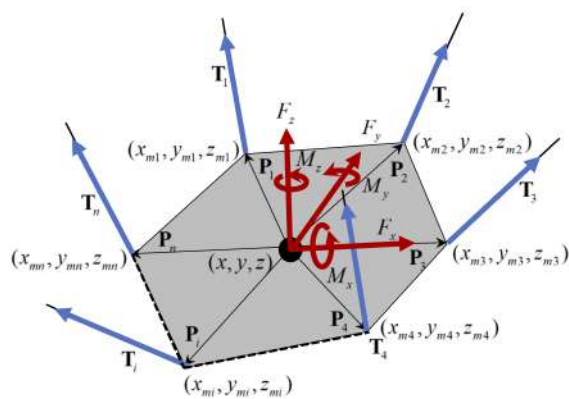
$$\begin{Bmatrix} x_{mi} \\ y_{mi} \\ z_{mi} \end{Bmatrix} = \begin{Bmatrix} x \\ y \\ z \end{Bmatrix} + \mathbf{R} \begin{Bmatrix} P_{i0x} \\ P_{i0y} \\ P_{i0z} \end{Bmatrix} \quad (2.13)$$

$$\mathbf{P}_i = P_{ix}\hat{\mathbf{i}} + P_{iy}\hat{\mathbf{j}} + P_{iz}\hat{\mathbf{k}} = \mathbf{R} \begin{Bmatrix} P_{i0x} \\ P_{i0y} \\ P_{i0z} \end{Bmatrix} \quad (2.14)$$

where  $\mathbf{R}$  is the rotation matrix of the moving platform w.r.t. the  $xyz$  coordinate system using a fixed axis rotation sequence of  $\phi_1$ ,  $\phi_2$ , and  $\phi_3$  about  $x$ ,  $y$ , and  $z$  axes, respectively, and can be written as



(a) Spatial cable robot



(b) Moving platform

Figure 2.2: Spatial cable robot consisting of a platform supported by  $n$  cables whose lengths are to be changed by winding rotary actuators to translate and rotate the platform

$$\mathbf{R} = \begin{bmatrix} \cos \phi_3 \cos \phi_2 & -\sin \phi_3 \cos \phi_1 + \cos \phi_3 \sin \phi_2 \sin \phi_1 & \sin \phi_3 \sin \phi_1 + \cos \phi_3 \sin \phi_2 \cos \phi_1 \\ \sin \phi_3 \cos \phi_2 & \cos \phi_3 \cos \phi_1 + \sin \phi_3 \sin \phi_2 \sin \phi_1 & -\cos \phi_3 \sin \phi_1 + \sin \phi_3 \sin \phi_2 \cos \phi_1 \\ -\sin \phi_2 & \cos \phi_2 \sin \phi_1 & \cos \phi_2 \cos \phi_1 \end{bmatrix} \quad (2.15)$$

The cable vectors denoted by  $\mathbf{l}_i$  ( $i = 1, 2, \dots, n$ ) are given by

$$\mathbf{l}_i = (x_{fi} - x_{mi})\hat{\mathbf{i}} + (y_{fi} - y_{mi})\hat{\mathbf{j}} + (z_{fi} - z_{mi})\hat{\mathbf{k}} \quad (2.16)$$

Then, the cable forces,  $\mathbf{T}_i$  ( $i = 1, 2, \dots, n$ ), acting on the platform are given as follows.

$$\mathbf{T}_i = T_i \frac{\mathbf{l}_i}{\|\mathbf{l}_i\|} = T_i \frac{\mathbf{l}_i}{l_i} \quad (2.17)$$

This tension force  $\mathbf{T}_i$  generates a moment  $\mathbf{P}_i \times \mathbf{T}_i$  about the centroid of the moving platform. By denoting the external load with  $(F_x\hat{\mathbf{i}} + F_y\hat{\mathbf{j}} + F_z\hat{\mathbf{k}}, M_x\hat{\mathbf{i}} + M_y\hat{\mathbf{j}} + M_z\hat{\mathbf{k}})$ , which include forces and moments about all the three axes acting at the centroid of the platform, static equilibrium equations can be written as follows.

$$\sum_{i=1}^n \mathbf{T}_i + (F_x\hat{\mathbf{i}} + F_y\hat{\mathbf{j}} + F_z\hat{\mathbf{k}}) = 0 \quad (2.18)$$

$$\sum_{i=1}^n (\mathbf{P}_i \times \mathbf{T}_i) + M_x\hat{\mathbf{i}} + M_y\hat{\mathbf{j}} + M_z\hat{\mathbf{k}} = 0 \quad (2.19)$$

Eqs. 2.18 and 2.19 can be represented in matrix form as given below:

$$\mathbf{L}\mathbf{t} + \mathbf{f} = \mathbf{0} \quad (2.20)$$

where

$$\mathbf{L} = \left\{ \mathbf{L}_1 \quad \mathbf{L}_2 \quad \dots \quad \mathbf{L}_n \right\} \quad (2.21)$$

$$\mathbf{L}_i = \left\{ \begin{array}{c} \left( \frac{\mathbf{l}_i}{l_i} \right)^T \\ \left( \mathbf{P}_i \times \frac{\mathbf{l}_i}{l_i} \right)^T \end{array} \right\} \quad (2.22)$$

$$\mathbf{t} = \left\{ \begin{array}{c} T_1 \\ T_2 \\ \vdots \\ T_n \end{array} \right\} \quad (2.23)$$

$$\mathbf{f} = \left\{ \begin{array}{c} F_x \\ F_y \\ F_z \\ M_x \\ M_y \\ M_z \end{array} \right\} \quad (2.24)$$

Basic geometric models were established in the early works on cable robots in [12, 34, 102]. The total wrench applied at the centroid of the platform by  $n$  cables must be equal to the external load acting at the centroid of the platform for it to be in static equilibrium. Eq. 2.7 in the case of planar cable robots and Eq. 2.20 for spatial cable robots play a key role in the kinematics, statics, and dynamics of cable robots. A variety of situations can be covered by properly defining load vector  $\mathbf{f}$ . For static conditions,  $\mathbf{f}$  represents the load induced by gravity on the platform. If dynamics is considered, then  $\mathbf{f}$  represents the load induced by gravity plus the inertial effects associated with the platform motion. In haptics applications,  $\mathbf{f}$  also includes the external forces and moments applied to the platform by the user [31]. Most of the analytical results produced in the literature are based on the equations presented in this section.

### 2.2.3 Workspace

Using Eqs. 2.7 and 2.20, basic problems related to analysis, design, and control of parallel mechanisms have been addressed. Several studies have targeted the determination of the workspace

of cable robots for a set of given geometric parameters. Several definitions of the workspace have been proposed. One such definition is mentioned here. Workspace can be defined as the set of positions and orientations of the platform for which an applied load on the platform  $\mathbf{f}$  can be balanced by a set of cable tensions [31]. Mathematically, it can be described as the set of platform positions and orientations for which, for a load applied on the platform  $\mathbf{f}$ , there exists at least one vector of cable tensions,  $\mathbf{t} \in \mathbb{R}^n$  such that  $\mathbf{L}\mathbf{t} + \mathbf{f} = \mathbf{0}$  and  $\mathbf{t} \succeq \mathbf{0}$ .

Several theorems were proposed in [76], ([103]–[106]) for obtaining the wrench-closure workspace (WCW). It can be defined as the set of positions and orientations of the mobile platform for which the cables can balance an external wrench  $\mathbf{f}$ , i.e., for which the platform of the mechanism is fully constrained. Six DoF cable robot driven by seven cables is dealt with in [103] and the two theorems provided in it are the efficient means to examine whether a given position and orientation of the moving platform belongs to the WCW. In [104], these theorems are used to find the parts of the reachable workspace that belong to WCW. Also, an efficient algorithm that determines the constant-orientation cross-sections of these parts was introduced. Stiemke’s theorem used in [105] provides an effective way of determining the boundaries of the WCW. To this end, tools from convex analysis and linear algebra are used to derive closed-form expressions for the workspace boundaries. The approach used in [105] lends itself to other numerical implementations using techniques such as interval analysis [76] and others [106]. In [104], it was shown that the boundary of the constant-orientation wrench-closure workspace of a planar parallel cable-driven mechanism (PPCDM) is composed of segments of conic sections, but the relationship between the geometry of the mechanism and the types of these conic sections is undetermined. For this, a graphical method for determining the types of these conic sections from the mechanism geometry was proposed in [106]. It was shown that the proposed method can be applied to find the constant-orientation singularities of a 3-RPR planar parallel robot because these conic sections correspond to the boundary segment of the analogous three-cable driven planar parallel mechanism.

It was observed that WCW is a rather restrictive property and that it is not necessarily the best design criterion. It is preferable to use wrench feasible workspace (WFW or it can also be called as force-feasible workspace) for the design of a cable robot when information on the tasks to be performed is available [31]. WFW can be defined as the set of positions and orientations in which the cables can balance any platform wrench belonging to a set of prescribed wrenches ([107]–[111]). [107] presents a means for analytically deriving WFW for the case of a point-mass end-effector, which has been validated via numerical simulation. Furthermore,

in [107], characteristics and trends of the WFW are observed and analyzed, and correlations between cable robot design parameters and observed workspace properties are determined. In [108], geometric properties of the available net wrench set are exploited to permit geometric calculation of the boundaries of the WFW. Net wrench set is the set of all wrenches that a cable robot can apply to its surroundings without violating tension constraints of the cables. It was shown that size and shape of WFW are highly dependent on the geometry of the robot and on the ranges of allowed cable tensions. Approach to obtain WFW in [109, 110] is based on interval analysis. Two sufficient conditions, namely, a sufficient condition for a box of poses to be fully inside the WFW and a sufficient condition for a box of poses to be fully outside the WFW and means to test them were presented in [109].

There are other definitions to workspace such as the dynamic workspace [112, 113] or the force-closure workspace [114]. Dynamic workspace is the workspace whose shape depends on the accelerations of the platform. In [112], it was shown that any subset of the workspace can be considered as a combination of three-cable workspaces, with boundaries being of two kinds: two-cable equilibrium loci and three-cable singularity loci [113].

Finally, necessary and sufficient conditions for a cable-suspended robot to stay in a given configuration (i.e., to achieve static equilibrium) are presented in [93]. Also, conditions for completely constraining the robot are derived. The problems of achieving static equilibrium and fully constraining the robot are derived [93]. An example of a four-cable planar robot is presented. In that example, feasible orientations of the rectangular platform are obtained at multiple points in the workspace of the cable robot. It was shown that a feasible pose of the platform must be part of the workspace and should have tension vector with non-negative elements. Procedure to obtain the tension vector for different cases of planar cable robots is discussed in the next sub-section.

#### 2.2.4 Tension vector

In Eq. 2.7, since  $\mathbf{L}$  is of size  $3 \times n$ ,  $\mathbf{t}$  of size  $n \times 1$ , and  $\mathbf{f}$  of size  $3 \times 1$ , for the simplest and trivial case of  $n = 1$  (i.e., for a one-cable robot, shown in Fig. 2.3),  $\mathbf{L}$  will be a  $3 \times 1$  column vector,  $\mathbf{t}$  a  $1 \times 1$  scalar, and  $\mathbf{f}$  a  $3 \times 1$  column vector. Therefore, a solution exists for  $\mathbf{t}$  (i.e.,  $T_1$ ), if and only if the elements of  $\mathbf{f}$  are proportional to the corresponding elements of  $\mathbf{L}$ . That is,

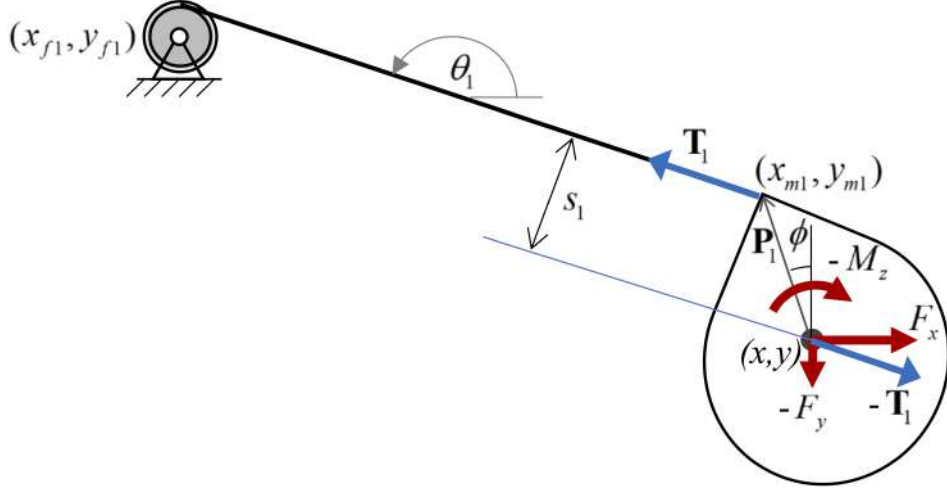


Figure 2.3: The trivial case of a planar one-cable robot

$$\begin{pmatrix} \cos \theta_1 \\ \sin \theta_1 \\ P_{1x} \sin \theta_1 - P_{1y} \cos \theta_1 \end{pmatrix} T_1 = - \begin{pmatrix} F_x \\ F_y \\ M_z \end{pmatrix} \quad (2.25)$$

It may be noted that not only the cable tension vector should be a resultant of the applied forces in  $x$  and  $y$  directions but also they should be separated by a distance  $s_1$  so that their couple cancels the applied moment,  $M_z$ . Note that  $T_1$  should be positive as a cable can only apply tension.

For  $n = 2$  (a two-cable robot, shown in Fig. 2.4),  $\mathbf{L}$ ,  $\mathbf{t}$ , and  $\mathbf{f}$  are of size  $3 \times 2$ ,  $2 \times 1$ , and  $3 \times 1$ , respectively.

$$\begin{bmatrix} \cos \theta_1 & \cos \theta_2 \\ \sin \theta_1 & \sin \theta_2 \\ P_{1x} \sin \theta_1 - P_{1y} \cos \theta_1 & P_{2x} \sin \theta_2 - P_{2y} \cos \theta_2 \end{bmatrix} \begin{pmatrix} T_1 \\ T_2 \end{pmatrix} = - \begin{pmatrix} F_x \\ F_y \\ M_z \end{pmatrix} \quad (2.26)$$

In order to have values of  $T_1$  and  $T_2$  that are non-negative, we can follow the following approach. Recall that  $\theta_i = \tan^{-1} \left( \frac{y_{fi} - y_{mi}}{x_{fi} - x_{mi}} \right)$  and  $(x_{mi}, y_{mi})$  for  $i = 1, 2$  depend on  $x, y$ , and  $\phi$  (i.e., the

coordinates of the centroid of the platform and its orientation). First, for given  $F_x$  and  $F_y$ , we can find all values of  $\theta_1$  and  $\theta_2$  using only the first two equations of Eq. 2.26 so that  $T_1$  and  $T_2$  are non-negative. Following this, for given  $M_z$ , we can find feasible values of  $x, y$ , and  $\phi$  that satisfy the third equation of Eq. 2.26 and other aforementioned relationships. In detail analysis of the workspace of a two-cable planar robot was presented in [3, 5].

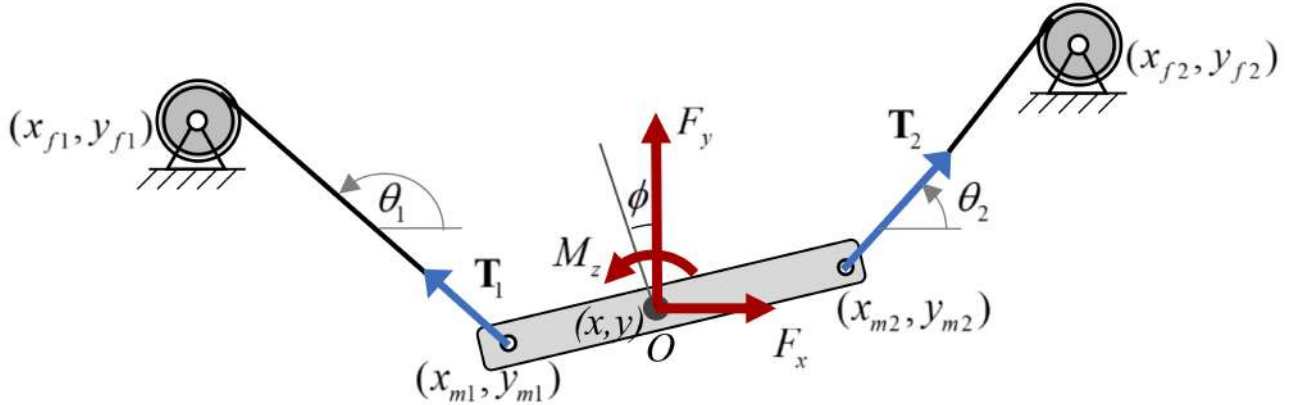


Figure 2.4: A planar two-cable robot

When  $n = 3$ ,  $\mathbf{L}$  is a  $3 \times 3$  square matrix. Therefore, there will be a unique solution to Eq. 2.7 if  $\mathbf{L}$  has full rank of three. Then,

$$\mathbf{t} = \mathbf{L}^{-1}(-\mathbf{f}) \quad (2.27)$$

Orientation  $\phi$  of the platform with its centroid at  $(x, y)$  is considered feasible only if the elements of  $\mathbf{t}$  are non-negative. For all the other remaining cases (i.e.,  $n > 3$  and rank deficient  $\mathbf{L}$  when  $n = 3$ ), Eq. 2.7 is an underdetermined system of equations and has many solutions if  $(\mathbf{L}\mathbf{L}^T)$  is invertible. Then, general solution of Eq. 2.7 can be written as

$$\mathbf{t} = \bar{\mathbf{t}} + \mathbf{N}\boldsymbol{\alpha} \quad (2.28)$$

Here,  $\bar{\mathbf{t}}$  is obtained using the pseudoinverse of matrix  $\mathbf{L}$  as given by

$$\bar{\mathbf{t}} = \mathbf{L}^T(\mathbf{L}\mathbf{L}^T)^{-1}(-\mathbf{f}) \quad (2.29)$$

and  $\mathbf{N}$  is the nullspace or kernel matrix of  $\mathbf{L}$ ; and  $\boldsymbol{\alpha}$  is a  $(n - r)$ -dimensional column vector,

where  $r$  is the rank of  $\mathbf{L}$ . For example, for a three-cable robot, when the rank of  $\mathbf{L}$  is 2, i.e.,  $r = 2$ ,  $\alpha$  is a scalar and  $\mathbf{N}$  will be  $3 \times 1$  nullspace vector. In such case, we can find a suitable range of  $\alpha$  so that all three elements of  $\mathbf{t}$  are non-negative even if  $\bar{\mathbf{t}}$  itself does not have non-negative elements. There may exist many solutions for  $\mathbf{t}$  depending on the range of  $\alpha$  for a given loading. Likewise, when  $r = 2$  for a four-cable robot, from Eq. 2.7, we have

$$\mathbf{t} = \begin{Bmatrix} t_1 \\ t_2 \\ t_3 \\ t_4 \end{Bmatrix} = \bar{\mathbf{t}} + \mathbf{N}\boldsymbol{\alpha} = \begin{Bmatrix} \bar{t}_1 \\ \bar{t}_2 \\ \bar{t}_3 \\ \bar{t}_4 \end{Bmatrix} + \begin{bmatrix} N_{11} & N_{12} \\ N_{21} & N_{22} \\ N_{31} & N_{32} \\ N_{41} & N_{42} \end{bmatrix} \begin{Bmatrix} \alpha_1 \\ \alpha_2 \end{Bmatrix} \quad (2.30)$$

In this case, values of  $\alpha_1$  and  $\alpha_2$  need to be found such that  $t_1, t_2, t_3$ , and  $t_4$  are all non-negative. This also leads to multiple solutions for  $\mathbf{t}$ . This is advantageous when a path is being planned for a cable robot so that tensions can be kept as small as possible or as large as possible. In fact, one can find  $\alpha_1$  and  $\alpha_2$  from the suitable range of  $\boldsymbol{\alpha}$  by minimizing or maximizing the  $\|\mathbf{t}\|$ .

For  $n > 3$  or rank-deficient  $n = 3$  cases, procedure to obtain suitable  $\boldsymbol{\alpha}$  for non-negative tensions in the cables is provided in [1]. It can be understood from Eq. 2.28 that a feasible solution for  $\{x, y, \phi\}^T$  is characterized by a convex region bounded by  $n$  linear inequalities on the elements of  $\boldsymbol{\alpha}_i$ ,  $i = 1, 2, \dots, m$ , where  $m = (n - r)$ , is the number of linearly independent columns of  $\mathbf{N}$ . To determine feasible range for  $\boldsymbol{\alpha}$ , we choose  $m$  out of  $n$  pair of inequalities and convert them into equations. Note that  $m$  out of  $n$  inequations can be chosen in  ${}^nC_m$  ways. We then find the inequalities by considering every pair of  $m$  equations to ensure that all components of  $\mathbf{t}$  are non-negative in Eq. 2.28. Thus, we get one-sided bounds on subsets of  $\boldsymbol{\alpha}$ , which denote with  $\bar{\boldsymbol{\alpha}}$ . Following this, we check if each  $\bar{\boldsymbol{\alpha}}$  satisfies all the remaining  $(n - m)$  inequalities. As the number of cables increase, complexity of the procedure increases.

### 2.2.5 The determinant approach

There is an alternative perspective to determining if a position and orientation is part of the workspace of a cable robot and hence can be in static equilibrium for given loading. Irrespective of the sign of the elements of  $\bar{\mathbf{t}}$ , if linear combinations of the elements of the column vectors of nullspace of  $\mathbf{L}$  are strictly positive ( $\mathbf{N}\boldsymbol{\alpha} \succ \mathbf{0}$ ), then the robot will achieve static equilibrium.

This is a sufficient condition. Towards this, Eq. 2.7 can be rewritten as follows.

$$\mathbf{L}_{\text{aug}}\mathbf{t}_{\text{aug}} = \mathbf{0} \quad (2.31)$$

where  $\mathbf{L}_{\text{aug}} = \{ \mathbf{L} \ \mathbf{f} \}$  and  $\mathbf{t}_{\text{aug}} = \{ \mathbf{t}^T \ 1 \}^T$ . It is possible for a planar cable robot to achieve static equilibrium for a given configuration (i.e., pose) if there is a nullspace vector of  $\mathbf{L}_{\text{aug}}$  such that its components are all non-negative and its last component is positive. Components of  $\mathbf{t}_{\text{aug}}$  determine the feasible set of cable tensions where the zero components of  $\mathbf{t}_{\text{aug}}$  correspond to slack cables. Roberts et al. (1998) presented an approach to determine the static equilibrium of the cable robot with the aid of  $\mathbf{L}_{\text{aug}}$ , as explained next.

Let  $\mathbf{N}_{\text{aug}}$  be the nullspace of  $\mathbf{L}_{\text{aug}}$  and its size be  $c \times d$  where  $d < c$ . Let  $\begin{bmatrix} \mathbf{v}_1 & \mathbf{v}_2 & \cdots & \mathbf{v}_c \end{bmatrix}$  be linearly independent row vectors of  $\mathbf{N}_{\text{aug}}$ . Choose  $(d - 1)$  linearly independent  $\mathbf{v}_j$  vectors, which are denoted with  $\mathbf{v}_{j_1}, \mathbf{v}_{j_2}, \dots, \mathbf{v}_{j_{d-1}}$ . They can be chosen in  ${}^cC_{d-1}$  ways. Compute the determinant  $\begin{vmatrix} \mathbf{v}_{j_1} & \mathbf{v}_{j_2} & \cdots & \mathbf{v}_{j_{d-1}} & \mathbf{v}_j \end{vmatrix}$  where  $j$  varies from 1 to  $c$ , excluding  $j_1, j_2, \dots, j_{d-1}$ . Cable forces will be non-negative if the values of determinants are either non-positive or non-negative else the procedure is repeated for other combination until all  ${}^cC_{d-1}$  combinations are exhaustively checked. If the values of determinants of all the  ${}^cC_{d-1}$  combinations are neither non-negative nor non-positive, then the cable robot cannot achieve static equilibrium for the considered configuration. With this approach, we can only determine whether a position and orientation belongs to workspace or not, but the tension vector cannot be obtained.

### 2.2.6 Force capabilities

It is interesting to determine the force capabilities of a cable robot for given actuator limits when it is at a feasible position and orientation. In other words, we ought to obtain the set of wrenches that the cable robot is capable of applying to its environment via its platform given its geometry and the limitations of its actuators or transmissions. This problem was tackled by mapping the cable force vector onto the platform wrench space [108, 115, 116], using Eqs. 2.7 and 2.20. In [115], it is shown that available wrench set of a cable robot can be represented mathematically by a zonotope, a special class of convex polytopes. A zonotope is a polytope composed of pairs of parallel faces. Using the properties of zonotopes, two methods to construct the available wrench set are discussed. From the representation of available wrench set, computationally efficient and non-iterative tests are presented to verify if this set includes the task wrench set (set of wrenches needed for a given task).

Cable-suspended robots are characterized by the use of gravity—the weight of the platform—to maintain cables in tension. One such example is the NIST ROBOCRANE [2, 12, 84]. In these mechanisms, gravity is considered as an additional actuator that always acts downwards on the moving platform. Cable-suspended robots do not generally have a WCW. They can also be called underactuated. They are like pendulum-type mechanisms whose DoF are not all controlled ([117]–[121]). They possess the advantage of not requiring redundant actuation since the number of cables does not have to exceed the number of DoF. Downwards vertical acceleration produced solely by gravity limits their acceleration capabilities. In [117], a simple, compact, yet powerful robotic winch, called Winch-Bot, is presented. It is an underactuated robot having only one controllable axis. Hanging a load with merely one cable, it is capable of moving it in a large workspace by swinging the load dynamically based on parametric self-excitation. [118, 119] present a novel planar three DoF pendulum-like underactuated robot. The robot consists of an end-effector with an actuated arm suspended on a cable wound on a reel. This robot can achieve full planar point-to-point motion, i.e., position and orientation with zero-velocity landing by swinging itself as children do on playground swings.

### 2.2.7 Determination of a static pose

For a given geometry of the attachment points and cable lengths of underactuated cable-suspended robots, an interesting issue is to determine its static pose. The problem is involved, because kinematics and statics are coupled and they must be solved simultaneously. A simplified case was solved in [122] for applications in cooperating flying vehicles. The general case of a body suspended on four cables was treated in [123]. Elimination procedure presented in it provides the complete solution set, thus proving that when all cables are in tension, 216 potential solutions exist in the complex field. A least-degree univariate polynomial free of spurious factors is obtained in the ideal governing the problem and solutions are numerically computed via both an eigenvalue formulation and homotopy continuation. Body suspended on three cables was treated in [124]. The univariate polynomial obtained in this case was of degree 156. The three-cable problem was also addressed in [125] using interval analysis. In [126], problem related to finding the lowest stable-equilibrium pose of a rigid body subjected to gravity and suspended in space by an arbitrary number of cables is solved. It is an optimization problem with well-defined properties. The proposed method for yielding equilibrium with the lowest potential energy in [126] is mildly sensitive to the number of suspending cables. An example involving a platform suspended by 1000 cables is solved to illustrate the generality and the effectiveness of the method.

Synthesis of planar cable robots was formulated mathematically using optimization formalisms in [127, 128]. In [127], problem related to dimensional synthesis was tackled, i.e., to find a geometry for a planar parallel cable-driven robot whose WCW contains a prescribed workspace. Geometry of a planar parallel cable-driven robot whose constant orientation WCW contains a prescribed workspace was found out in [128]. In [50], two 6-DoF cable robots sharing a common workspace to obtain the mechanical base for the design of a locomotion interface is proposed. Numerical optimization was used to synthesize these cable robots while ensuring wrench capabilities and avoiding mechanical interferences between all the entities of the locomotion interface (cables and moving bodies).

Determination of potential interferences between cables or between cables and other bodies are included in the problems related to analysis and synthesis of cable robots. In [129], algorithms that allow to study the influence of wire/wire and wire/end-effector interference on the workspace, assuming a fixed orientation of the end-effector were proposed. These algorithms exactly determine the region of the workspace which is interference free. Cable is assumed as a line segment in space. When a mechanical contact occurs between two cables or between a cable and an edge of the end effector, these entities necessarily lie in the same plane, and then the 3-D problem becomes 2-D. In [130], this fact was used to simplify the equations and it led to exhaustive descriptions of the associated interference loci in the constant-orientation workspace of cable-driven mechanism. Obtained results provided a fast method to graphically represent all interference regions in the manipulator workspace, given its geometry and the orientation of its end effector. Compared to rigid link mechanisms, cable robots may also be able to tolerate some cable interferences, due to the flexibility of the cables. This approach was taken in order to handle the potential interferences that may occur in a locomotion interface based on two adjacent platforms each driven by eight cables in [131].

## 2.3 Dynamics and control

### 2.3.1 Fully constrained cable robots

When the platform is fully constrained, reduced weight of the components in cable robots makes them appropriate for high-speed and high-performance applications [8]. In high-speed applications, load vector  $\mathbf{f}$  includes gravity plus the inertial effects associated with the platform motion. Most of the studies on cable robots neglect the mass of the cables in order to make the computation of the inertial effects simple. It is equivalent to the application of Newton-Euler

equations on a single moving rigid body on which pure forces are exerted. If the number of cables exceeds the number of DoF of the platform, Eqs. 2.7 and 2.20 lead to an underdetermined system of equations and in general there exist infinitely many solutions for the cable tensions as discussed in Section 2.2.4 and these may not be properly distributed. Thus, it provides an opportunity for the use of optimization in order to generate a proper distribution of the cable tensions for given platform trajectories and avoid large internal forces.

In [87], a six DoF tendon-based parallel manipulator moves the platform with high speed using seven cables. For this, nonlinear feed-forward control laws in the cable length coordinates are used to control the motion of the platform along desired trajectories in space. Using a method based on the analysis of the workspace condition, tension constraints, and limiting torque constraints of actuators, an analytical solution for optimum tension distribution is found and used to compute the force in each cable for compensation of dynamic errors. In [88], different algorithms for tendon force distribution are proposed and investigated w.r.t. their usability on a real time system. Methods of improving energy efficiency by leveraging nonlinear trajectories and energy-optimal tension distributions are proposed in [132]. Experimental and simulated results in it showed that energy efficiency can be improved significantly by using optimized parabolic trajectories. In [133], force and torque capacity (i.e., capability of the end-effector for applying force and torque to external object) of the manipulator is illustrated in 3D space whose axes are force or torque components. It is shown that the force and torque capacity have a convex cone and parallelepiped shape, respectively. The design of the cable robot is then reduced to the sizing of these shapes according to the design requirements and manufacturing limitations.

Linear programming used in [87, 132] is simple and systematic, but it cannot guarantee the continuity of the solution, which may lead to instabilities. On the other hand, quadratic programming used in [88, 133] provides continuity but at the expense of less predictable computation time. As the number of cables increase, situation becomes more complex. Dykstra’s alternating projection method is used to find the minimum-2-norm solution for actuator forces in [134]. Lower and upper bounds are imposed on the actuator forces. The lower bound is to obtain desired pretension in the cables and upper bound is to limit the maximum allowable forces in the cables. Algorithm presented in it is a systematic numerical method to determine whether or not a solution exists to the cable forces within the bounds imposed. And, if it does exist, calculate the minimum-2-norm solution for the cable forces for a given task. In [135], an algorithm for tendon force distribution calculations capable for usage on a real-time

system is proposed. The algorithm is designed in such a way that tendon force distributions is continuous to avoid steps in the motor torques. A real-time algorithm is proposed in [136] also. A real-time capable tension distribution algorithm for  $n$ -DOF cable robot actuated by  $(n + 2)$  cables is proposed in [137]. The approach for the design of fast tension distribution algorithm in it is based on Mikelson’s barycenter approach.

Implementation of control in CDPMs with actuation redundancy is a complicated task. For controlling the distribution of the forces in the cables, they have to be monitored continuously. Different means of measuring these forces is proposed in [138]. One approach for the proper distribution of force is to rely on the compliance of the cables and the attachment points [35]. Force control capabilities are compromised in this approach by simplifying the control. Controller that deals with cable tensions is first proposed in [139]. Optimal solution is computed off-line and then the solution is uploaded in to real-time controller. In [19], a fuzzy plus proportional-integral control (FPPIC) method, which enhances the control performance for steady-state errors, is utilized to control the wind-induced vibration of the trajectory tracking of the feed cabin (i.e., moving platform). A three DoF cable robot is made to trace a desired trajectory in [140]. Control law used in this system is designed based on backstepping technique. In [141], robust sliding mode control is utilized in order to set-point control of the suspended cable-driven robot at the presence of unknown but bounded disturbances. The asymptotic stability and robustness of the proposed control law is proved using second method of Lyapunov. [142] also includes a three-cable robot controlled by a sliding mode control system. Flexibility of the cables is considered in the development of a complex dynamic model that is used for the control in [143, 144].  $H_\infty$  controller (which suits for multi-input multi-output systems including flexible modes) was proposed in order to mitigate the effects of the flexibility of the cables in a cable robot in [145]. Multitude of control strategies have been proposed in the literature (e.g., [146]).

### 2.3.2 Cable-suspended robots

In cable-suspended robots, the dynamics and control become tough because there generally exists no configuration in which internal forces can be generated, i.e., these systems are not tensionable [147]. In [1], an approach to design positive tension controllers for cable-suspended robots with redundant cables is discussed. The tension distribution problem in the context of very large cable-suspended robots was studied in [20, 26]. A technique proposed in [73, 74] for the design of dynamic trajectories can guarantee the tensions in the cables of cable-suspended robots. [117] deals with the dynamics of underactuated (pendulum-like) cable-

suspended robots (Winch-Bot, one-cable robot). This was further developed to a pendulum-like three dof underactuated cable-driven robot in [118, 121]. In [120], control was simplified by providing differential flatness and integrability. The trajectory planning and control techniques proposed in the literature focus on the prescription of target configurations to be reached because the trajectory of underactuated cable-suspended robots cannot be fully controlled. One of the key concepts is then the design of input functions that can either inject or extract energy from the underactuated mechanism. One such engineering system was studied in [148] i.e., famous censer (Botafumeiro). When very long cables are used, mass of the cables are considered as non-negligible [19, 21, 27, 148, 149, 150, 151]. The inverse dynamic formulation of cable-suspended parallel robot based on the inverse kinematic analysis with non-negligible cable mass is established using Lagrangian dynamic formulation in [19]. Dynamic model of a cable robot including cable mass, cable bending, and cable torsional stiffness is formulated in [27]. Solution of the inverse kinematic problem of cable robots while considering the mass of the cables requires the numerical solution of a set of nonlinear equations. It was shown that cable sag can have a significant effect on both the inverse kinematics and stiffness of cable-driven robotic manipulators in [149]. The importance of maintaining a minimum level of cable tension to minimize the effect of cable sagging on the mechanism’s stiffness and workspace is demonstrated in [150].

### 2.3.3 Calibration

Dynamic modelling and control strategies require the knowledge of kinematic and inertial parameters of the cable robots. For efficient modelling, additional parameters such as friction characteristics, dynamic response of transmission components and others can be included. For proper behavior and kinematic accuracy of cable robots, calibration and identification must be done in proper order. For this, self-calibration of a novel biologically-inspired cable-driven robotic arm was proposed in [152]. The model is formulated based on the differential change in the cable end-point distances. A computationally efficient algorithm using iterative least-squares is employed to identify the errors in the geometric model parameters. In [153], a novel two DoF cable-driven robot with self-calibration and online drift correction capabilities is proposed. Two novel self-calibration methods have been developed in [153] that leverage the robot’s actuation redundancy. The first uses an incremental displacement, or jitter method, whereas the second uses variations in cable tensions to determine the end effector location. Other calibration techniques are proposed in ([154]–[157]). An algorithm for the extended kinematics taking into account cable pulleys is discussed and implemented in real-time in [158] for parallel cable robots. A methodology for the identification of the combined kinematic and dynamic

parameters of a six DoF cable robots model is proposed in [159]. This methodology ensures that the errors on the kinematic parameters do not affect the performances of the dynamic parameters estimation step. Another similar identification issue is addressed in [77]. Other issues such as the determination of the optimal number of measurement points and the choice of identification reference frames are also addressed in [77, 159]. Cable robots are considered to be ideal for portable reconfigurable systems that can be rapidly installed and operated. In such applications, calibration is key. For that, self-calibrating cable robots have been proposed in the literature.

## Closure

In this chapter, modelling of both the planar and spatial cable robots is carried out. By properly defining  $\mathbf{f}$  in Eqs. 2.7 and 2.20, a variety of situations covered in the literature are discussed. Tools and algorithms used for obtaining different workspaces are presented. Procedure to obtain the tension vector, used in the later chapters of this thesis, for different cases of planar cable robots is explained. To confirm the feasibility of the pose of the platform, one has to go through the tedious process of obtaining tension vector with non-negative elements. To circumvent this, an alternate approach that confirms the feasibility of the pose of the platform with the aid of nullspace is discussed. Several techniques implemented to obtain the set of wrenches that the platform is capable of applying to its environment for the given geometry of cable robot and the limitations of its actuators are explained. Different approaches used by various research groups for the determination of static pose of the platform for the given geometry of the attachment points and cable lengths of underactuated cable-suspended robots are presented. Finally, dynamics and control of cable robots are considered.

With this background, we present the work done in this thesis in the subsequent chapters, beginning with the orientability of cable robots in the next.

# Chapter 3

## Orientability of the Moving Platform

### Summary

In this chapter, we present the workspace analysis of  $n$ -cable planar robots for given external loading. In particular, we note that the orientability of the moving platform of a cable robot is rather limited. This point is illustrated by presenting a few examples that show the nature of the workspace and the extent of orientability in it. We consider moment load in addition to in-plane forces. The enhancement of orientability with and without a moment load is illustrated through examples. Finally, we present examples of feasible cable tensions for given loading along prescribed trajectories.

### 3.1 Feasibility of the orientation of the moving platform

As discussed in Section 2.2.4, the orientation  $\phi$  of the moving platform with its centroid at  $(x, y)$  is considered feasible only if the elements of  $\mathbf{t}$  are non-negative. Configuration 1 is feasible but not Configuration 2 as can be seen in Figs. 3.1a and 3.1b. Table 3.1 lists the details of the two configurations. Eq. 2.27 is used to obtain the tension vector for both the configurations as the rank of  $\mathbf{L}$  is 3. Non-negative cable forces for the first configuration indicate that the platform is in static equilibrium, while two negative cable forces for the second configuration indicate that the platform is not in static equilibrium with cables.

The data for two different planar cable robots can be found in Table 3.2. Eqs. 2.28 and 2.29 are used for obtaining the tension vector. In the first case, for which  $n = 4$ , we see in the 14<sup>th</sup> row and third column that there is no intersection for the value of  $\alpha$ . Furthermore,  $\bar{\mathbf{t}}$  does not have all non-negative components, hence, we can conclude that there is no solution for this data. This case is shown in Fig. 3.2a.

Table 3.1: Cable forces for two different configurations of the three-cable robot whose  $\mathbf{L}$  matrix has full rank. Cable forces of Configuration 2 are not all non-negative.

No.	Variables	Configuration 1	Configuration 2
1	$(x_{fi}, y_{fi})$ where (i=1,2,3)	(0,5.77) (5,-2.89) (-5,-2.89)	(0,5.77) (5,-2.89) (-5,-2.89)
2	$(x, y)$	(2,-2)	(2,-2)
3	$\phi$	$10^\circ$	$-5^\circ$
4	$(P_{i0x}, P_{i0y})$	(0,1.73) (1.5,-0.87) (-1.5,-0.87)	(0,1.73) (1.5,-0.87) (-1.5,-0.87)
5	$(x_{mi}, y_{mi})$	(1.70,-0.29) (3.63,-2.59) (0.67,-3.11)	(2.15,-0.27) (3.42,-2.99) (0.43,-2.73)
6	$\mathbf{L}$	$\begin{bmatrix} -0.27 & 0.98 & -0.99 \\ 0.96 & -0.21 & 0.04 \\ 0.17 & 0.23 & -1.16 \end{bmatrix}$	$\begin{bmatrix} -0.34 & 0.99 & -0.99 \\ 0.94 & 0.07 & -0.03 \\ 0.72 & 1.08 & -0.69 \end{bmatrix}$
7	$\mathbf{f}$	$\{0 \ -1 \ 0\}^T$	$\{0 \ -1 \ 0\}^T$
8	$\mathbf{t}$	$\{1.16 \ 0.62 \ 0.30\}^T$	$\{1.16 \ -2.75 \ -3.14\}^T$

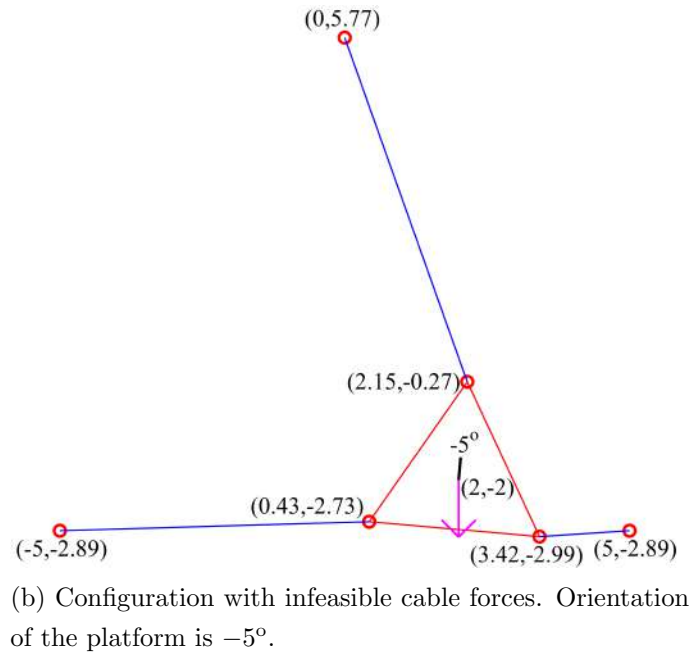
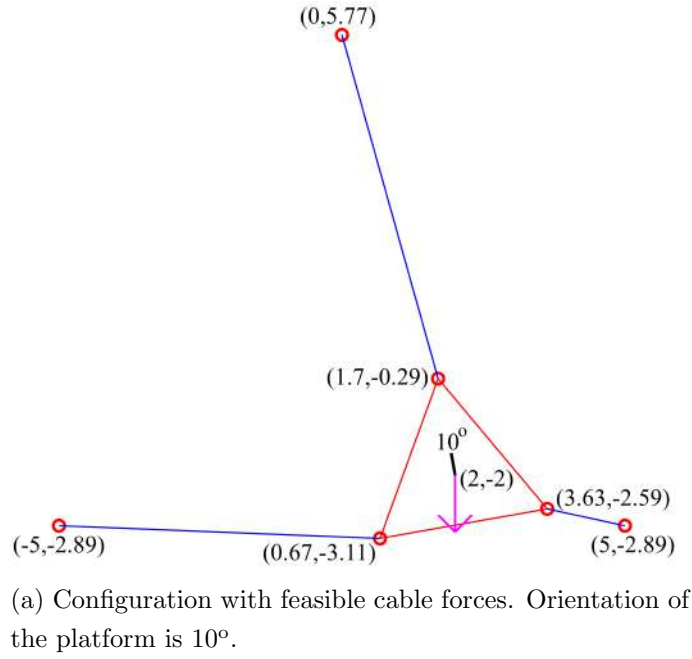


Figure 3.1: Two different configurations of a three-cable robot. Pink arrow indicates the direction of the external load acting at the centroid of the platform.

On the other hand, for  $n = 5$  case in the 4<sup>th</sup> column of Table 3.2, it can be checked that  $\bar{\alpha}_{10}$  and  $\bar{\alpha}_3$  satisfy other three inequalities. Hence, feasible  $\alpha$  lies on the line joining between  $\bar{\alpha}_{10}$  and  $\bar{\alpha}_3$ . Any point on this line satisfies all the five inequalities of  $\bar{\mathbf{t}} + \mathbf{N}\alpha \succeq \mathbf{0}$ . Therefore, the platform will be in static equilibrium for any values of  $\alpha$  on this line. This case is depicted

in Fig. 3.2b.

Table 3.2: Data for two different configurations of the planar cable robots i.e., for  $n = 4$  and 5

No.	Variables	Four-cable robot	Five-cable robot
1	$(x_{fi}, y_{fi})$	(10,10) (10,-10) (-10,-10) (-10,10)	(0,7.5) (5,5) (5,-5) (-5,-5) (-5,5)
2	$(x, y)$	(0,0)	(3,2)
3	$\phi$	18°	10°
4	$(P_{i0x}, P_{i0y})$	(2,1.5) (2,-1.5) (-2,-1.5) (-2,1.5)	(0,0.5) (1,0.5) (1,-0.5) (-1,-0.5) (-1,0.5)
5	$(x_{mi}, y_{mi})$	(1.44,2.04) (2.37,-0.81) (-1.44,-2.04) (-2.37,0.81)	(2.91,2.49) (3.90,2.67) (4.07,1.68) (2.10,1.33) (1.93,2.32)
6	$n$	4	5

Continued on the next page

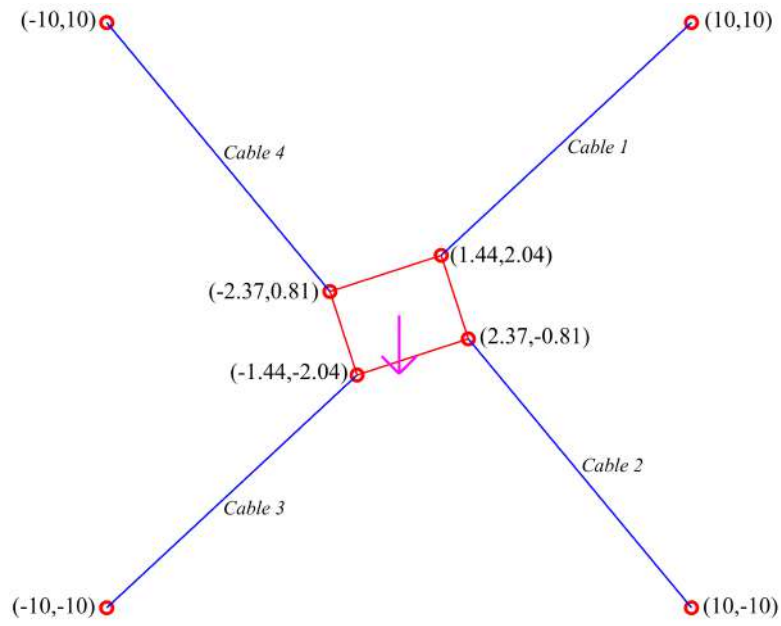
Table 3.2 – continued from the previous page

No.	Variables	Four-cable robot	Five-cable robot
7	$r$	3	3
8	$m$	1	2
9	$\mathbf{f}$	$\{0 \ -1 \ 0\}^T$	$\{0 \ -1 \ 0\}^T$
10	$\bar{\mathbf{t}}$	$\begin{Bmatrix} 0.32 \\ -0.37 \\ -0.32 \\ 0.37 \end{Bmatrix}$	$\begin{Bmatrix} 0.48 \\ 0.23 \\ 0.11 \\ -0.57 \\ 0.32 \end{Bmatrix}$
11	$\mathbf{N}$	$\begin{Bmatrix} -0.66 \\ 0.26 \\ -0.66 \\ 0.26 \end{Bmatrix}$	$\begin{Bmatrix} 0.02 & -0.73 \\ 0.78 & 0.16 \\ 0.44 & -0.12 \\ 0.44 & -0.22 \\ 0.06 & 0.62 \end{Bmatrix}$
12	$\mathbf{t}$	$\begin{Bmatrix} 0.32 \\ -0.37 \\ -0.32 \\ 0.37 \end{Bmatrix} + \begin{Bmatrix} -0.66 \\ 0.26 \\ -0.66 \\ 0.26 \end{Bmatrix} \alpha_1$	$\begin{Bmatrix} 0.48 \\ 0.23 \\ 0.11 \\ -0.57 \\ 0.32 \end{Bmatrix} + \begin{Bmatrix} 0.02 & -0.73 \\ 0.78 & 0.16 \\ 0.44 & -0.12 \\ 0.44 & -0.22 \\ 0.06 & 0.62 \end{Bmatrix} \begin{Bmatrix} \alpha_1 \\ \alpha_2 \end{Bmatrix}$
13	${}^n C_m$	${}^4 C_1 = 4$	${}^5 C_2 = 10$

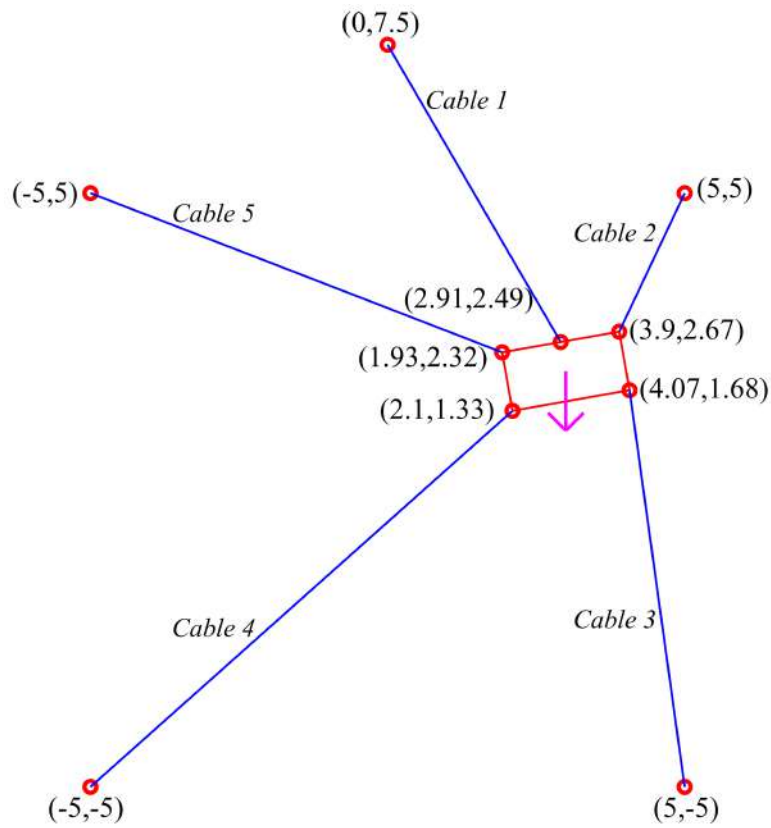
Continued on the next page

Table 3.2 – continued from the previous page

No.	Variables	Four-cable robot	Five-cable robot
14	$\bar{\alpha}_i$	$\bar{\alpha}_1 \leq 0.49$ $\bar{\alpha}_2 \geq 1.42$ $\bar{\alpha}_3 \leq -0.49$ $\bar{\alpha}_4 \geq -1.42$	$\bar{\alpha}_1 = \begin{Bmatrix} -0.43 \\ 0.65 \end{Bmatrix}$ $\bar{\alpha}_2 = \begin{Bmatrix} -0.09 \\ 0.65 \end{Bmatrix}$ $\bar{\alpha}_3 = \begin{Bmatrix} 1.62 \\ 0.69 \end{Bmatrix}$ $\bar{\alpha}_4 = \begin{Bmatrix} -10.41 \\ 0.44 \end{Bmatrix}$ $\bar{\alpha}_5 = \begin{Bmatrix} -0.28 \\ -0.08 \end{Bmatrix}$ $\bar{\alpha}_6 = \begin{Bmatrix} 0.17 \\ -2.28 \end{Bmatrix}$ $\bar{\alpha}_7 = \begin{Bmatrix} -0.19 \\ -0.49 \end{Bmatrix}$ $\bar{\alpha}_8 = \begin{Bmatrix} -2.06 \\ -6.85 \end{Bmatrix}$ $\bar{\alpha}_9 = \begin{Bmatrix} -0.38 \\ -0.48 \end{Bmatrix}$ $\bar{\alpha}_{10} = \begin{Bmatrix} 0.99 \\ -0.61 \end{Bmatrix}$



(a) Four-cable robot's configuration with infeasible cable forces



(b) Five-cable robot's configuration with feasible cable forces

Figure 3.2: Two different planar cable robots i.e., four and five-cable robots

## 3.2 Feasible orientations of the moving platform at a point

As noted in Chapter 1, at any  $(x, y)$  that belongs to the workspace, there might exist a range of feasible orientations. To obtain these orientations, we vary  $\phi$  from  $-180^\circ$  to  $180^\circ$  with an increment of  $1^\circ$ . For each angle, we obtain  $\mathbf{L}$  using Eq. 2.8 and tension vector as discussed in Section 2.2.4. Every feasible orientation should have non-negative cable forces. An example is presented next.

Cable robot parameters used for this example are provided in Table 3.3. Orientations that are feasible at  $(2, -1)$  in the workspace of the three-cable robot are shown as black sectors in Figs. 3.3 and 3.4. Their range varies from  $-179^\circ$  to  $-168^\circ$  and then from  $1^\circ$  to  $9^\circ$ . Non-negative cable forces of these feasible angles are shown in Fig. 3.5.

Table 3.3: Parameters of the three-cable robot

No.	$(x_{fi}, y_{fi})$	$(P_{i0x}, P_{i0y})$	$(x, y)$	$\mathbf{f}$
1	$(0, 5.77)$	$(0, 1.73)$	$(2, -1)$	$\left\{ \begin{array}{c} 0 \\ -1 \\ 0 \end{array} \right\}$
	$(5, -2.89)$	$(1.5, -0.87)$		
	$(-5, -2.89)$	$(-1.5, -0.87)$		

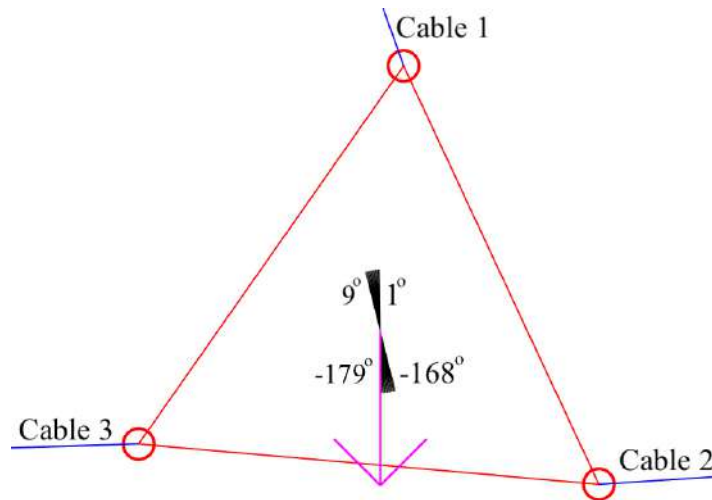


Figure 3.3: Black sectors represent feasible orientations of the platform at  $(2, -1)$

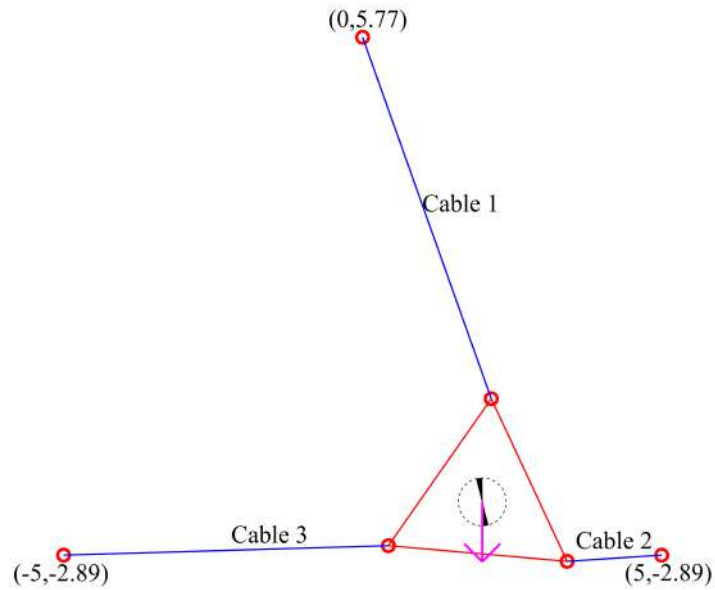


Figure 3.4: Feasible orientations of the platform of the planar three-cable robot at  $(2,-1)$

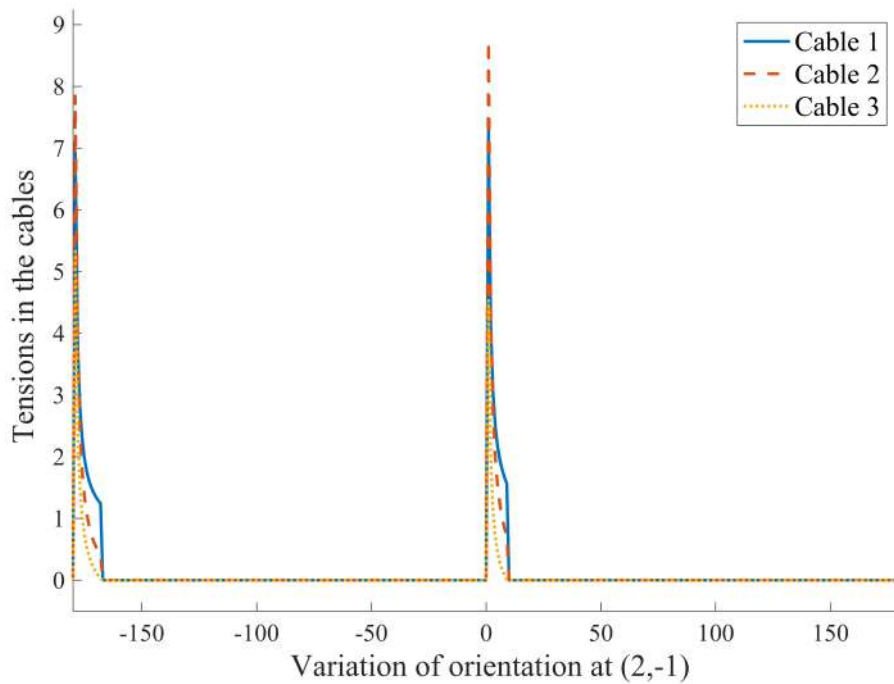


Figure 3.5: Non-negative cable forces for the feasible orientations. Cable forces for non-feasible orientations are shown with the values of zero.

Instead of obtaining and checking the tension vector at each increment, the determinant approach presented in Section 2.2.5 can also be implemented for checking the feasibility of the orientation of the platform. This will reduce the computation time.

### 3.3 Feasible orientations of the platform at multiple points

A grid is defined with uniform step size along both  $x$  and  $y$  axes. It is confined to the rectangular region formed by  $(x_l, y_l)$ ,  $(x_l, y_u)$ ,  $(x_u, y_l)$ , and  $(x_u, y_u)$ , where  $x_l$ ,  $x_u$ ,  $y_l$ , and  $y_u$  represent lower and upper limits of  $x$  and  $y$  values. At every point in the grid, the procedure discussed in Section 3.2 is carried out to obtain feasible orientations. These orientations are shown as black sectors at each grid point. An example of a three-cable robot is considered here to present feasible orientations for different load vectors. Parameters used for this example are given in Table 3.4. Fig. 3.6 depicts feasible orientations of the three-cable robot considered for this example at  $(4, 3)$ .

Table 3.4: Parameters of the three-cable robot

No.	$(x_{fi}, y_{fi})$	$(P_{i0x}, P_{i0y})$	$x_l$	$x_u$	$y_l$	$y_u$	Step size
1	$(4, 2)$	$(0.8, 0.4)$					
	$(0, -4)$	$(0, -0.8)$	-8	8	-8	6	1
	$(-4, 2)$	$(-0.8, 0.4)$					

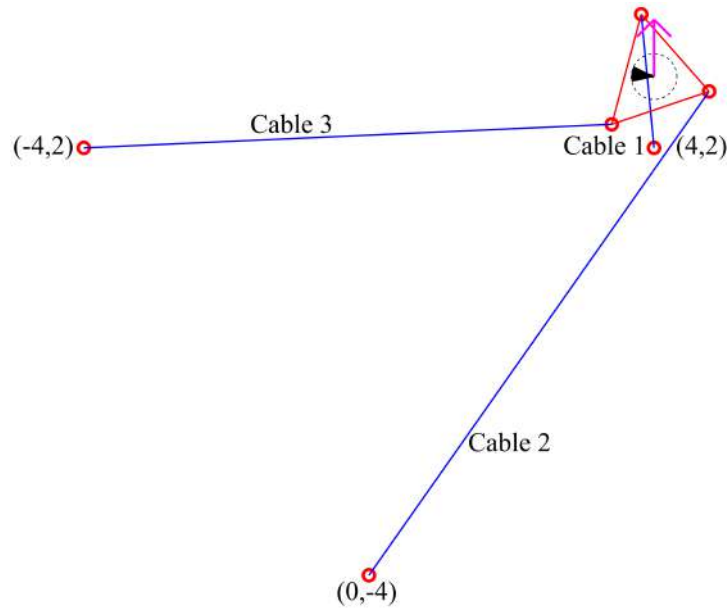
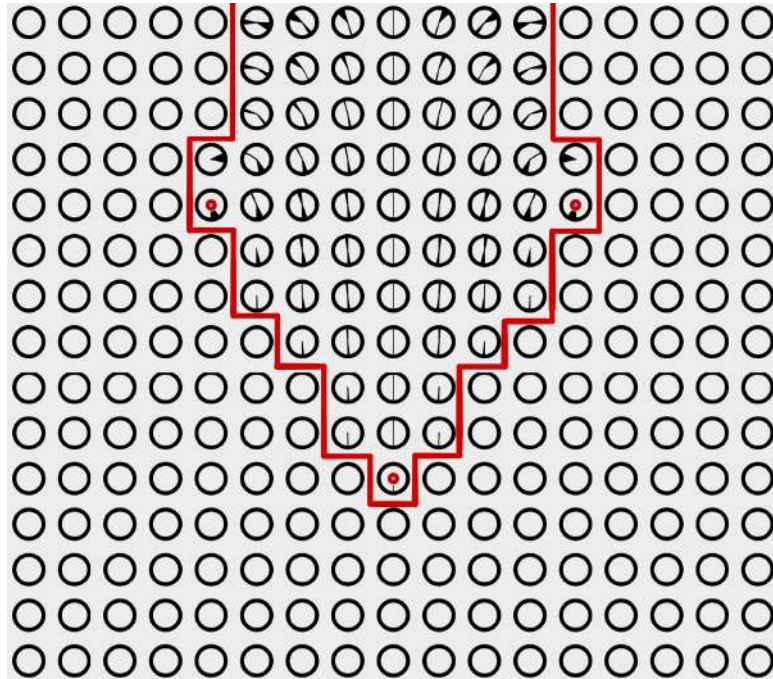
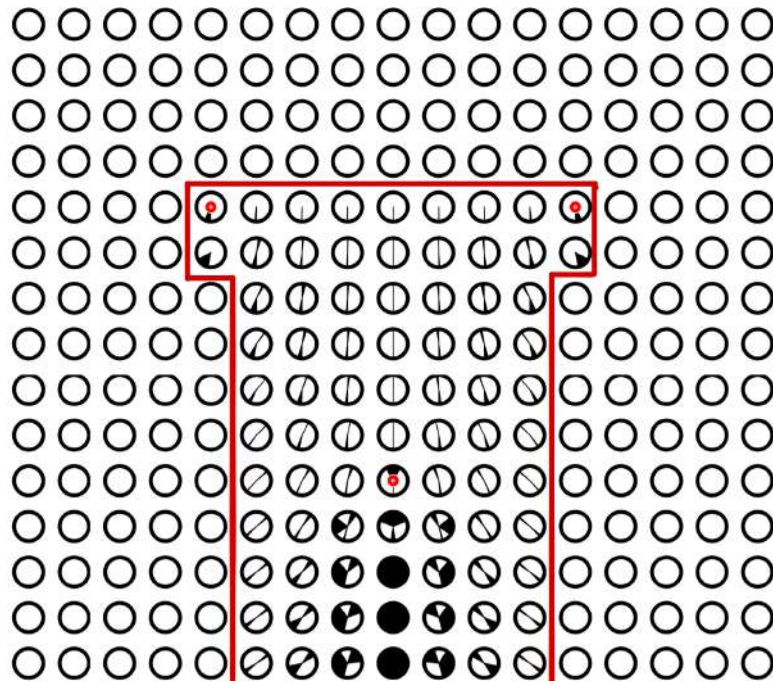


Figure 3.6: Platform is in static equilibrium at  $(4, 3)$  for the load vector  $\{0 \ 1 \ 0\}^T$ . Orientation of the platform is  $75^\circ$ . Range of the feasible orientations is from  $64^\circ$  to  $102^\circ$ .

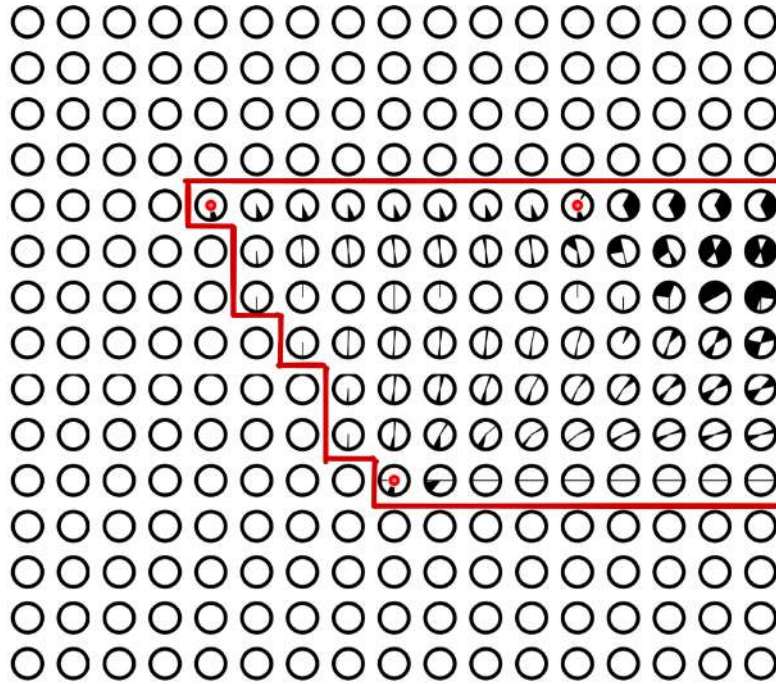


(a) Feasible orientations for  $\{0 \ 1 \ 0\}^T$

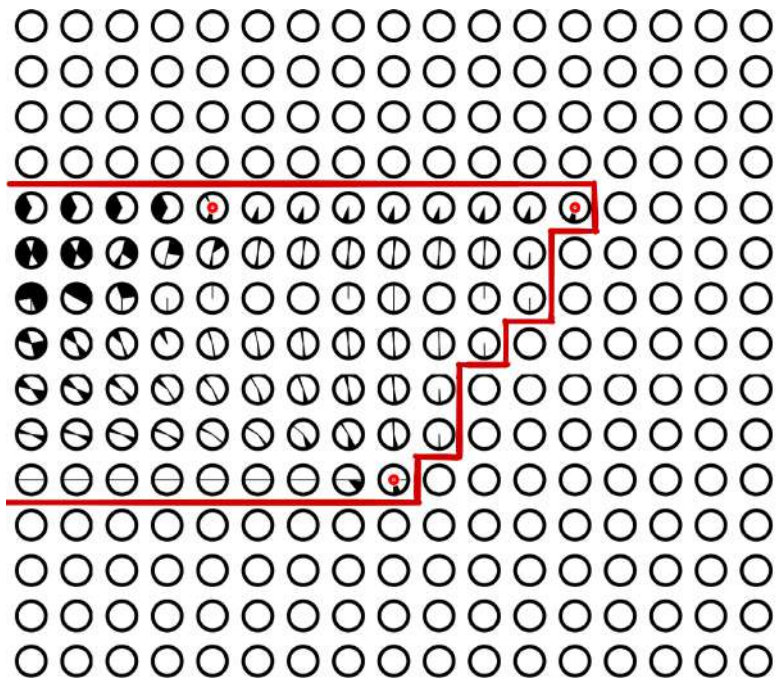


(b) Feasible orientations for  $\{0 \ -1 \ 0\}^T$

Figure 3.7: Feasible orientations of the triangular platform for two different load vectors (i.e., along the  $y$ -axis) with same magnitude but in opposite directions. Tiny red circles indicate the fixed pivots of the three-cable robot. The boundary of the workspace is indicated with a red curve.

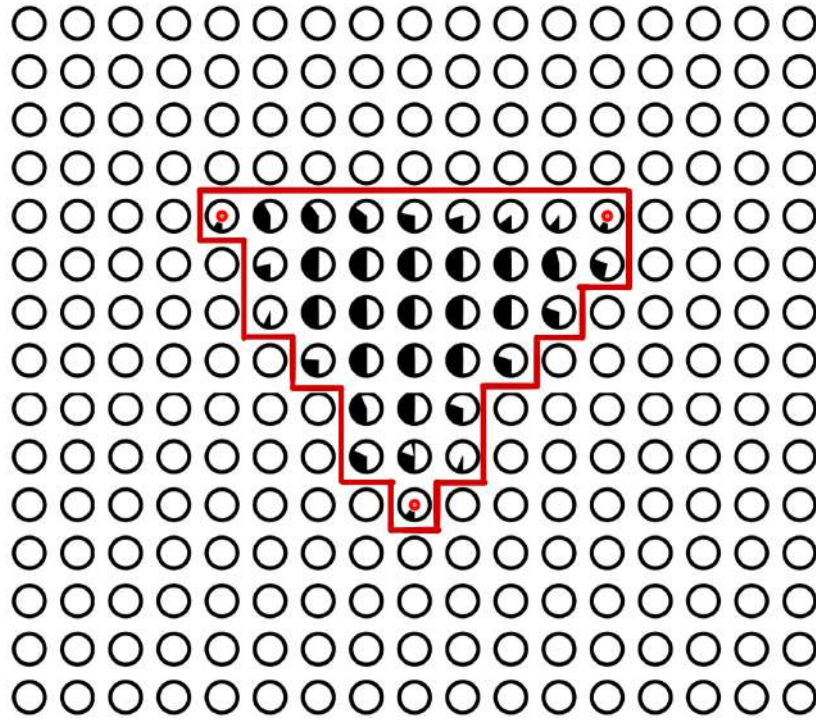


(a) Feasible orientations for  $\{1\ 0\ 0\}^T$

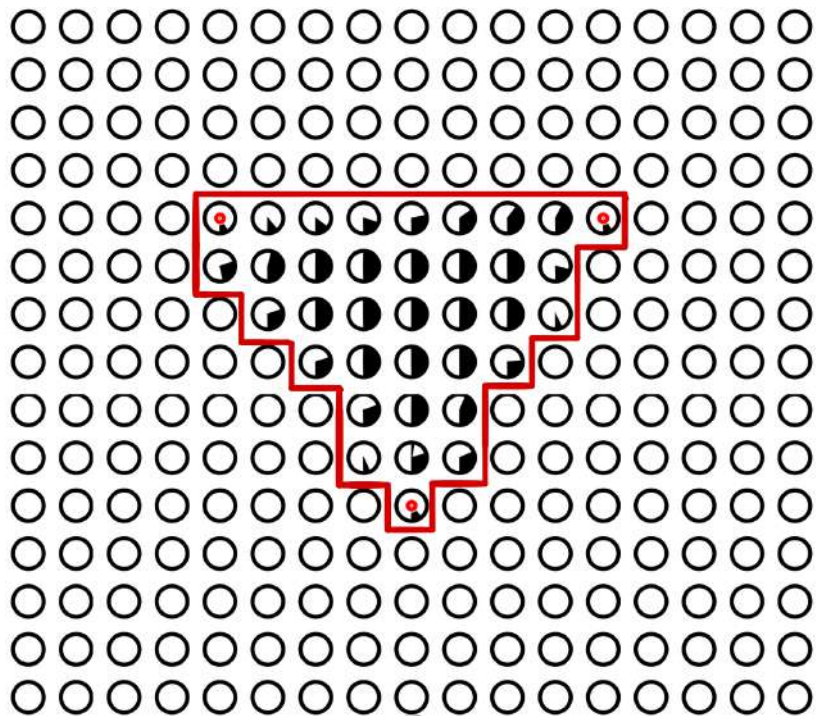


(b) Feasible orientations for  $\{-1\ 0\ 0\}^T$

Figure 3.8: Feasible orientations of the triangular platform for two different load vectors (i.e., along the  $x$ -axis) with same magnitude but in opposite directions. The boundary of the workspace is indicated with a red curve.



(a) Feasible orientations for  $\{0\ 0\ 1\}^T$



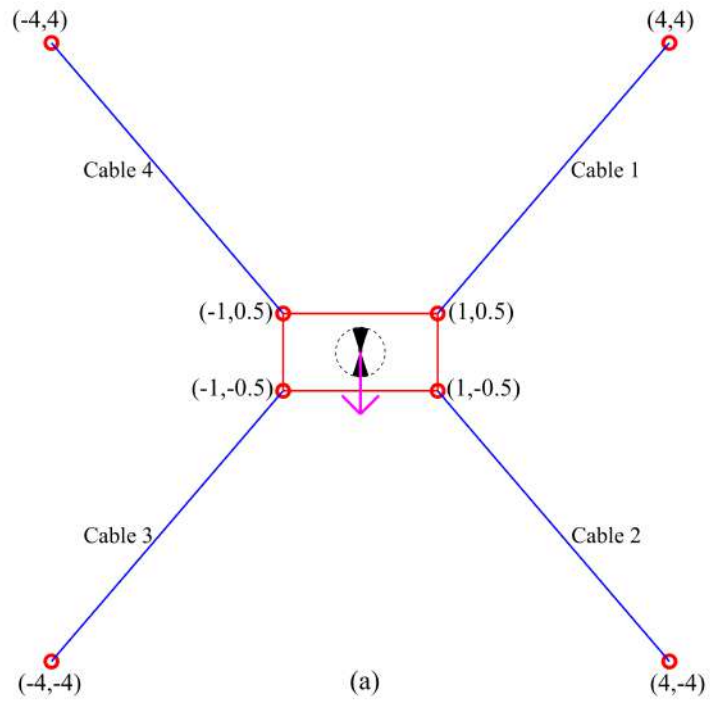
(b) Feasible orientations for  $\{0\ 0\ -1\}^T$

Figure 3.9: Feasible orientations of the triangular platform for two different load vectors (i.e., about the  $z$ -axis) with same magnitude but in opposite directions. The boundary of the workspace is indicated with a red curve.

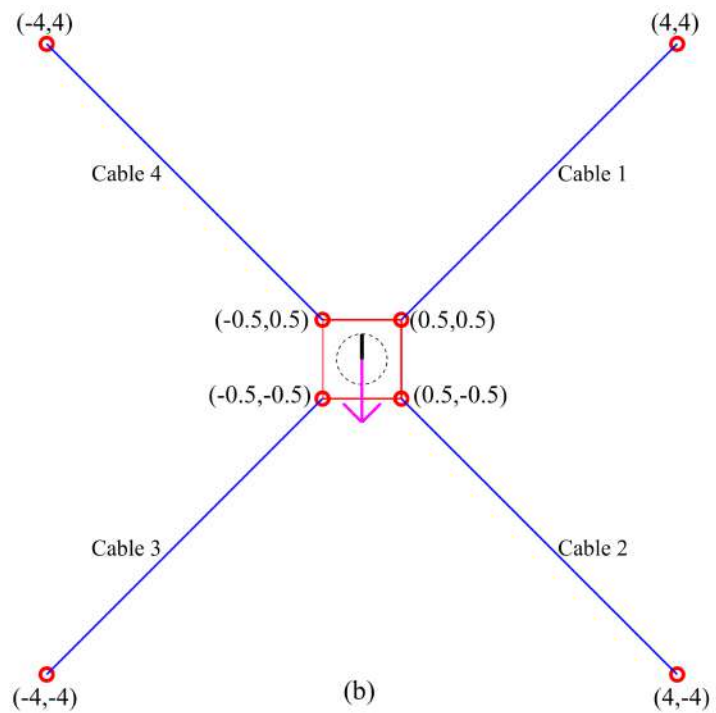
Empty circles in the preceding (i.e., Figs. 3.7a–3.9b) and subsequent figures indicate that no orientation is feasible and thus the platform cannot be in static equilibrium for any orientation at that point. Hence, that point does not belong to the workspace. In Fig. 3.7a, feasible orientations are more towards the top than the bottom portion of the grid. This is because cables 1 and 3 start supporting the orientability of the platform in addition to cable 2, for the load vector  $\{0 \ 1 \ 0\}^T$ , as it approaches the top portion of the grid. In Fig. 3.7b, feasible orientations are more in the bottom portion as compared to the top portion of the grid because of the nature of the load acting on the robot. In it, cables 1 and 3 i.e., two cables support the orientability of the platform in the convex hull of the fixed pivots, but for the case of Fig. 3.7a, there is only one cable i.e., cable 2. In Fig. 3.7b, the platform will be hanging with the aid of three cables beyond the second fixed pivot. Hence, the orientability of the platform suddenly increases beyond the second fixed pivot.

Feasible angles of the platform shown in Figs. 3.8a and 3.8b are exactly the mirror images of each other; this is due to the reversal of the sign of the  $x$ -force. The same pattern can also be observed in Figs. 3.9a and 3.9b. It can be inferred from Figs. 3.7a – 3.8b that feasible orientations always lie in the direction of the net external load acting on the platform. As compared to the other four cases, feasible angles in Figs. 3.9a and 3.9b are confined within the convex hull of the fixed pivots because of the moment load that is acting on the platform. From these two figures, it can be inferred that the orientability of the platform increases within the convex hull of the fixed pivots when a moment load is acting at the centroid of the platform. From the points discussed above, we can conclude that the nature of the load acting on the platform will strongly influence the feasible orientations of the platform.

An additional example of a four-cable robot (i.e., cable robot with actuation redundancy) is considered here for two different platforms (rectangle and square). Parameters used for this example are given in Table 3.5. Fig. 3.10 depicts feasible orientations of the four-cable robot at  $(0, 0)$ . In Fig. 3.10a, for the rectangular platform, feasible angles are  $-180^\circ$  to  $-162^\circ$ ,  $-18^\circ$  to  $18^\circ$ , and  $162^\circ$  to  $180^\circ$  and for the square platform, in Fig. 3.10b, only three angles are feasible and they are  $-180^\circ$ ,  $0^\circ$ , and  $180^\circ$ . Orientability of the square platform is limited as compared to that of the rectangular platform. This is because of the geometric similarity between the vertices on the square platform and the fixed pivots of the cable robot.



(a) Rectangular platform with  $0^\circ$  orientation



(b) Square platform with  $0^\circ$  orientation

Figure 3.10: Feasible orientations of two different platforms for the same fixed pivots of the four-cable robot

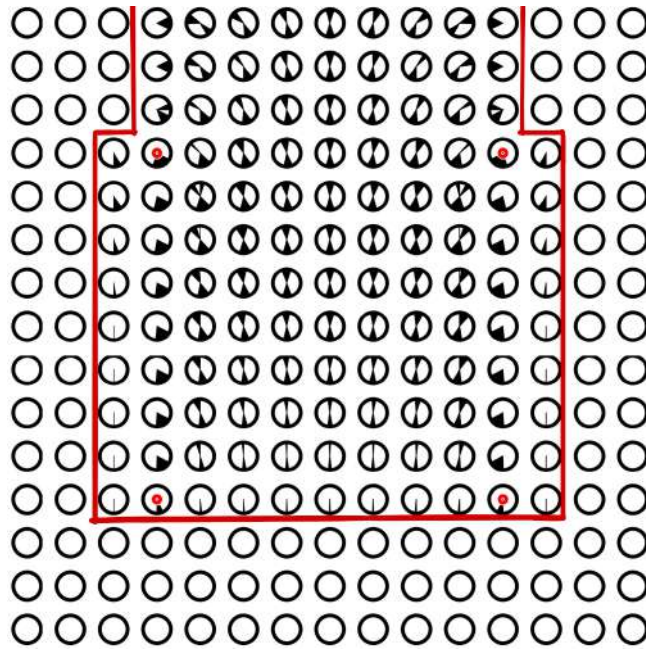
Table 3.5: Parameters of the four-cable robot. Columns 3 and 4 indicate the initial vertices of the rectangular and square platforms respectively.

No.	$(x_{fi}, y_{fi})$	$(P_{i0x}, P_{i0y})$	$(P_{i0x}, P_{i0y})$	$x_l$	$x_u$	$y_l$	$y_u$	Step size
1	(4, 4)	(1, 0.5)	(0.5, 0.5)	-7	7	-7	7	1
	(4, -4)	(1, -0.5)	(0.5, -0.5)					
	(-4, -4)	(-1, -0.5)	(-0.5, -0.5)					
	(-4, 4)	(-1, 0.5)	(-0.5, 0.5)					

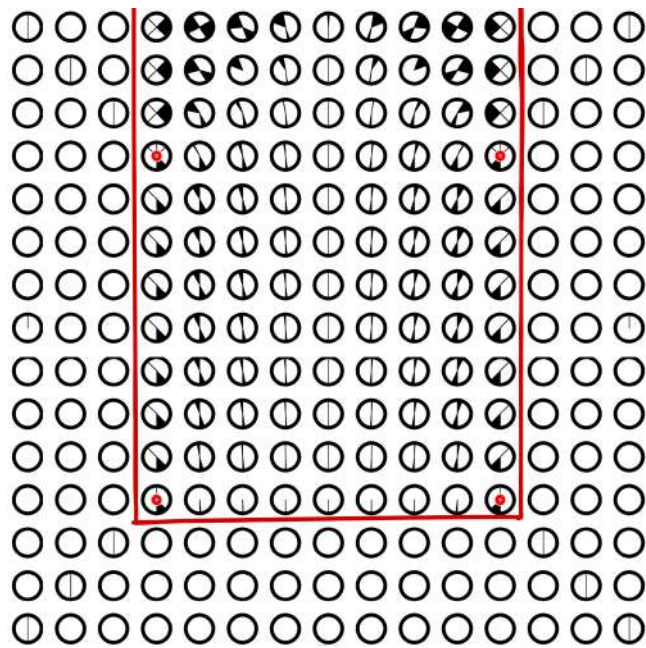
Feasible orientations of the four-cable robot follow the same pattern as observed in the case of the three-cable robot with some differences. In the case of the three-cable robot, feasible orientations were confined within the convex hull of the fixed pivots when a moment load was acting at the centroid of the platform, but for the case of the four-cable robot, this pattern is not followed. Feasible orientations can be observed in the region outside of the convex hull. Furthermore, the orientability of the platform has increased in the case of the four-cable robot as compared to that of the three-cable robot for the same load vector acting at the centroid of the platform. From Figs. 3.11a – 3.13b, it can be observed that feasible orientations of the square platform throughout the grid are limited as compared to those that correspond to the rectangular platform. This behaviour of the feasible orientations can be attributed to the geometric similarity between the vertices on the square platform and the fixed pivots of the cable robot. From the points discussed above, it can be concluded that as the number of cables increase, the orientability of the platform increases. And when there is a geometric similarity between the platform vertices and the fixed pivots of the cable robot, the orientability of the platform gets restricted i.e., the shape of the platform vertices plays an important role in the behaviour of the feasible orientations. An additional point to be noted is that the increase in the number of cables increases the orientability (i.e., only until certain extent), but it does not require complex control strategies. Research groups working in the area of cable robots have worked on cable robots consisting of six to ten cables with simple control strategies. One such group is Charlotte et al. [14].

Now, for the same fixed pivots of the four-cable robot, size (i.e., length and breadth) of the platforms (i.e., rectangular and square platforms) is doubled and the results obtained are presented in Figs. 3.14a – 3.16b. It can be observed that orientability of the platform has got

increased slightly as the size of the platform is doubled for both the cases.



(a) Rectangular platform

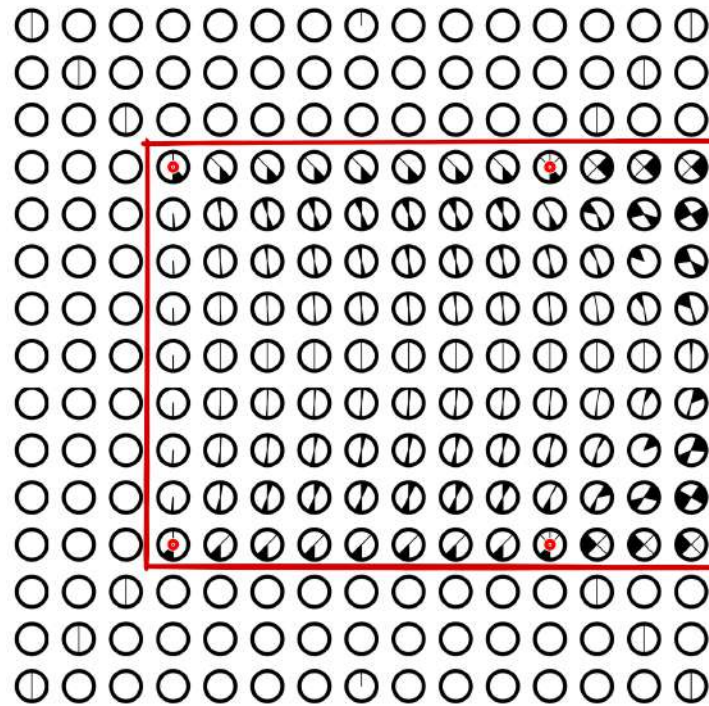


(b) Square platform

Figure 3.11: Feasible orientations of two different platforms for the same fixed pivots of the four-cable robot for the load vector  $\{0 \ 1 \ 0\}^T$

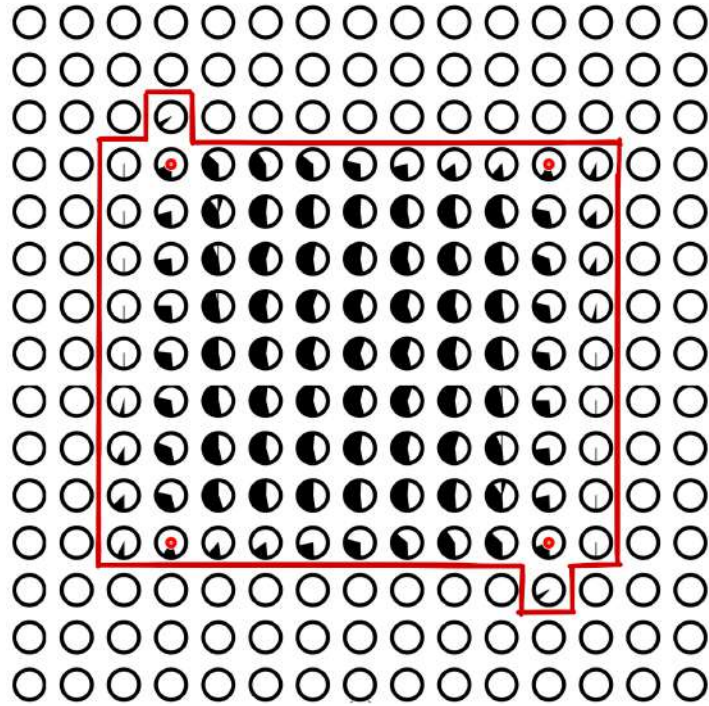


(a) Rectangular platform

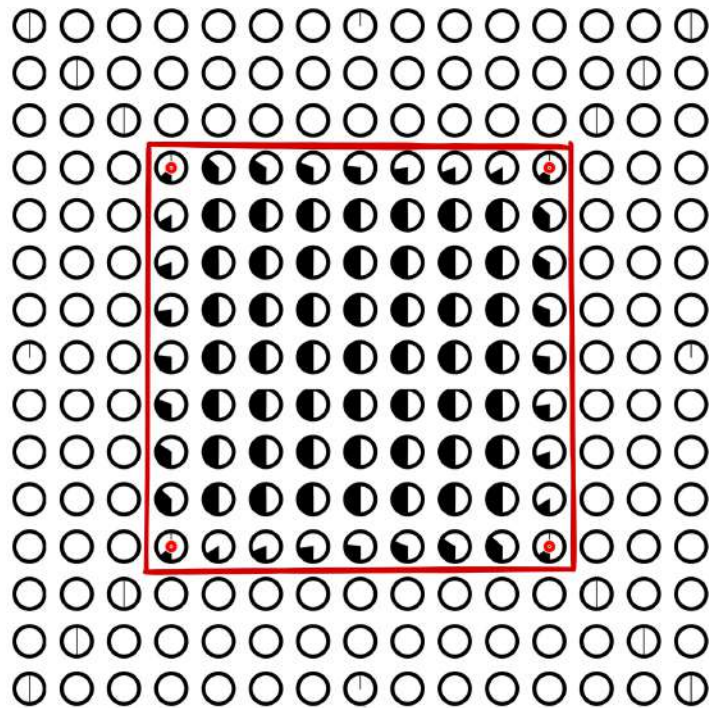


(b) Square platform

Figure 3.12: Feasible orientations of two different platforms for the same fixed pivots of the four-cable robot for the load vector  $\{1\ 0\ 0\}^T$

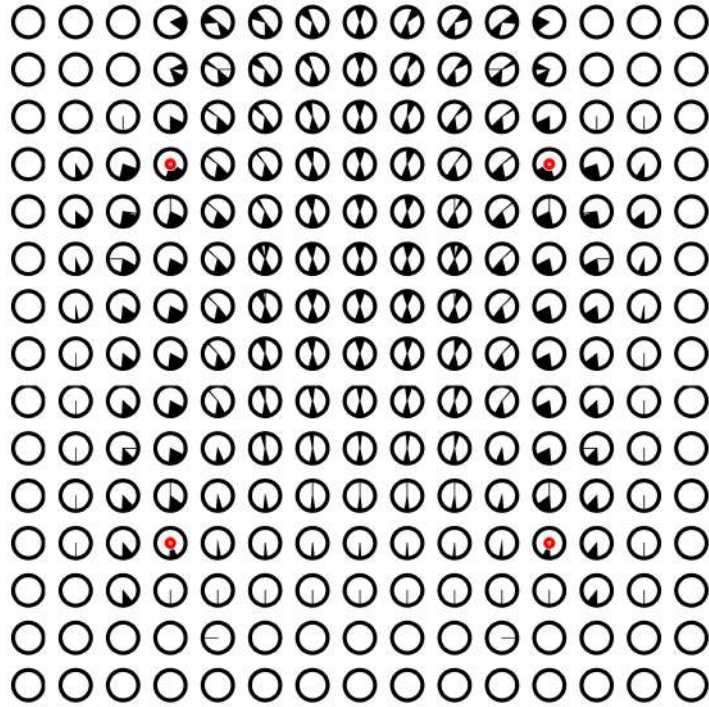


(a) Rectangular platform

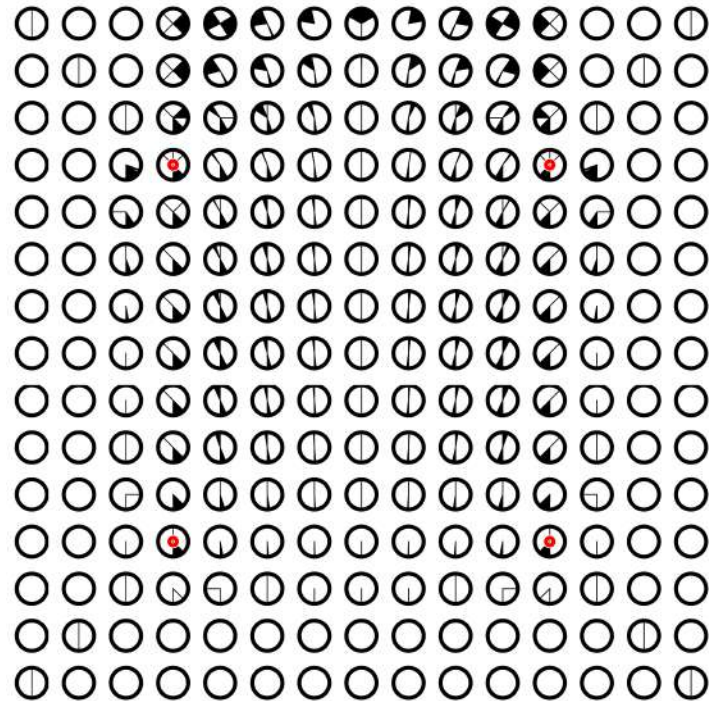


(b) Square platform

Figure 3.13: Feasible orientations of two different platforms for the same fixed pivots of the four-cable robot for the load vector  $\{0 \ 0 \ 1\}^T$

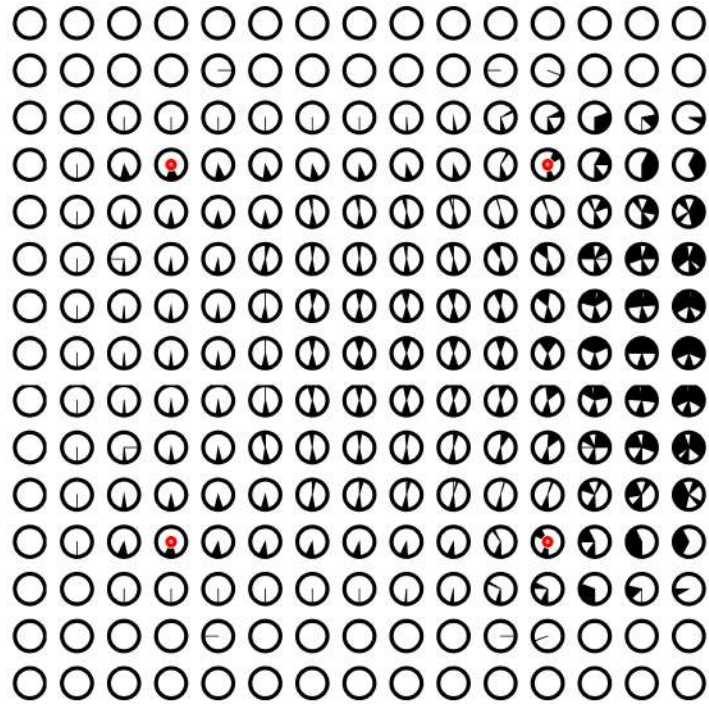


(a) Double-sized rectangular platform

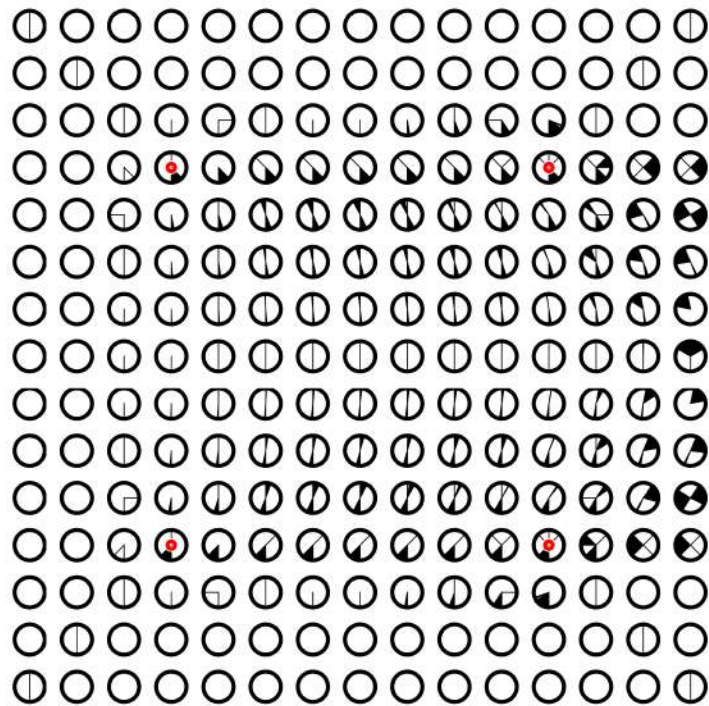


(b) Double-sized square platform

Figure 3.14: Feasible orientations of two different platforms for the same fixed pivots of the four-cable robot for the load vector  $\{0 \ 1 \ 0\}^T$

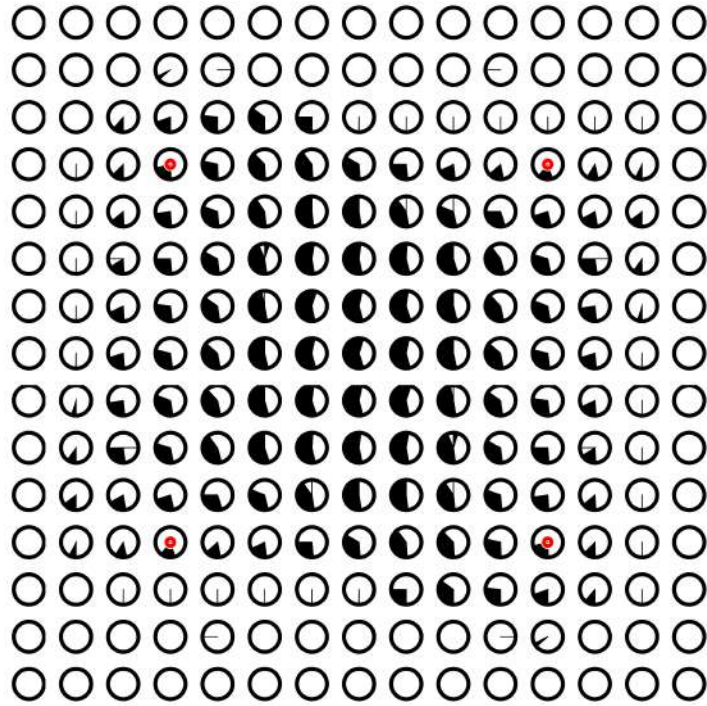


(a) Double-sized rectangular platform

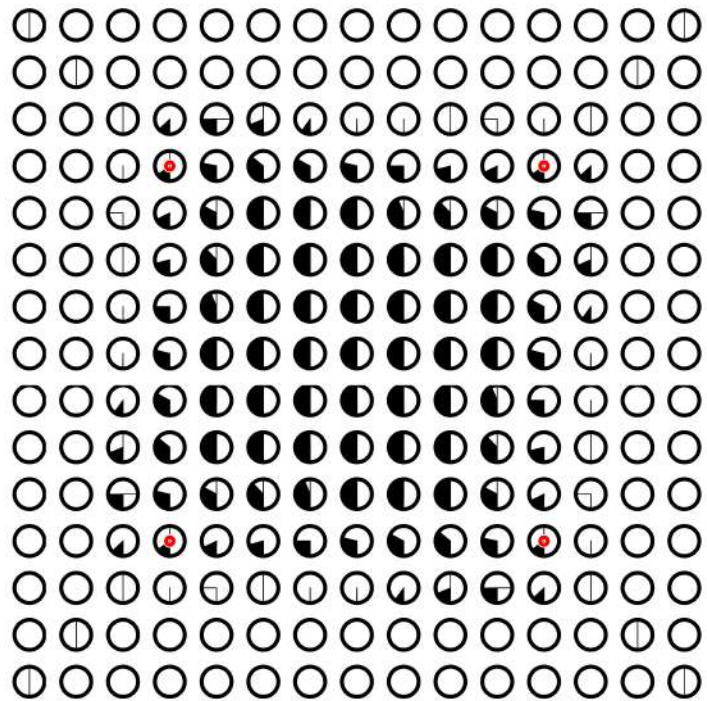


(b) Double-sized square platform

Figure 3.15: Feasible orientations of two different platforms for the same fixed pivots of the four-cable robot for the load vector  $\{1\ 0\ 0\}^T$



(a) Double-sized rectangular platform



(b) Double-sized square platform

Figure 3.16: Feasible orientations of two different platforms for the same fixed pivots of the four-cable robot for the load vector  $\{0 \ 0 \ 1\}^T$

## 3.4 Feasible orientations that fully constrain the moving platform

### 3.4.1 Fully constrained configuration

For any given position and orientation of the robot in the workspace, there is a corresponding set of cable lengths. A robot configuration is said to be fully constrained when its position and orientation cannot be changed without changing the cable lengths and if each motion of the robot requires at least one cable length to become longer and any other cable length to become shorter [93]. The under-constrained configuration is the configuration that is not fully constrained. In an under-constrained configuration, there are motions of the robot that can cause the cables to become slack. A cable robot in a pendulum-like configuration, NIST ROBOCRANE for example, is under-constrained not only because it can swing back and forth but also because the cables can become slack when the robot is lifted by an external force [93].  $\mathbf{L}$  matrix of a fully constrained configuration robot has full rank and has the property that every nonzero vector in its row space has both positive and negative components. This is taken as the local definition of a kinematically fully constrained configuration. A non-negative or a non-positive vector with some zero components can still correspond to a constrained robot and in this case, one would need to check second-order or higher-order derivatives [93]. A non-singular configuration is kinematically fully constrained if and only if there exists a nullspace or kernel matrix of  $\mathbf{L}$  with the property that the elements of linear combinations of the column vectors are strictly positive.

$$\mathbf{N}\boldsymbol{\alpha} \succ \mathbf{0} \tag{3.1}$$

where  $\mathbf{N}$  is  $n \times m$  nullspace or kernel matrix of  $\mathbf{L}$ , and  $\boldsymbol{\alpha}$  is a  $m \times 1$  underdetermined vector. As Eq. 3.1 contains strictly positive elements, tension vector  $\mathbf{t}$  with non-negative elements can always be obtained for a fully constrained configuration. Thus, any configuration that is fully constrained can always be held in static equilibrium but vice versa cannot be guaranteed. Statics problem is in some sense a generalization of the fully constrained problem. Two problems are nearly the same when gravity is absent. Gravity acts as an additional actuator and thus the range of orientations that can be held in static equilibrium at a position  $(x, y)$  is necessarily a superset of the orientations for which the robot is fully constrained for the same position.

For example, consider a four-cable robot with relevant information provided in Table 3.6.  $\mathbf{N}$  is a  $4 \times 1$  column vector for a four-cable robot with full rank  $\mathbf{L}$ . At  $(0,0)$ , when the orientation of the platform is  $0^\circ$ , elements of  $\mathbf{N}$  are  $\{0.5 \ 0.5 \ 0.5 \ 0.5\}^T$  and when the orientation is  $12^\circ$ ,  $\mathbf{N}$  is  $\{0.70 \ 0.08 \ 0.70 \ 0.08\}^T$ . Thus, the platform is fully constrained for both the cases as the elements of  $\mathbf{N}$  are strictly positive, but when the orientation of the platform is  $18^\circ$ ,  $\mathbf{N}$  is  $\{0.70 \ -0.07 \ 0.70 \ -0.07\}^T$ . Here, it can be observed that the elements of the nullspace are neither negative nor positive. Hence, the platform is not fully constrained at  $(0,0)$  for  $\phi = 18^\circ$ .

It is an easy procedure to decide whether an orientation of the platform fully constrains the robot or not in the case of a four-cable robot whose  $\mathbf{L}$  has full rank. But for the cases where  $n > 4$  and the four-cable robot with rank deficient  $\mathbf{L}$ , we must use the determinant approach discussed in Section 2.2.5 with two modifications to obtain feasible orientations that fully constrain the robot at a given point. The first modification is that the values of the determinants must be either negative or positive rather than non-negative or non-positive. The second modification is that the nullspace of  $\mathbf{L}$  should be used instead of that of  $\mathbf{L}_{\text{aug}}$  for the determinant approach. This procedure is used to obtain the feasible orientations throughout the workspace that fully constrain the cable robot in the next section.

Table 3.6: Parameters of the four-cable robot

No.	$(x_{fi}, y_{fi})$	$(P_{i0x}, P_{i0y})$	$(x, y)$	$\mathbf{f}$
1	(10, 10)	(1.73, 1)	(0,0)	$\left\{ \begin{array}{c} 0 \\ -1 \\ 0 \end{array} \right\}$
	(10, -10)	(1.73, -1)		
	(-10, -10)	(-1.73, -1)		
	(-10, 10)	(-1.73, 1)		

### 3.4.2 Feasible orientations that fully constrain the moving platform at multiple points

Eq. 3.1 indicates that the feasible orientations that fully constrain the cable robot are independent of the load acting on the platform. To obtain these feasible orientations, a grid is created as discussed in Section 3.3 and at every point in it,  $\phi$  is varied from  $-180^\circ$  to  $180^\circ$  with an increment of  $1^\circ$ . At every increment,  $\mathbf{N}$  is obtained with the aid of  $\mathbf{L}$ . The determinant approach

is carried out to check whether the orientation considered is feasible or not. To illustrate this, we once again consider the example of the four-cable robot presented in Section 3.3. Figs. 3.17 and 3.18 present feasible orientations for both the rectangle and square platforms, respectively. It is observed that orientations of the square platform are limited as compared to those of the rectangular platform for the same fixed pivots (arranged in square shape) of the four-cable robot. As noted in Section 3.3, we recall that the orientability of the square platform is limited as compared to that of the rectangular platform for the same fixed pivots of the cable robot. An important point to be noted here is that the orientability of the platform gets highly restricted when vertices of the platform and fixed pivots of the cable robot are arranged in a geometrically similar shape. It can also be observed that feasible orientations that fully constrain the robot belong to a subset of the feasible orientations that allow the platform to be in static equilibrium for the same configuration of the cable robot. Furthermore, feasible orientations are confined within the convex hull of the fixed pivots. It is observed for this example that the change in the size of the square platform does not affect feasible orientations that fully constrain it, but the change in the size of the rectangular platform affects the feasible orientations.

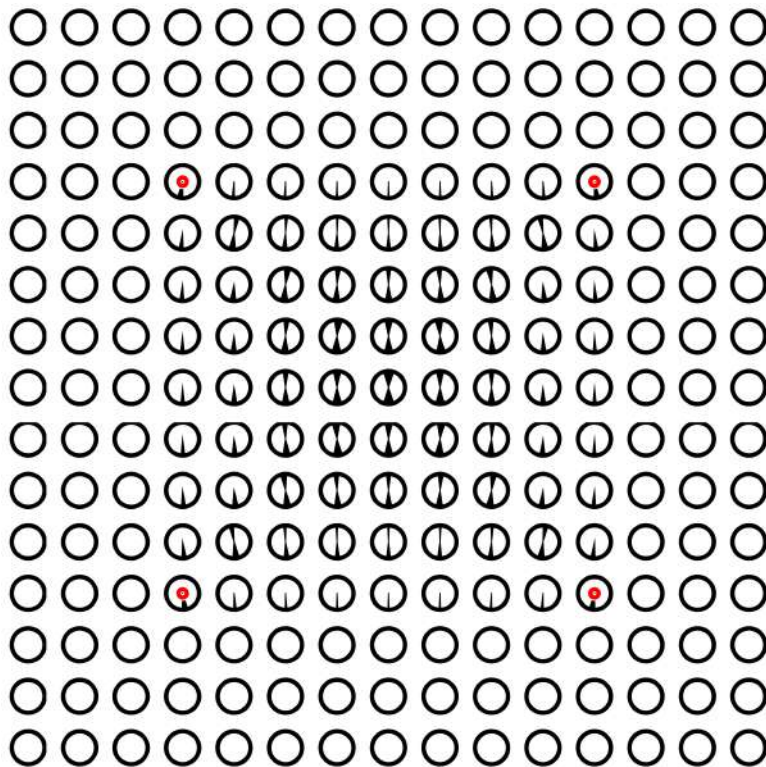


Figure 3.17: Feasible orientations that fully constrain the rectangular platform

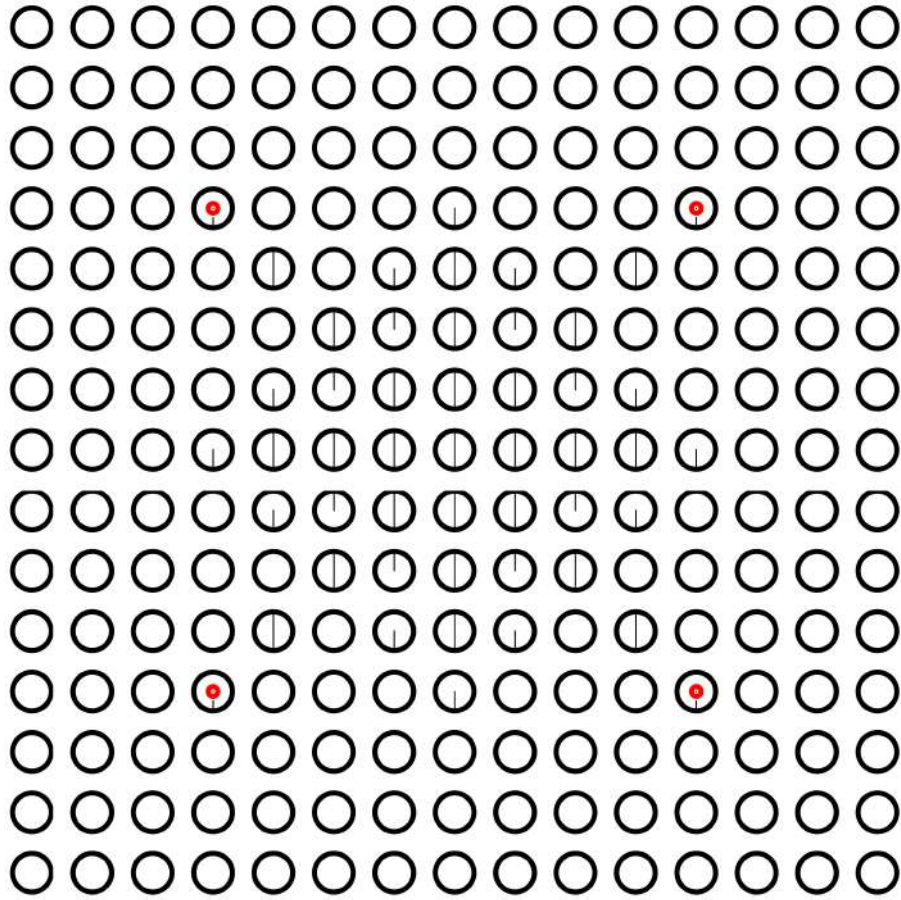


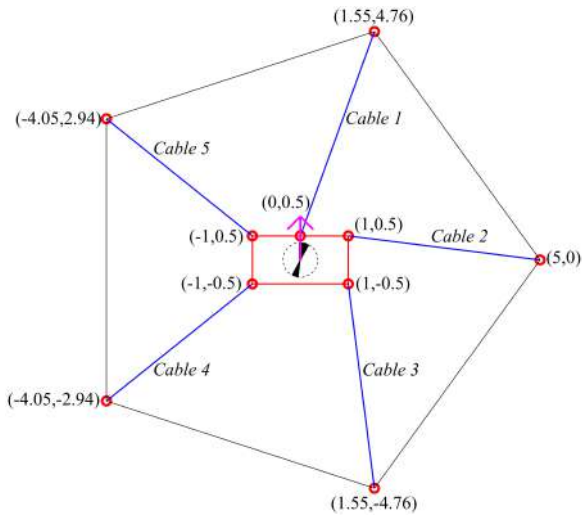
Figure 3.18: Feasible orientations that fully constrain the square platform

An additional example of a five-cable robot is considered here for the two different platforms (i.e., a rectangle and a pentagon). Parameters used for this example are given in Table 3.7. Fig. 3.19 depicts feasible orientations that fully constrain the five-cable robot at  $(0, 0)$ . In Fig. 3.19a, for a rectangular platform, feasible angles vary from  $-30^\circ$  to  $-6^\circ$  and then from  $151^\circ$  to  $173^\circ$  and for the pentagonal platform, shown in Fig. 3.19b, only three angles are feasible and they are  $-180^\circ$ ,  $0^\circ$ , and  $180^\circ$ . Note that  $0^\circ$  orientation of the rectangular platform shown in Fig. 3.19a does not fully constrain the five-cable robot.

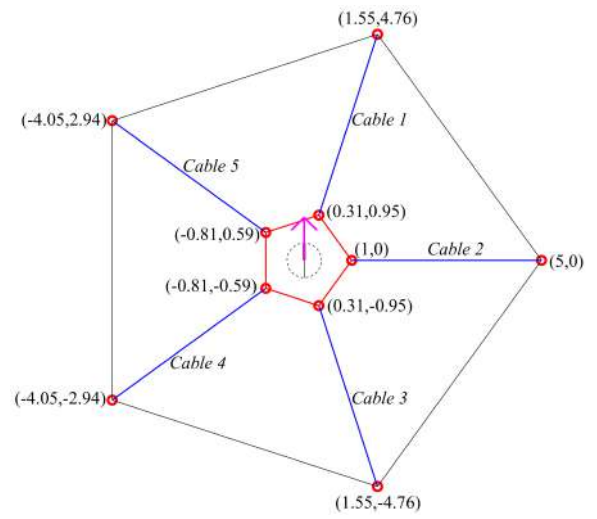
From Figs. 3.20a and 3.20b, it can be concluded that feasible orientations of the pentagonal platform are more restricted as compared to those of the rectangular platform for the same fixed pivots (arranged in a pentagon shape) of the five-cable robot. Also, the orientability of the platform got enhanced in the case of a five-cable robot as compared to that of the four-cable robot.

Table 3.7: Parameters of the five-cable robot

No.	$(x_{fi}, y_{fi})$	Rectangular	Pentagonal	$x_l$	$x_u$	$y_l$	$y_u$	Step size
		platform $(P_{i0x}, P_{i0y})$	platform $(P_{i0x}, P_{i0y})$					
1	(5, 0)	(1, 0.5)	(1, 0)	-8	9	-7	9	1
	(1.55, 4.76)	(0, 0.5)	(0.31, 0.95)					
	(-4.05, 2.94)	(-1, 0.5)	(-0.81, 0.59)					
	(-4.05, -2.94)	(-1, -0.5)	(-0.81, -0.59)					
	(1.55, -4.76)	(1, -0.5)	(0.31, -0.95)					

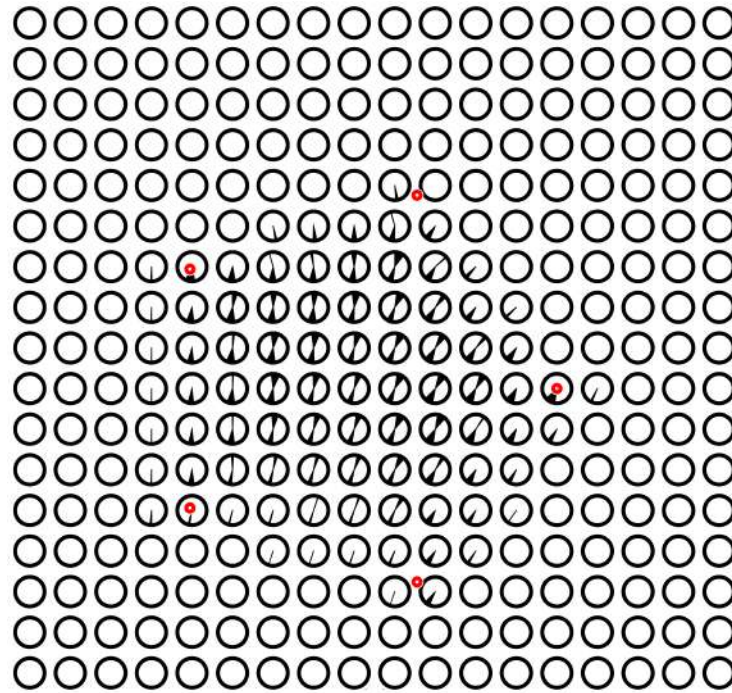


(a) Feasible orientations of the rectangular platform

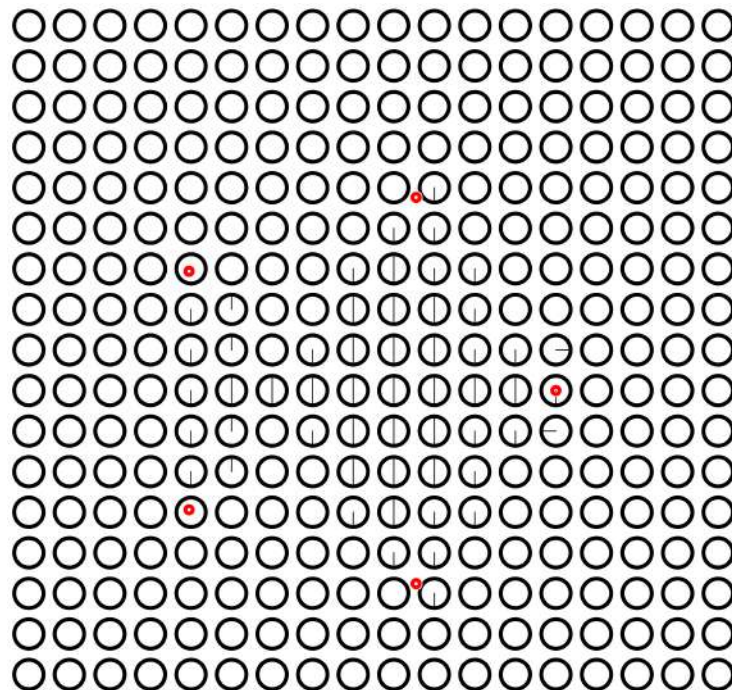


(b) Feasible orientations of the pentagonal platform

Figure 3.19: Feasible orientations of two different platforms at  $(0,0)$  for the same fixed pivots of the five-cable robot for the load vector  $\{0 \ 1 \ 0\}^T$



(a) Rectangular platform



(b) Pentagonal platform

Figure 3.20: Feasible orientations that fully constrain the two different platforms for the same fixed pivots of the five-cable robot

## 3.5 Platform tracing a prescribed trajectory

In this section, a path comprising a finite number of waypoints is given to the moving platform of the cable robot. We discuss two ways of tracing the trajectory. The first case deals with obtaining an optimal orientation of the platform at every waypoint to achieve maximum or minimum tensions in the cables at that point. This procedure is described in Section 3.5.1. In the next case, we specify the desired orientation for the platform at every waypoint, which is elaborated in Section 3.5.2.

### 3.5.1 Trajectory tracing with an optimal orientation at every waypoint

At every waypoint, feasible orientations are obtained according to the procedure discussed in Section 3.2. At every waypoint, corresponding to every feasible orientation, there will be multiple tension values depending on the value of  $\alpha$ . For every feasible orientation at a waypoint, the criterion for the selection of  $\alpha$  depends on the maximum or minimum tensions (i.e., maximum or minimum of  $\|\mathbf{t}\|$ ). Note that there is an exception, which is the case of a three-cable robot whose  $\mathbf{L}$  has rank three. It will always have a unique solution given by Eq. 2.27. The criterion for the selection of the most favorable orientation (i.e., the optimal orientation) at a point depends again on the maximum or minimum tensions among the set of maximum or minimum tensions corresponding to every orientation. Therefore, we are selecting the maximum from the set of maximum tensions or the minimum from the set of minimum tensions of the cables. From this procedure, we obtain the optimal  $\phi$  and the optimal  $\alpha$  corresponding to it. Thus, we have minimum or maximum possible tensions at every waypoint.

A point to be noted is that in search of the optimal orientation, the algorithm selects an orientation which is nearly  $180^\circ$  apart from the optimal orientation corresponding to the previous waypoint. This results in the sudden flipping of the platform between two consecutive waypoints. To avoid this, we search for feasible orientations within the range of  $-90^\circ$  to  $90^\circ$  instead of  $-180^\circ$  to  $180^\circ$  as done in Section 3.2.

To illustrate the preceding procedure, an example of a five-cable robot tracing a horizontal path is presented here. Parameters used for this example are given in Table 3.8. The path is made of 20 equidistant points w.r.t. each other between the points  $(-2, 2)$  and  $(2, 2)$  inclusive. For this example, we consider the minimum  $\|\mathbf{t}\|$  as the criteria for obtaining optimal orientations. Fig. 3.21 shows the simulated task at the ending point  $(2, 2)$ . In the figure, the path is

shown as a series of red points. Black arrows indicate the direction of the tensions in the cables and their size varies according to the magnitude of the tensions in the cables. The tension value with magnitude greater than 0.1 is shown next to its respective cable.

Table 3.8: Parameters of the five-cable robot

No.	$(x_{fi}, y_{fi})$	$(P_{i0x}, P_{i0y})$	$\mathbf{f}$
1	(0, 7.5)	(0, 0.5)	$\begin{Bmatrix} 1 \\ 0 \\ 0 \end{Bmatrix}$
	(5, 5)	(1, 0.5)	
	(5, -5)	(1, -0.5)	
	(-5, -5)	(-1, -0.5)	
	(-5, 5)	(-1, 0.5)	

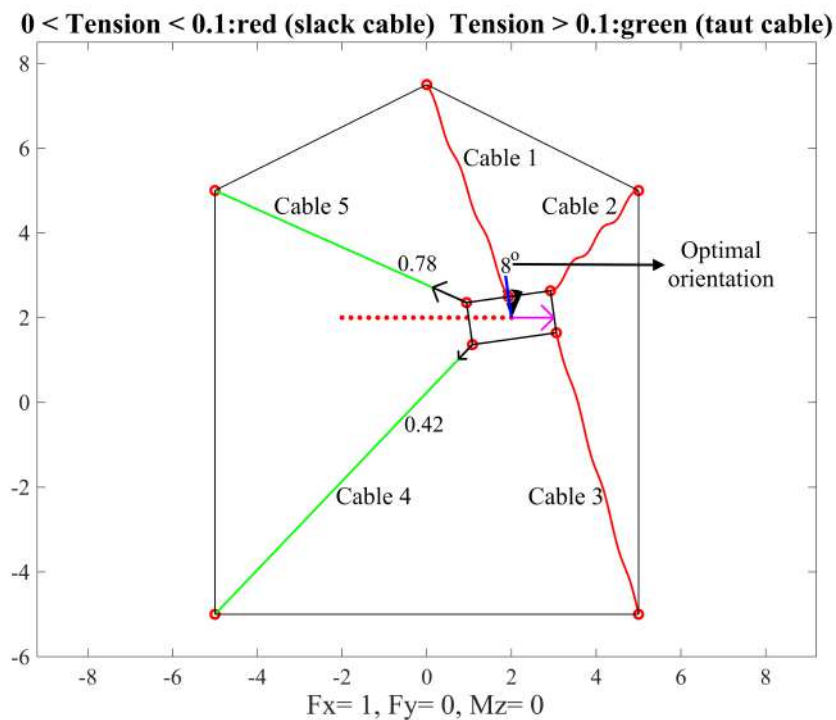


Figure 3.21: Horizontal path traced by the moving platform of the five-cable robot

Figs. 3.22 and 3.23 correspond to tensions and lengths of the cables. In Fig. 3.23, lengths of the cables 2 and 3 are decreasing because the platform is moving closer towards fixed pivots

2 and 3. Conversely, lengths of the cables 4 and 5 are increasing because of the movement of the platform away from the fixed pivots 4 and 5. Length of the cable 1 partially decreases and then increases because the platform initially approaches and then moves away from the first fixed pivot. Fig. 3.24 is the plot of the optimal orientation at every waypoint corresponding to minimum tensions in the cables. Fig. 3.25 corresponds to the optimal  $\alpha$  of the optimal orientation at every waypoint.

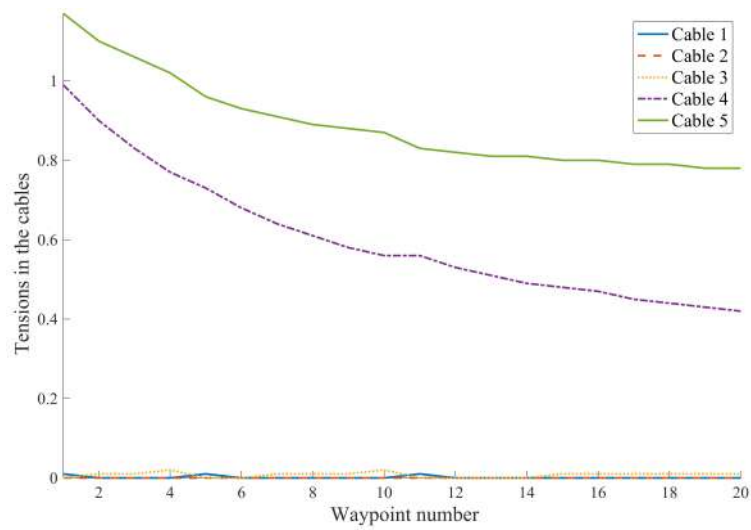


Figure 3.22: Fourth and fifth cables support the platform for the entire path as the net external force is in the direction of the positive  $x$ -axis

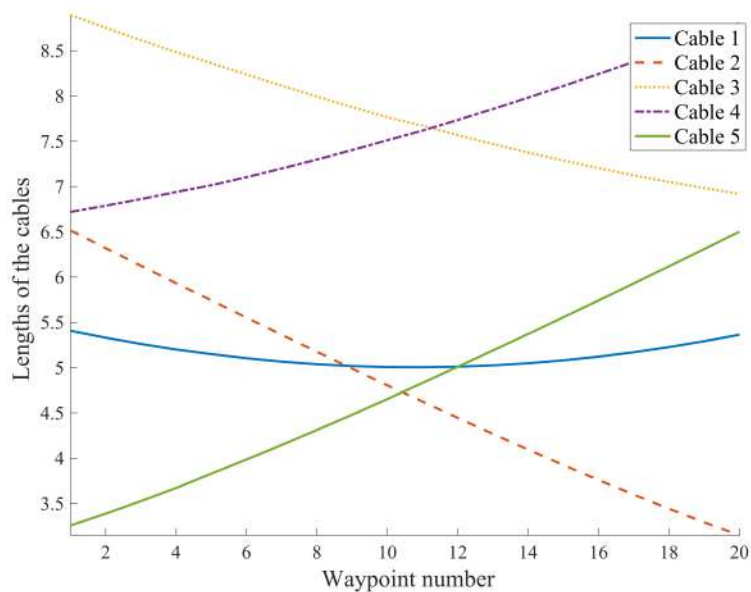


Figure 3.23: Lengths of the cables at every waypoint

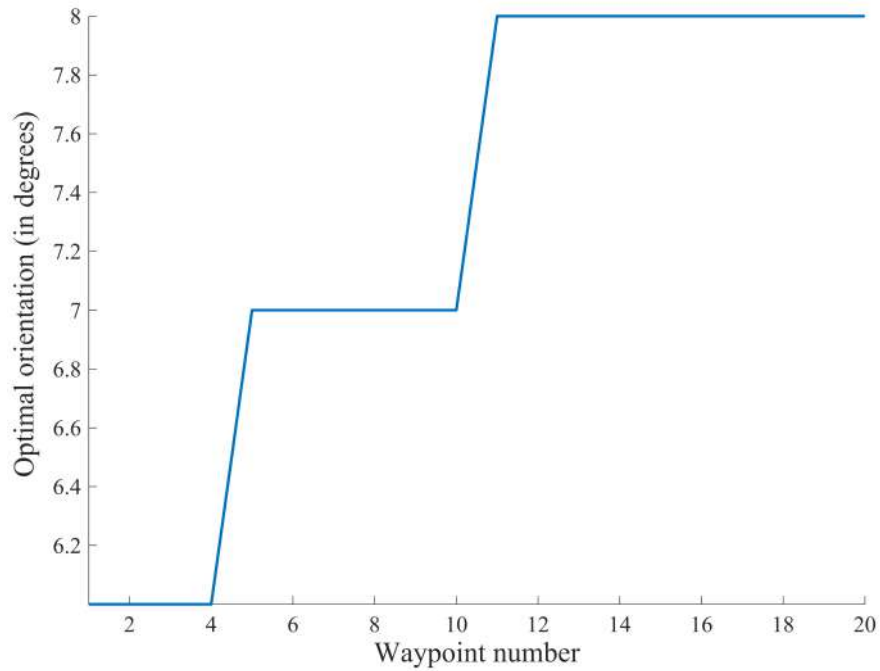


Figure 3.24: Orientation chosen at every waypoint, by the algorithm, for minimum  $\|\mathbf{t}\|$

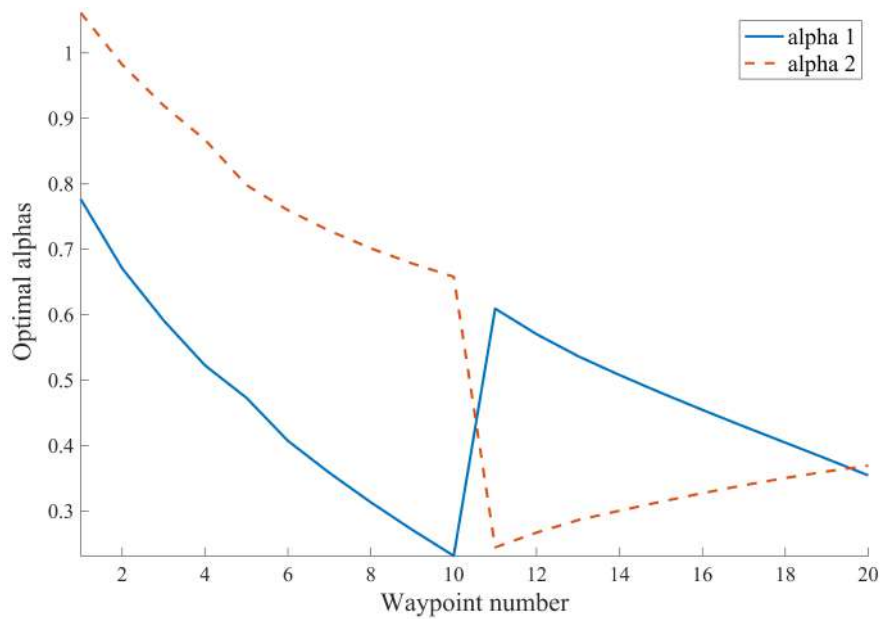


Figure 3.25: Optimal  $\alpha$  corresponding to the optimal orientation at every waypoint

### 3.5.2 Trajectory tracing with specified orientation at every waypoint

As an extension from the previous section, here, we consider the case where the desired orientation of the platform is specified at every waypoint. As discussed in the previous section, every

orientation has multiple possible tension values. We can consider either maximum or minimum tensions in the cables as a criterion to choose  $\alpha$ . The algorithm has to be given the required orientation at every waypoint and  $\alpha$ -selection criterion (i.e., maximum or minimum  $\|\mathbf{t}\|$ ). As an example, a case of the six-cable robot with a vertical path and a set of desired orientations is considered. Let the criterion for the selection of  $\alpha$  be maximum  $\|\mathbf{t}\|$ . Since tension values are proportional to the elements of  $\alpha$ , the algorithm may choose values of  $\alpha$  which may push tension values to infinity. To prevent this, elements of  $\alpha$  are bounded between  $-20$  and  $20$ . Parameters of the six-cable robot are given in Table 3.9. The path is made of 10 equidistant points w.r.t. each other between both the points  $(-2, -2)$  and  $(-2, 2.5)$  inclusive. Desired orientation at every waypoint is specified in Table 3.9. Fig. 3.26 shows the simulated task at the ending point  $(-2, 2.5)$  for  $15^\circ$  orientation of the platform. Figs. 3.27 and 3.28 correspond to tensions and lengths of the cables. Fig. 3.29 corresponds to optimal  $\alpha$  chosen at every waypoint for maximum  $\|\mathbf{t}\|$  within the bounds provided.

Table 3.9: Parameters of the six-cable robot

No.	$(x_{fi}, y_{fi})$	$(P_{i0x}, P_{i0y})$	$\mathbf{f}$	Desired $\phi$ at every waypoint
1				$10^\circ$ at $(-2, -2)$
				$13^\circ$ at $(-2, -1.5)$
	$(0, 7.5)$	$(0, 0.5)$	$\left\{ \begin{array}{c} 0 \\ 0 \\ 1 \end{array} \right\}$	$17^\circ$ at $(-2, -1)$
	$(5, 5)$	$(1, 0.5)$		$12^\circ$ at $(-2, -0.5)$
	$(5, -5)$	$(1, -0.5)$		$21^\circ$ at $(-2, 0)$
	$(0, -7.5)$	$(0, -0.5)$		$25^\circ$ at $(-2, 0.5)$
	$(-5, -5)$	$(-1, -0.5)$		$14^\circ$ at $(-2, 1)$
	$(-5, 5)$	$(-1, 0.5)$		$35^\circ$ at $(-2, 1.5)$
				$27^\circ$ at $(-2, 2)$
				$15^\circ$ at $(-2, 2.5)$

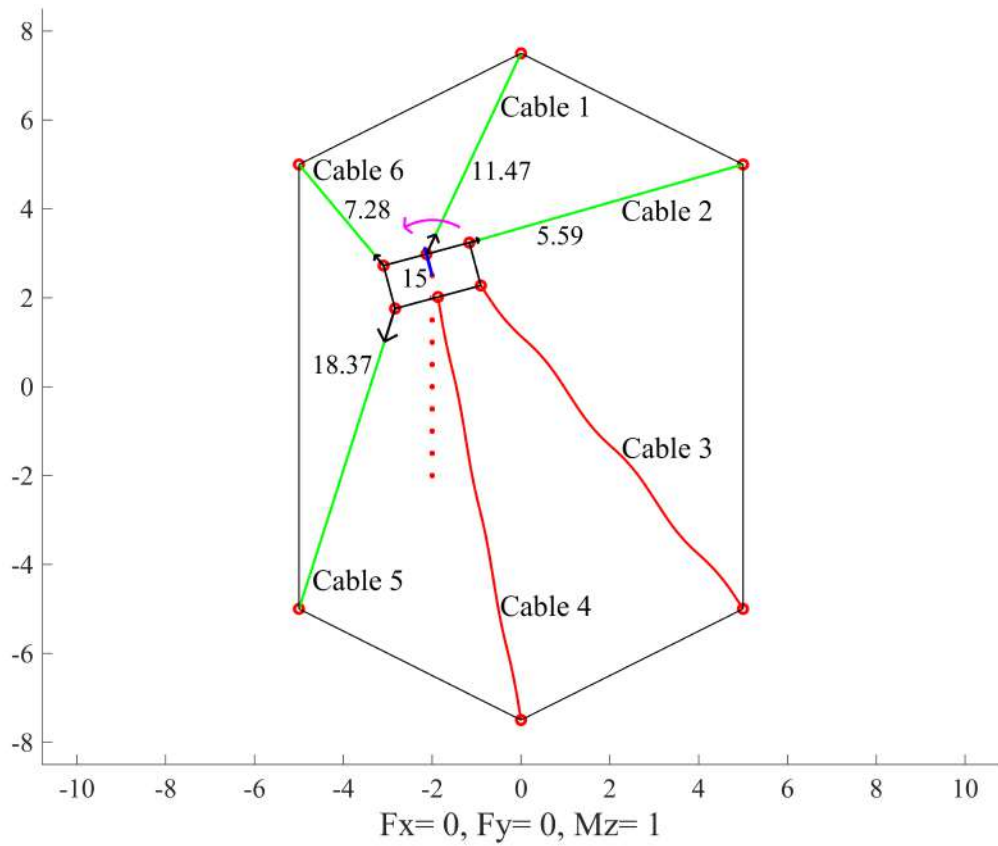


Figure 3.26: Vertical path traced by the moving platform of the six-cable robot. Curved pink arrow indicates that a positive moment load is acting on the platform.

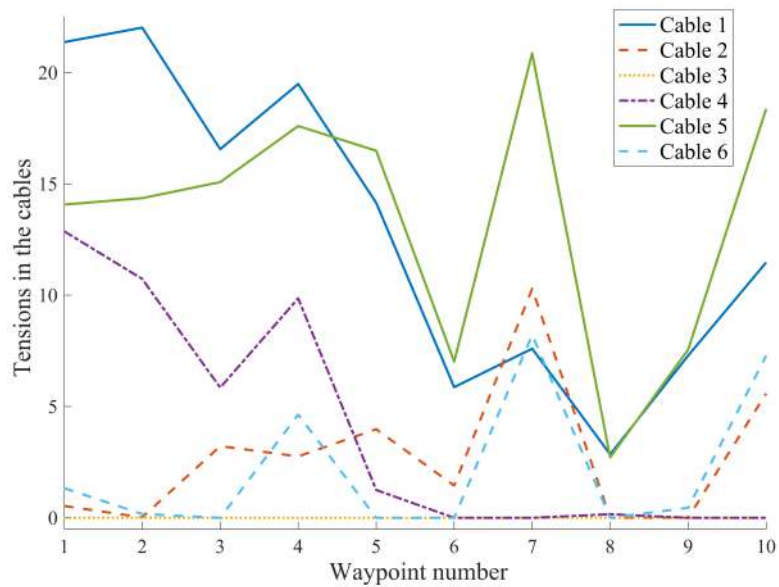


Figure 3.27: Tensions in the cables for maximum  $\|\mathbf{t}\|$

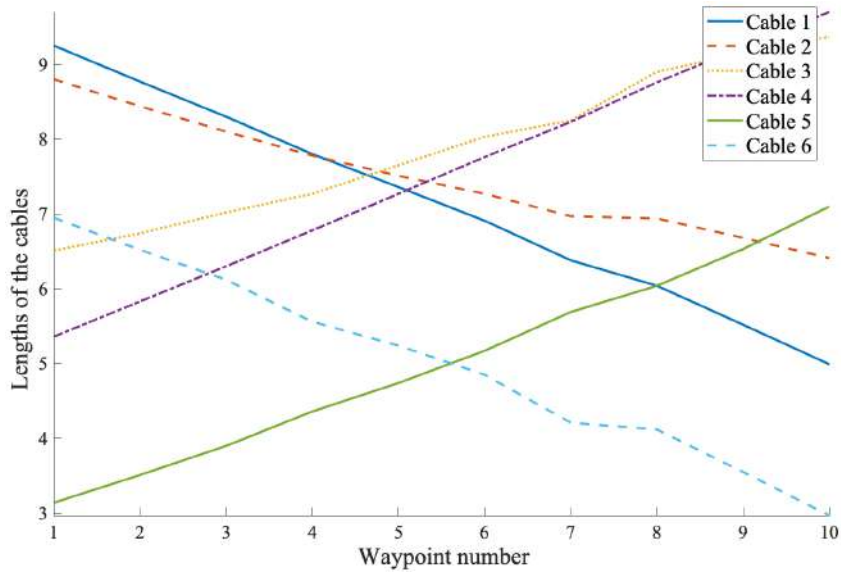


Figure 3.28: Lengths of the cables at every waypoint

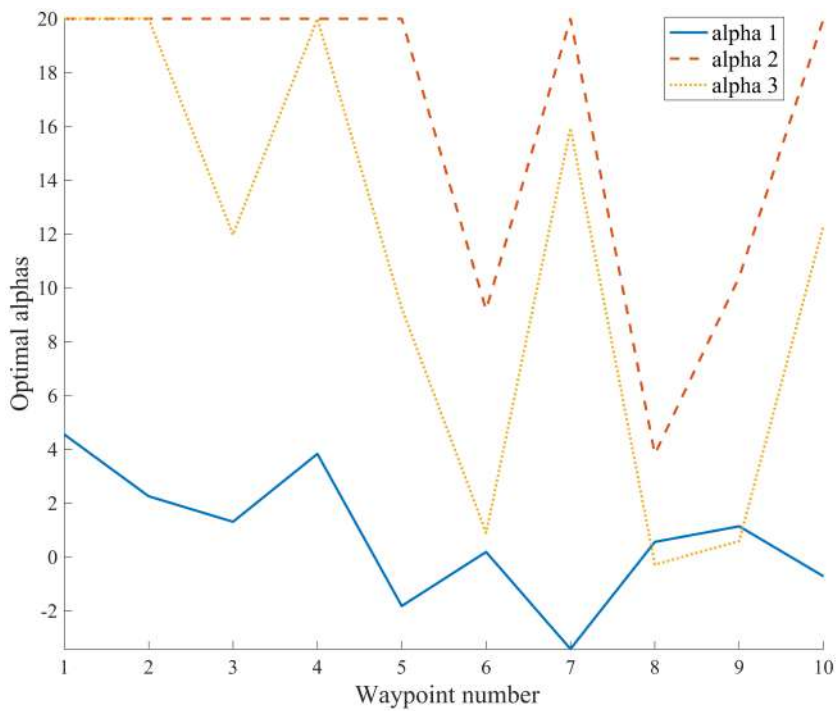


Figure 3.29: Optimal  $\alpha$  chosen at every waypoint for maximum  $\|\mathbf{t}\|$  within the bounds provided

## Closure

In this chapter, feasible orientations are obtained for two different cases. First, for static equilibrium of the cable robot and, second, for fully constrained condition. It is shown that the

nature of the load acting on the platform strongly influences the orientability of the platform for the first case whereas it does not play a role in the second case. Orientability of the platform in both cases improves as the number of cables increase. Also, the geometry of the cable robot influences feasible orientations. When a moment load is acting on the platform, its orientability enhances in the first case. If the initial vertices of the platform and fixed pivots of the cable robot are geometrically aligned, it curtails the orientability of the platform. It is shown, with the help of examples, that feasible orientations that fully constrain the cable robot are a subset of those that are required to maintain the cable robot in static equilibrium.

# Chapter 4

## Enhanced Orientability of the Cable Robot

### Summary

An approach to enhance the orientability of the cable robot is presented in this chapter. It involves the addition of a motor, an extra cable, and a spring. The equations governing the orientation are discussed and some examples presented.

### 4.1 Limited orientability of the moving platform

As presented in Chapter 3, there are limitations to the orientability of the platform in different regions of the workspace. At every point in the workspace, depending on the nature of the load and geometry of the cable robot, there is a limit to the range within which the platform can rotate. Although a cable robot with more cables increases the orientability of the platform, this enhanced range may not always cover the orientability requirements of intended applications. We solve the problem of limited range by adding a rotary degree of freedom on the moving platform, as discussed next (an alternate approach that used two-platforms was discussed in [160]).

### 4.2 Modification of the set-up to achieve an additional rotary degree of freedom

Consider a three-cable robot with a triangular platform. A spool (on which an end-effector can be mounted) is attached to the center of the platform with a pin joint, allowing it to freely rotate w.r.t. the platform. The spool contains a helical groove for winding a cable. The spool

behaves like a pulley since its rotation is controlled by the cable wound on it. This cable is attached at one end to an additional rotary actuator fixed at  $(x_r, y_r)$ , as shown in Fig. 4.1.

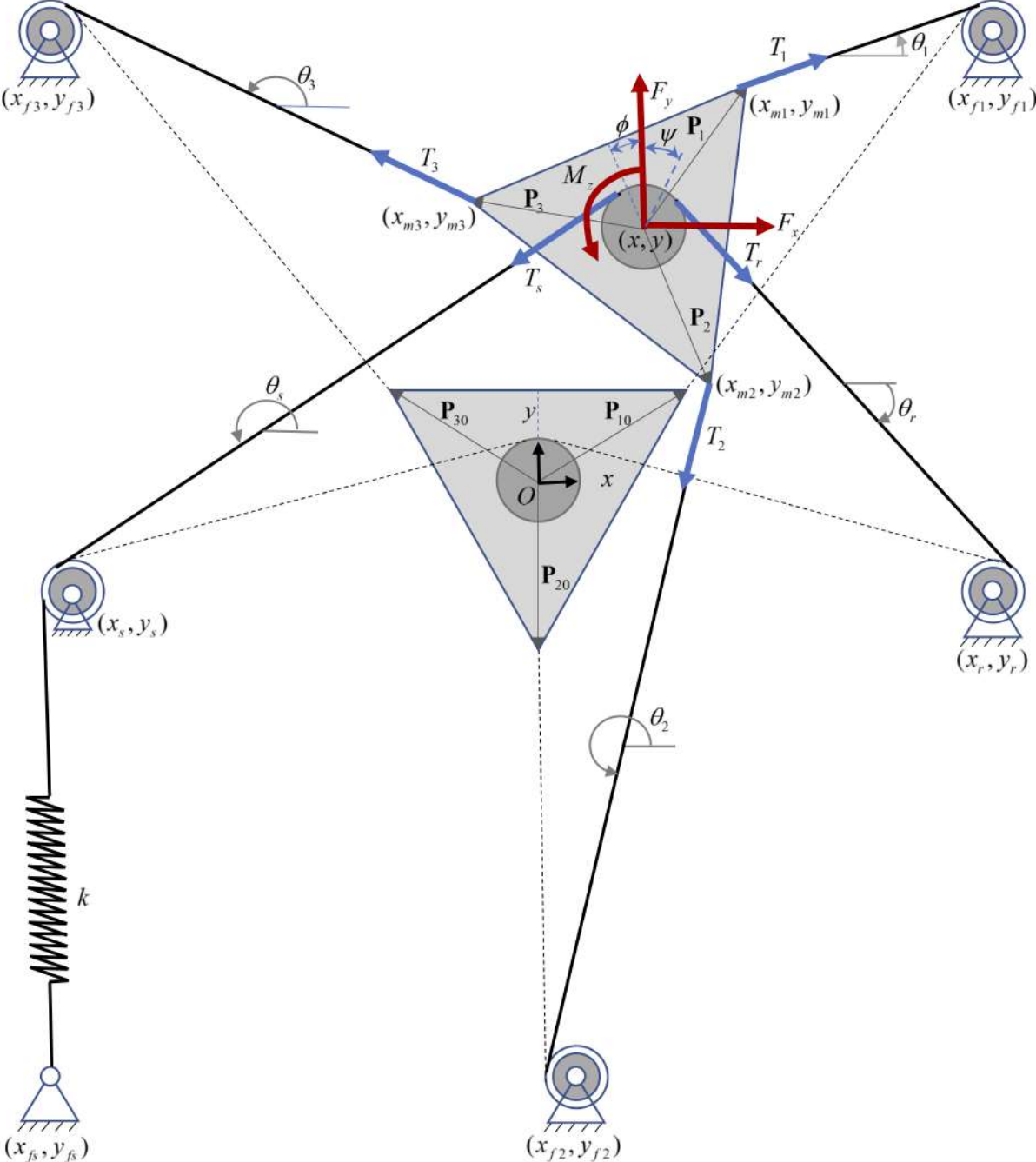
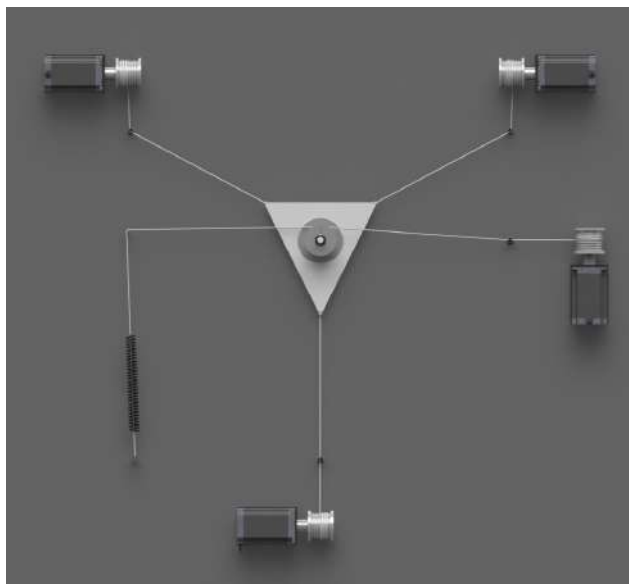


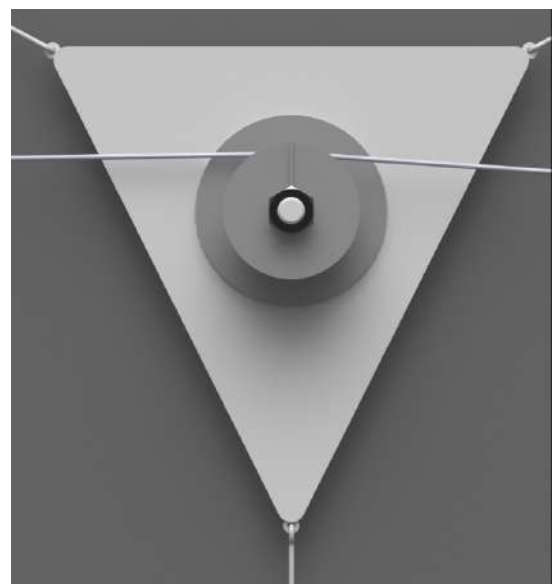
Figure 4.1: 2D model of the three-cable robot with an additional rotary degree of freedom

The other end of the cable passes through a pulley fixed at  $(x_s, y_s)$  and is then attached to a

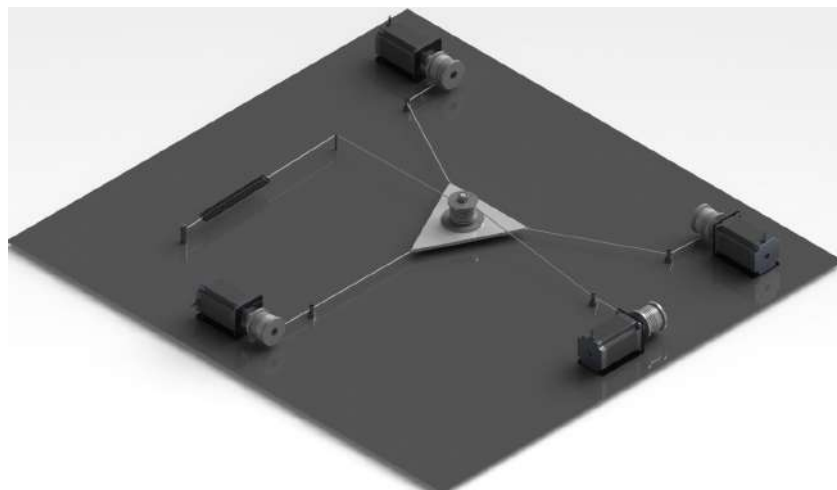
fixed point  $(x_{fs}, y_{fs})$  with a tension spring. This spring helps in restoring the orientation and also prevents the slacking of the cable. The spool has multiple windings of the cable along the helical groove so as to prevent slip. An end-effector is attached to the spool so that any orientation of the end-effector can be achieved when there is no load. Cable tensions need to be adjusted to maintain a particular orientation of the end-effector. Working of the set-up is discussed in Section 4.3. A 3D Solidworks model of the set-up is shown in Fig. 4.2.



(a) Top view of the set-up



(b) Spool with an indicator to show its orientation



(c) Perspective view of the set-up

Figure 4.2: 3D Solidworks model of the three-cable robot with a spool attached to the moving triangular platform

### 4.3 Working of the set-up

Let us consider the case where the coordinates of the centroid of the platform are  $(x, y)$  and its orientation is  $\phi$ . Let the orientation of the spool be  $\psi$ . Tension in the cable connecting the rotary actuator to the spool is  $T_r$  and the tension in the cable connecting spool to spring is  $T_s$ . The magnitude of  $\mathbf{T}_r$  can be controlled by controlling the input current to the motor controlling the orientation. The magnitude of  $\mathbf{T}_s$  depends on spring stiffness and the elongation of the spring, which can be given as follows.

$$T_s = k(\Delta s) \quad (4.1)$$

$$\Delta s = \delta - r_p \psi + \sqrt{(y + r_p - y_s)^2 + (x - x_s)^2} - \sqrt{(r_p - y_s)^2 + (x_s)^2} \quad (4.2)$$

where  $k$  is the spring stiffness,  $\Delta s$  the elongation of the spring,  $r_p$  the pitch circle radius of the helical groove on the spool, and  $\delta$  the initial elongation of the spring. When the orientation motor releases the cable, the spring tugs it back causing the spool to rotate in the counter-clockwise direction. To achieve this, the spring must always be in tension. Hence, the value of  $\delta$  must be chosen accordingly. First, let us consider the case where the orientation of the spool is not changing. For this to happen,  $T_r$  and  $T_s$  must be equal. The two tension vectors  $\mathbf{T}_r$  and  $\mathbf{T}_s$  are the external forces acting on the platform. Hence, their components must be added to the respective components of the load vector  $\mathbf{f}$ .

$$\hat{\mathbf{f}} = \begin{Bmatrix} \hat{F}_x \\ \hat{F}_y \\ \hat{M}_z \end{Bmatrix} = \begin{Bmatrix} F_x \\ F_y \\ M_z \end{Bmatrix} + \begin{Bmatrix} T_s \cos \theta_s + T_r \cos \theta_r \\ T_s \sin \theta_s + T_r \sin \theta_r \\ (T_s - T_r)r_p \end{Bmatrix} \quad (4.3)$$

where

$$\theta_s = \tan^{-1} \left( \frac{y_s - y - r_p \sin \left( \frac{\pi}{2} + \beta_1 \right)}{x_s - x - r_p \cos \left( \frac{\pi}{2} + \beta_1 \right)} \right) \quad (4.4)$$

$$\theta_r = \tan^{-1} \left( \frac{y_r - y - r_p \sin \left( \frac{\pi}{2} - \beta_2 \right)}{x_r - x - r_p \cos \left( \frac{\pi}{2} - \beta_2 \right)} \right) \quad (4.5)$$

$\theta_s$  and  $\theta_r$  are the angles of the fourth cable on either side of the spool w.r.t. the  $x$ -axis;  $\beta_1$  and  $\beta_2$  are the angles of wrap of the orientation (i.e., fourth) cable, as shown in Fig. 4.3. They can be positive, negative, or zero depending on the position  $(x, y)$  of the platform w.r.t. the fixed coordinates  $(x_s, y_s)$  and  $(x_r, y_r)$ . The possible values of  $\beta_1$  and  $\beta_2$  are presented in Table 4.1.

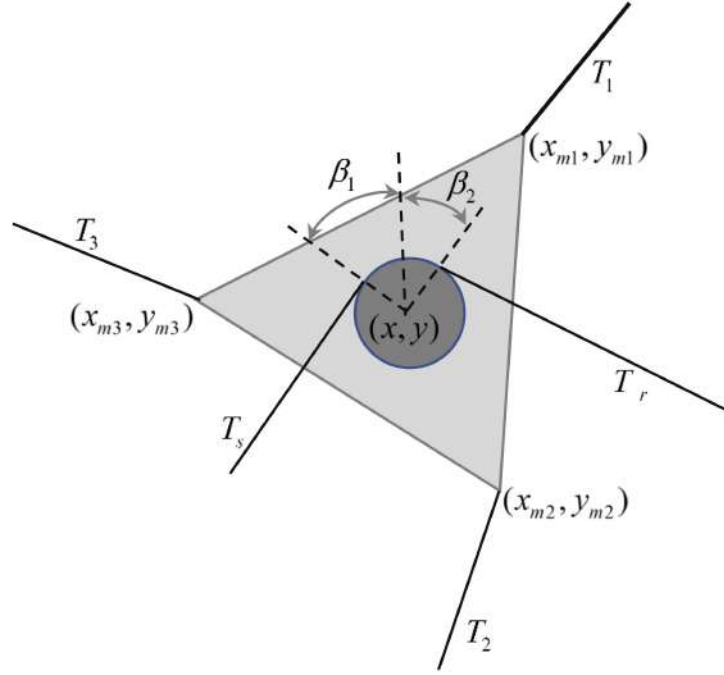


Figure 4.3: Angles of wrap of the fourth cable on either side of the spool

Table 4.1: Three different cases of  $\beta_1$  and  $\beta_2$

No.	Conditions for $\beta_1$	Values of $\beta_1$	Conditions for $\beta_2$	Values of $\beta_2$
1	$y + r_p > y_s$	$\sin^{-1} \left( \frac{r_p}{\sqrt{(x-x_s)^2 + (y-y_s)^2}} \right)$	$y + r_p > y_r$	$\sin^{-1} \left( \frac{r_p}{\sqrt{(x-x_r)^2 + (y-y_r)^2}} \right)$
2	$y + r_p = y_s$	0	$y + r_p = y_r$	0
3	$y + r_p < y_s$	$-\sin^{-1} \left( \frac{r_p}{\sqrt{(x-x_s)^2 + (y-y_s)^2}} \right)$	$y + r_p < y_r$	$-\sin^{-1} \left( \frac{r_p}{\sqrt{(x-x_r)^2 + (y-y_r)^2}} \right)$

Static equilibrium of the cable robot with the updated load vector  $\hat{\mathbf{f}}$  is given as follows.

$$\mathbf{L}\mathbf{t} + \hat{\mathbf{f}} = \mathbf{0} \quad (4.6)$$

where  $\mathbf{L}$ ,  $\mathbf{t}$ , and  $\hat{\mathbf{f}}$  are given by Eqs. 2.8, 2.11, and 4.3. The data for two examples is given in Table 4.2.

Table 4.2: Cable forces of the three-cable robot for the two different orientations of the spool

No.	Variables	Configuration 1	Configuration 2
1	$(x_{fi}, y_{fi})$ where $(i = 1, 2, 3)$	$(30, 17.32)$ $(0, -34.64)$ $(-30, 17.32)$	$(30, 17.32)$ $(0, -34.64)$ $(-30, 17.32)$
2	$(P_{i0x}, P_{i0y})$	$(9, 6)$ $(0, -12)$ $(-9, 6)$	$(9, 6)$ $(0, -12)$ $(-9, 6)$
3	$(x, y)$	$(5, 5)$	$(5, 5)$
4	$\phi$	$2^\circ$	$2^\circ$
5	$(x_{mi}, y_{mi})$	$(13.79, 11.31)$ $(5.42, -6.99)$ $(-4.2, 10.68)$	$(13.79, 11.31)$ $(5.42, -6.99)$ $(-4.2, 10.68)$
6	$\mathbf{f}$	$\begin{Bmatrix} 0 \\ -1 \\ 0 \end{Bmatrix}$	$\begin{Bmatrix} 0 \\ -1 \\ 0 \end{Bmatrix}$
7	$k$	3	3

Continued on the next page

Table 4.2 – continued from the previous page

No.	Variables	Configuration 1	Configuration 2
8	$\delta$	10	10
9	$r_p$	2.13	2.13
10	$\psi$	$10^\circ$	$-10^\circ$
11	$(x_s, y_s)$	(-30,0)	(-30,0)
12	$(x_r, y_r)$	(30,0)	(30,0)
13	$\Delta s$	15.27	16.02
14	$T_s$	45.81	48.05
15	$T_r$	45.81	48.05
16	$\theta_s$	$-168.45^\circ$	$-168.45^\circ$
17	$\theta_r$	$-16.01^\circ$	$-16.01^\circ$
18	$\beta_1$	$3.45^\circ$	$3.45^\circ$
19	$\beta_2$	$4.79^\circ$	$4.79^\circ$
20	$\hat{\mathbf{f}}$	$\begin{Bmatrix} -0.85 \\ -22.81 \\ 0 \end{Bmatrix}$	$\begin{Bmatrix} -0.89 \\ -23.87 \\ 0 \end{Bmatrix}$
21	$\mathbf{L}$	$\begin{bmatrix} 0.94 & -0.19 & -0.97 \\ 0.35 & -0.98 & 0.25 \\ -2.86 & -2.72 & 3.21 \end{bmatrix}$	$\begin{bmatrix} 0.94 & -0.19 & -0.97 \\ 0.35 & -0.98 & 0.25 \\ -2.86 & -2.72 & 3.21 \end{bmatrix}$

Continued on the next page

Table 4.2 – continued from the previous page

No.	Variables	Configuration 1	Configuration 2
22	$\mathbf{t}$	$\left\{ \begin{array}{c} 43.12 \\ 2.29 \\ 40.42 \end{array} \right\}$	$\left\{ \begin{array}{c} 45.12 \\ 2.40 \\ 42.29 \end{array} \right\}$

Positive cable forces indicate that the platform is in static equilibrium for the cases considered in Table 4.2. Note that for every orientation of the spool, there exist multiple feasible orientations of the platform. To find these feasible orientations,  $\phi$  is varied from  $-180^\circ$  to  $180^\circ$  with an increment of  $1^\circ$  similar to the procedure discussed in Section 3.2, but with a slight modification:  $\hat{\mathbf{f}}$  is used instead of  $\mathbf{f}$ . It may be noted that  $\hat{\mathbf{f}}$  varies with the orientation of the spool. For the first configuration considered in Table 4.2, feasible orientations of the platform are from  $-180^\circ$  to  $-177^\circ$  and then from  $0^\circ$  to  $2^\circ$ . Feasible orientations of the second configuration are same as that of the first configuration.

Next, let us consider a case where the platform's centroid is located at  $(x, y)$  and its pose is  $\phi$ . Initially, the spool is at rest with an orientation  $\psi_1$ . It then undergoes a rotation and comes to rest with an orientation  $\psi_2$  i.e.,  $\Delta\psi = \psi_2 - \psi_1$ . Sign of  $\Delta\psi$  indicates the direction of rotation.  $\Delta\psi > 0$  for counter-clockwise direction and  $\Delta\psi < 0$  for clockwise direction. In order to rotate the spool counter-clockwise,  $T_s$  must be greater than  $T_r$ . Conversely, to rotate it clockwise  $T_r$  must be greater than  $T_s$ . When the spool is at rest with the orientation  $\psi_1$ ,  $T_s$  and  $T_r$  are equal and are given as follows.

$$T_s = T_r = k(\delta - r_p\psi_1 + \sqrt{(y + r_p - y_s)^2 + (x - x_s)^2} - \sqrt{(r_p - y_s)^2 + (x_s)^2}) \quad (4.7)$$

While the spool is undergoing rotation from  $\psi_1$  to  $\psi_2$ , value of  $T_s$  depends on the stiffness and elongation of the spring given by Eqs. 4.1 and 4.2.  $T_r$  depends on  $T_s$ ,  $r_p$ , coefficient of sliding friction between pin joint and the spool ( $\mu$ ), radius of the pin joint ( $r_b$ ), and the direction of rotation of the spool.  $T_r$  value can be obtained by solving the equation below with the

constraint  $T_r > 0$ .

$$(|T_r - T_s|) r_p = \mu \left( \sqrt{T_s^2 + T_r^2 + 2T_s T_r \cos(\theta_s - \theta_r)} \right) r_b \quad (4.8)$$

When the spool comes back to rest with the orientation  $\psi_2$ ,  $T_s$  and  $T_r$  must be equal in order to prevent any further orientation change and their values can be given as follows.

$$T_s = T_r = k(\delta - r_p \psi_2 + \sqrt{(y + r_p - y_s)^2 + (x - x_s)^2} - \sqrt{(r_p - y_s)^2 + (x_s)^2}) \quad (4.9)$$

An example is considered here to illustrate this procedure.

The platform's centroid is placed at (5, 6) and its orientation is fixed at  $0^\circ$ . The spool rotates from  $30^\circ$  to  $60^\circ$  with an increment of  $1^\circ$ . Parameters of the three-cable robot considered for this example are given in Table 4.3. At every increment,  $T_s$  and  $T_r$  are obtained and  $\hat{\mathbf{f}}$  is calculated according to the Eq. 4.3. The tension vector ( $\mathbf{t}$ ) is obtained at every increment using Eq. 4.6. Figs. 4.4 – 4.7 shows the simulated task of the change in the orientation of the spool from  $30^\circ$  to  $60^\circ$ . In Figs. 4.4 – 4.7, the pink arrow indicates the direction of the updated load vector. Curved pink arrow represent the moment load acting on the platform. Black arrows indicate the direction of the tensions in the cables with magnitude greater than 0.1. Their size varies in accordance with the magnitude of the tension in the cable. Fig. 4.8 present the tension values of the cables for the simulated task. The figure also shows  $T_s$  and  $T_r$ . Fig. 4.9 shows the updated load vector  $\hat{\mathbf{f}}$  at every increment of the spool.

Table 4.3: Parameters used for the three-cable robot

No.	Parameters	Values
1	$(x_{fi}, y_{fi})$ where $(i = 1, 2, \dots, n)$	$(30, 17.32)$ $(0, -34.64)$ $(-30, 17.32)$
Continued on the next page		

Table 4.3 – continued from the previous page

No.	Parameters	Values
2	$(P_{i0x}, P_{i0y})$	$(9, 6)$ $(0, -12)$ $(-9, 6)$
3	$(x, y)$	$(5, 6)$
4	$\phi$	$0^\circ$
5	$k$	3
6	$\delta$	10
7	$r_p$	2.13
8	$r_b$	0.4
9	$\mu$	0.1
10	$\mathbf{f}$	$\begin{Bmatrix} 0 \\ -1 \\ 0 \end{Bmatrix}$
11	$\psi$	Varies from $30^\circ$ to $60^\circ$ with an increment of $1^\circ$
12	$(x_s, y_s)$	$(-30, 0)$
13	$(x_r, y_r)$	$(30, 0)$

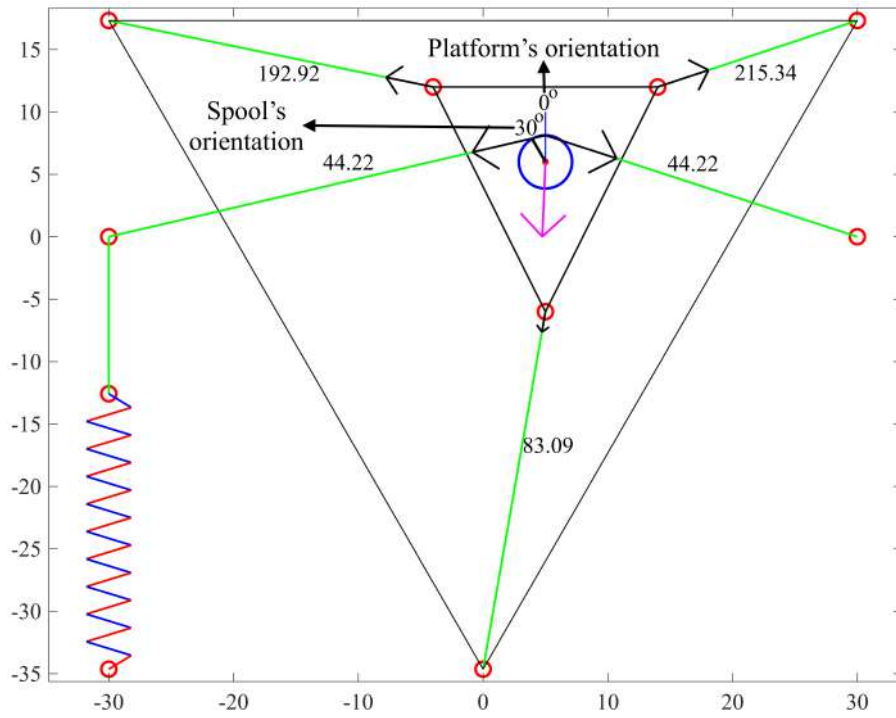


Figure 4.4: Orientation of the spool is  $30^\circ$

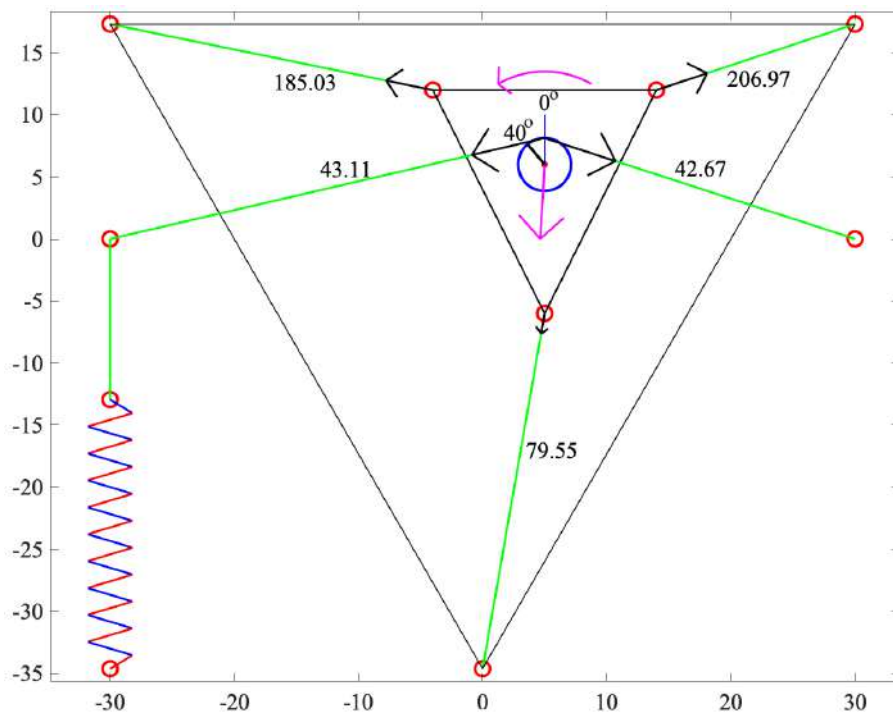


Figure 4.5: Orientation of the spool is  $40^\circ$

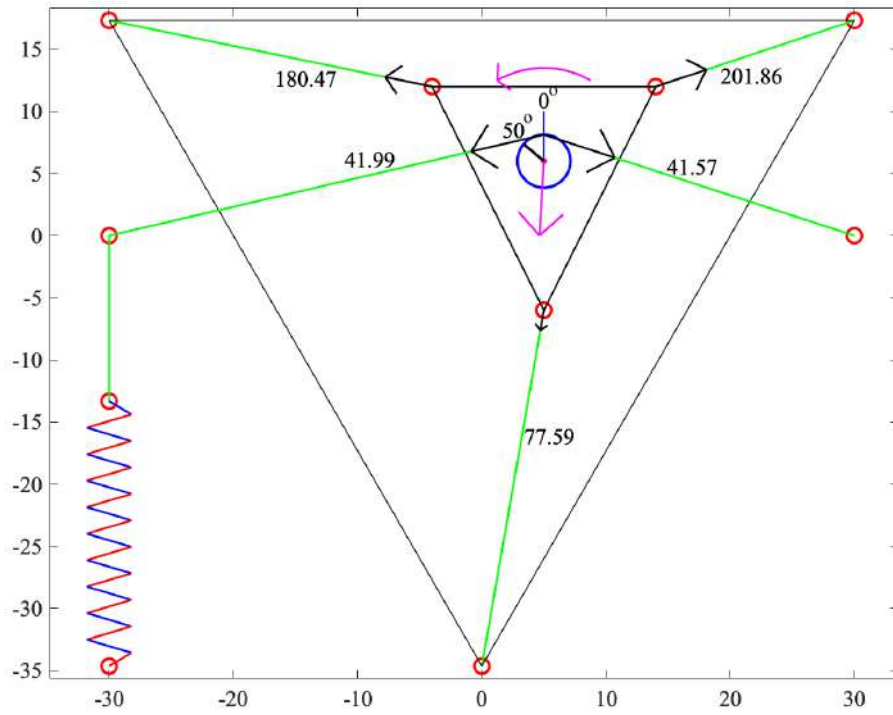


Figure 4.6: Orientation of the spool is  $50^\circ$

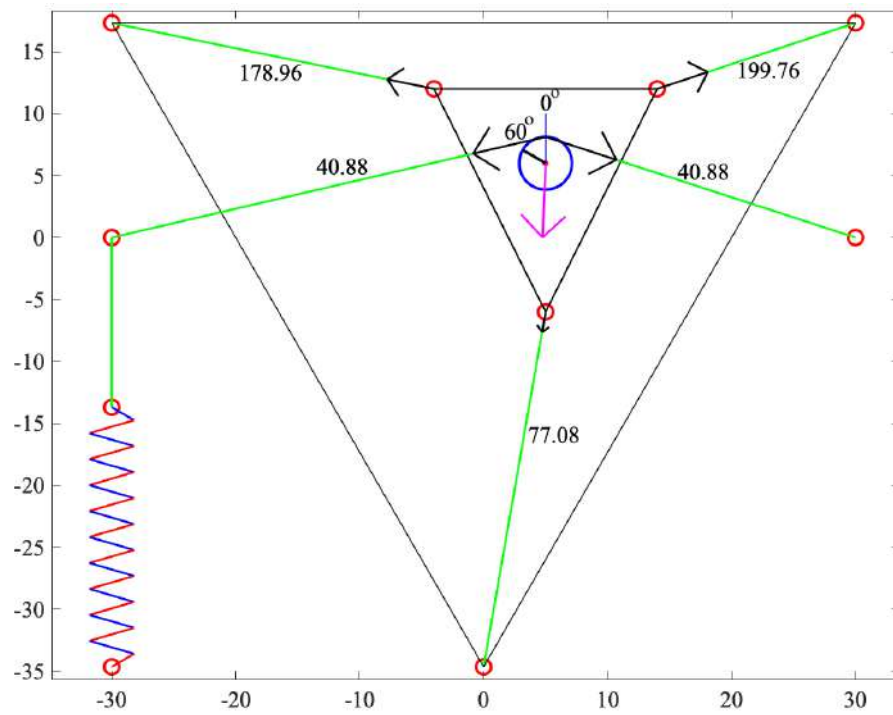


Figure 4.7: Orientation of the spool is  $60^\circ$

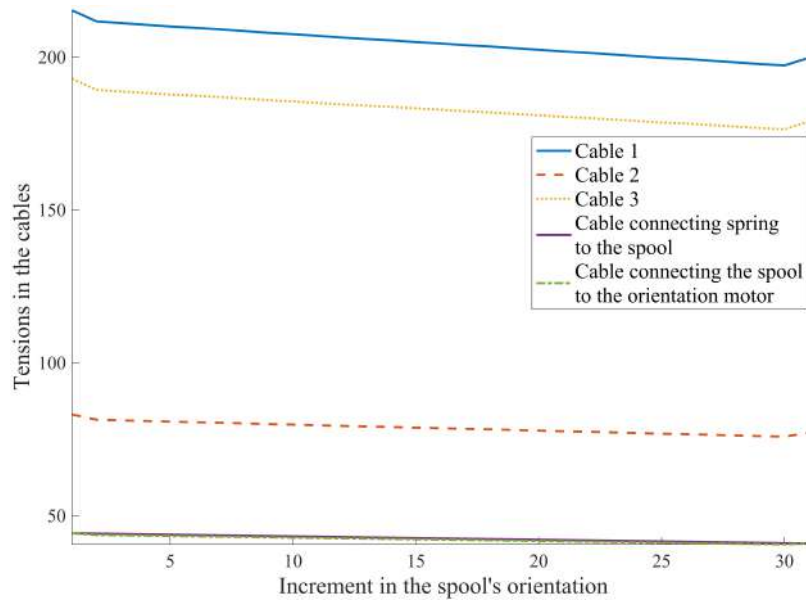


Figure 4.8: Tensions in the cables at every increment in the orientation of the spool

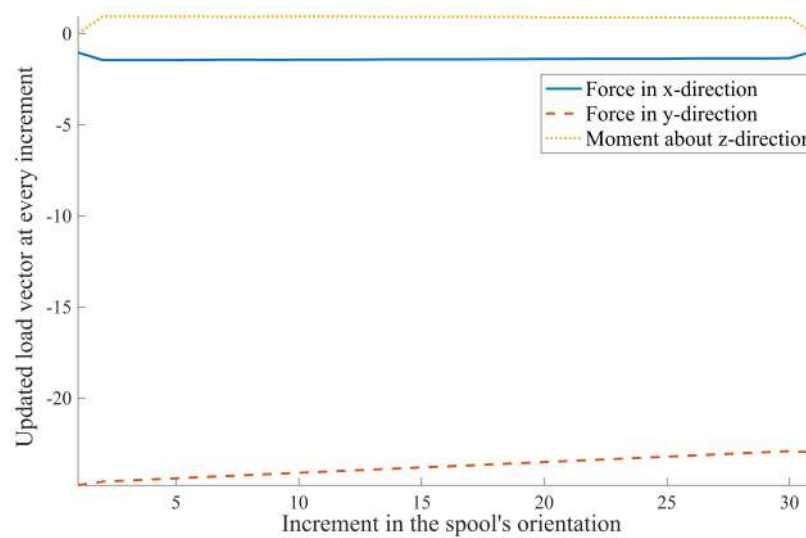


Figure 4.9: Updated load vector  $\hat{\mathbf{f}}$  at every increment in the orientation of the spool

#### 4.4 Platform tracing a prescribed trajectory with desired orientation of the spool

In this section, a path consisting of discrete waypoints to be traced by the moving platform is considered. At every waypoint, a desired orientation of the spool could be specified in accordance with an application. The load vector  $\hat{\mathbf{f}}$  is updated using Eq. 4.3 in conjunction

with either of the Eqs. 4.7 – 4.9. Optimal  $\phi$  of the platform is obtained as per the procedure discussed in Section 3.5.1. We consider an example where the platform of a three-cable robot is required to trace a path along the  $y$ -axis. The path is made up of 11 equidistant points between the points  $(-5, -5)$  and  $(-5, 5)$  including them. The parameters of the three-cable robot are the same as the parameters considered in Table 4.3 with the exemption of a few rows. They are third, fourth, and eleventh rows. For this example, we consider the minimum  $\|\mathbf{t}\|$  as the criteria for obtaining optimal orientations. Desired orientation of the spool at every waypoint is specified in Table 4.4. A simulated task at four-waypoints with the desired orientation of the spool is shown in Figs. 4.10 – 4.13. The range of the feasible orientations of the platform at every waypoint is shown as a black sector. Fig. 4.14 indicates the minimum tensions in the cables and Fig. 4.15 presents the updated load vector at every waypoint. Optimal orientations of the platform chosen for minimum tensions in the cables are shown in Fig. 4.16.

Table 4.4: Desired orientation of the spool at every waypoint

No.	Waypoint	Orientation of the spool
1	$(-5,-5)$	$-20^\circ$
2	$(-5,-4)$	$20^\circ$
3	$(-5,-3)$	$35^\circ$
4	$(-5,-2)$	$-50^\circ$
5	$(-5,-1)$	$-55^\circ$
6	$(-5,0)$	$30^\circ$
7	$(-5,1)$	$80^\circ$
8	$(-5,2)$	$0^\circ$
9	$(-5,3)$	$5^\circ$
10	$(-5,4)$	$-5^\circ$
11	$(-5,5)$	$11^\circ$

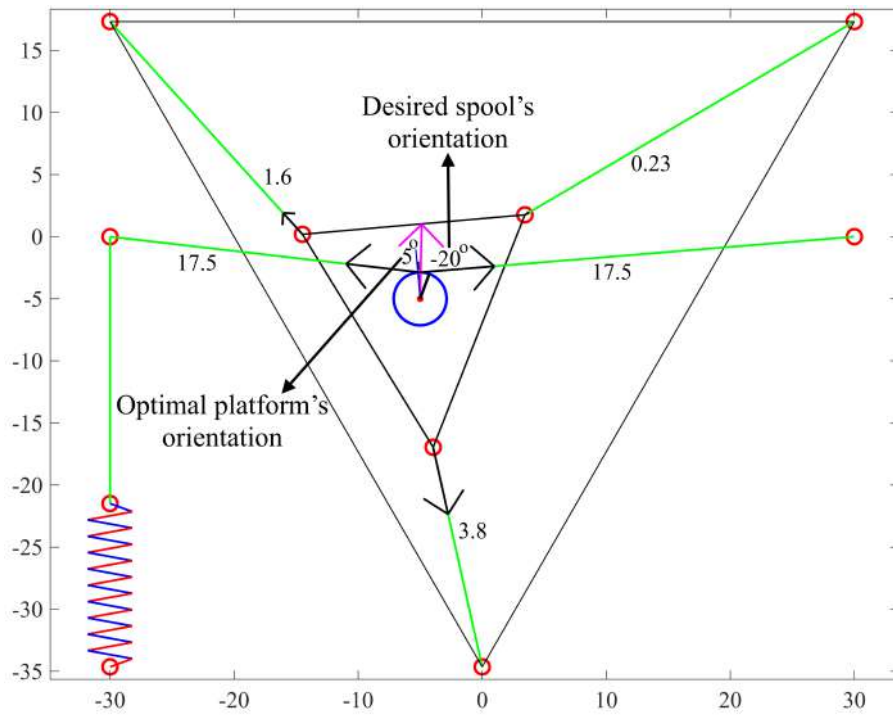


Figure 4.10: Orientation of the spool at  $(-5, -5)$  is  $-20^\circ$

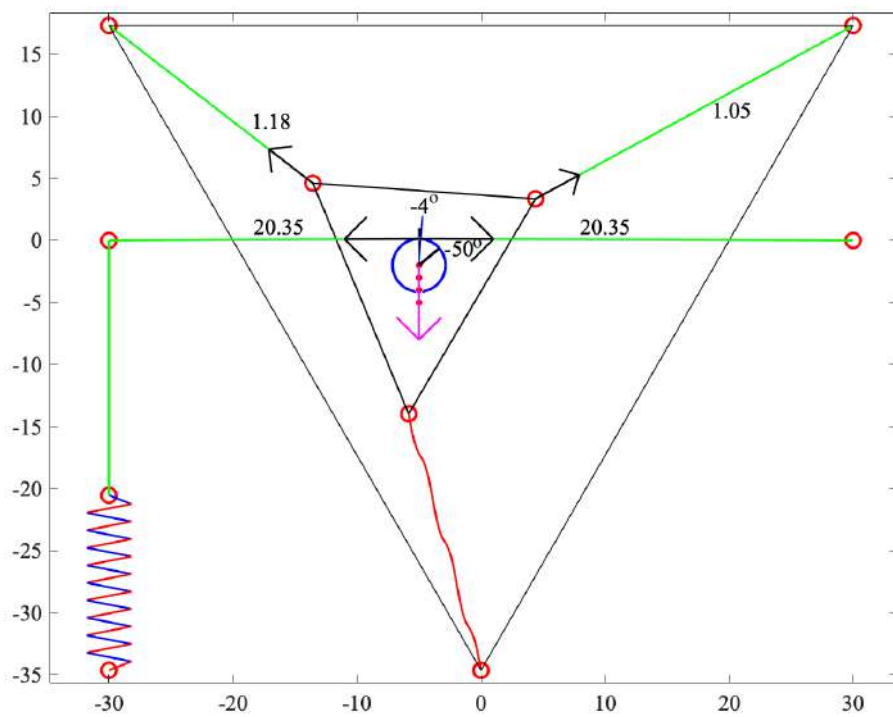


Figure 4.11: Orientation of the spool at  $(-5, -2)$  is  $-50^\circ$

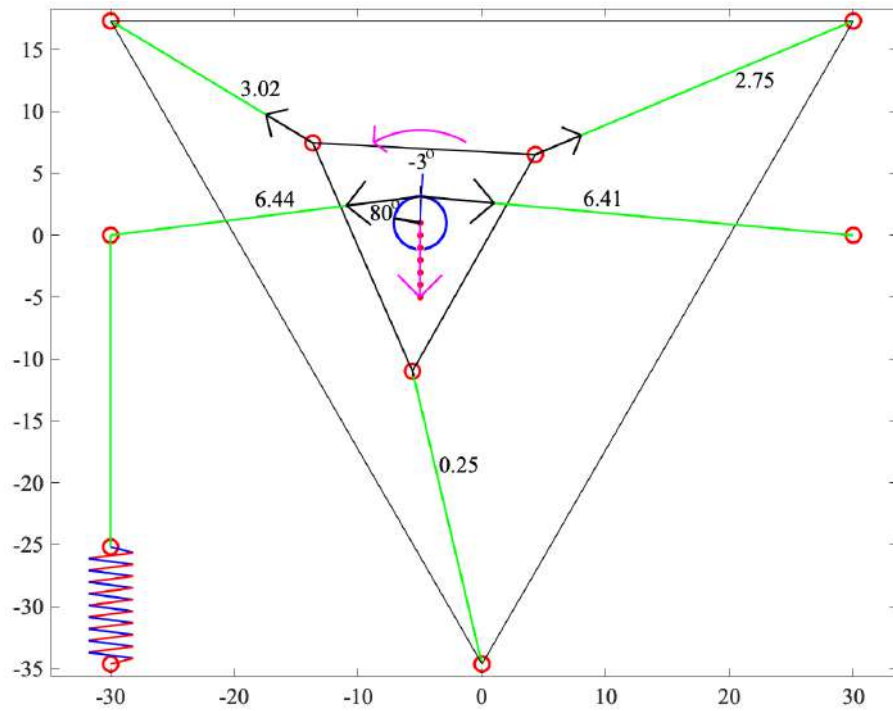


Figure 4.12: Orientation of the spool at  $(-5,1)$  is  $80^\circ$

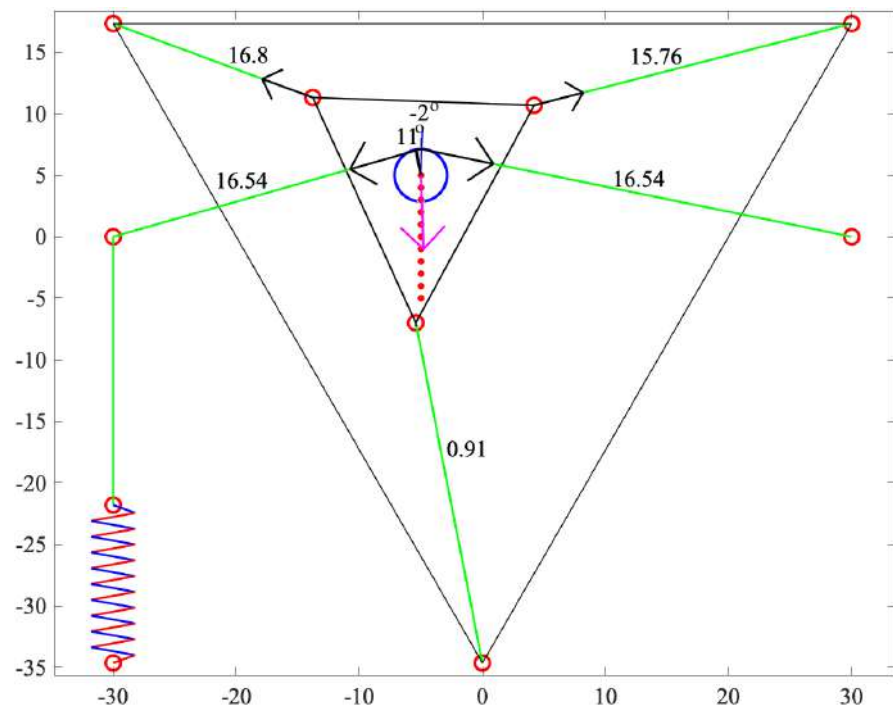


Figure 4.13: Orientation of the spool at  $(-5,5)$  is  $11^\circ$

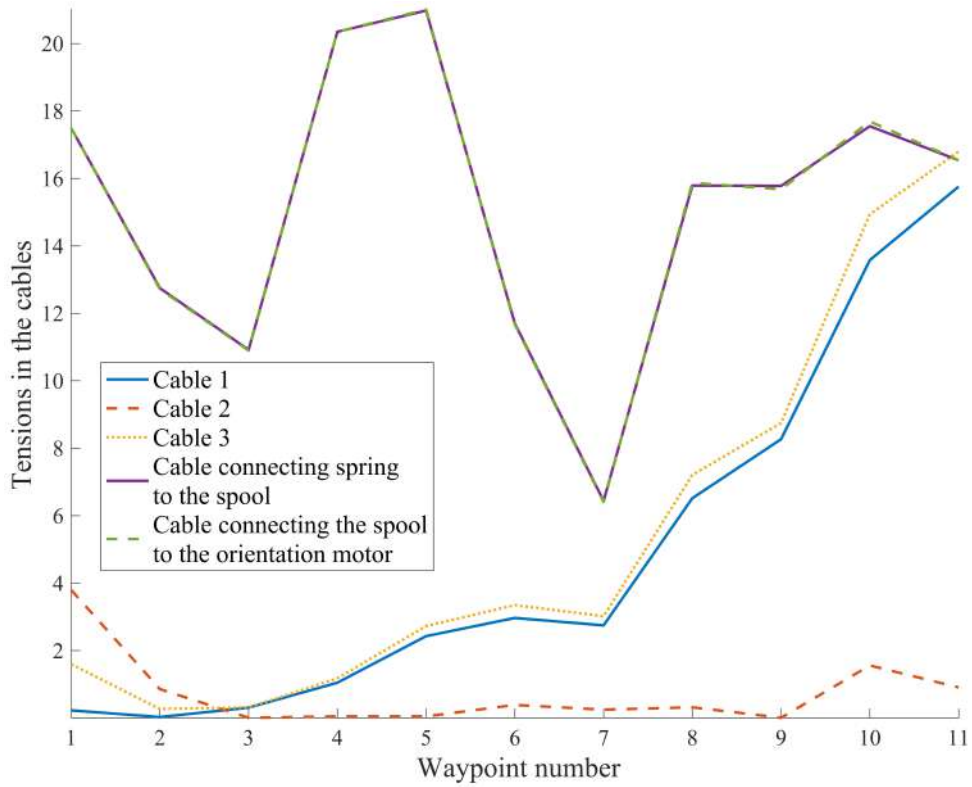


Figure 4.14: Minimum tensions (i.e.,  $\|\mathbf{t}\|$ ) in the cables at every waypoint

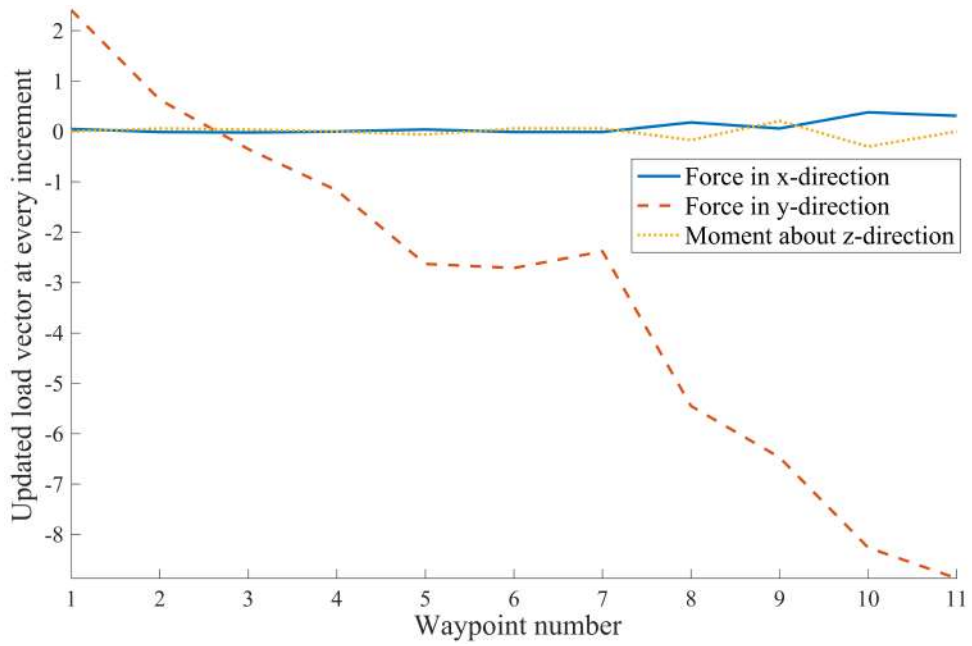


Figure 4.15: Updated load vector  $\hat{\mathbf{f}}$  at every waypoint

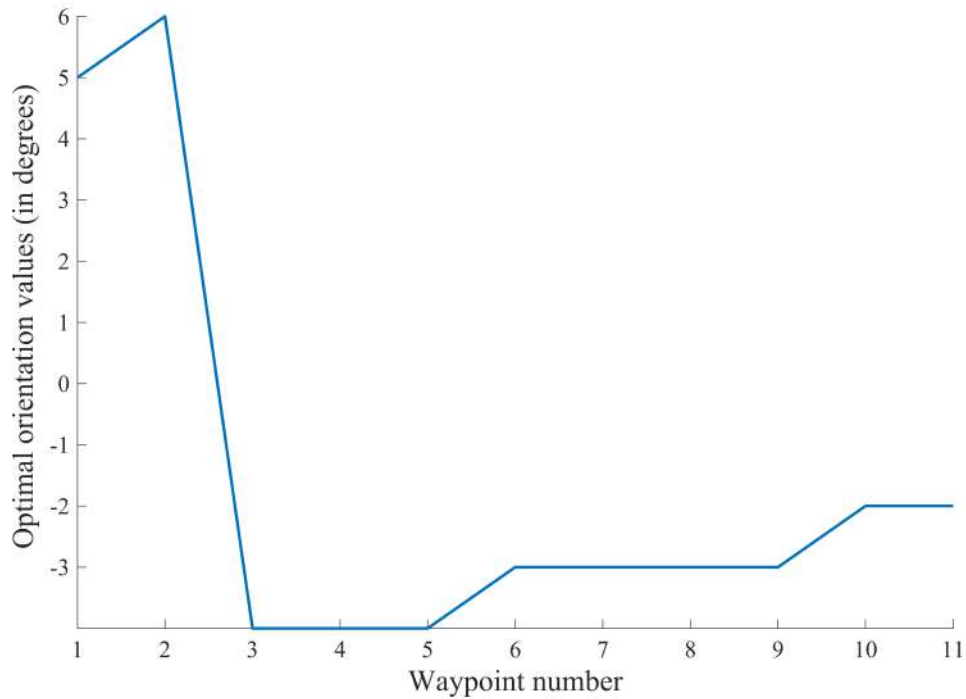


Figure 4.16: Optimal orientation of the platform, chosen by the algorithm, for the minimum tensions (i.e.,  $\|\mathbf{t}\|$ ) in the cables

## Closure

A method of enhancing the orientability of the cable robot with an appendage is described. Multiple examples are considered to illustrate the method. Note that a three-cable robot is considered for all the examples. This is because a three-cable robot has highly restricted orientability as compared to a four-cable robot, a five-cable robot, and so on. Considering how well the orientability of the three-cable robot is enhanced, we can infer that we can achieve much better orientability by adding the same modifications to a cable robot with more than three cables.

# Chapter 5

## Moment Load on the Moving Platform

### Summary

This chapter describes the behavior of a planar cable robot when a moment load is acting on its platform. The set-up used for enhancing the orientability of the cable robot can also be used to apply or support a moment load on the moving platform with a slight modification. The equations governing for the application of a specific moment load and the corresponding examples are presented. A simulated task where the platform of the three-cable robot was made to trace a path with a moment load specified along the path.

### 5.1 Modification of the set-up for the application of moment load

In Chapter 4, a method to enhance the orientability of the cable robot was proposed. This method requires an additional cable, a translational spring, a rotary actuator, and a spool with a helical groove. With the aid of a spring and a rotary actuator, the spool can be rotated either clockwise or counter-clockwise in accordance to the desired orientation. With a slight modification, this set-up can be used to support an external moment load applied on the platform. The modification of the set-up involves arresting the spool to the platform using set-screws as shown in Fig. 5.1. We can either provide positive or negative moment load on the platform. Working of this set-up is discussed next.

### 5.2 Working of the set-up

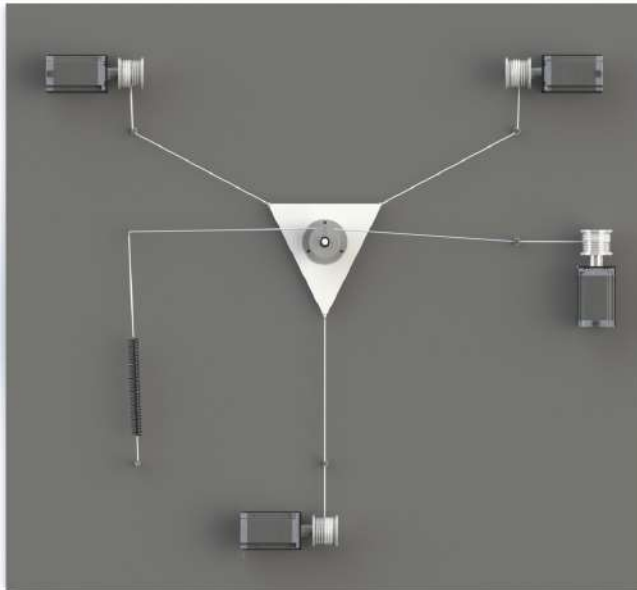
The spool is firmly attached to the platform using three set-screws to arrest its independent rotation. Platform's restriction to the rotation of the spool results in the moment load on the

platform. An attempt to rotate the spool counter-clockwise results in the positive moment load on the platform. Conversely, an attempt to rotate the spool clockwise results in the negative moment load on the platform. Let us consider a case without the moment load on the platform. For this, magnitude of  $\mathbf{T}_s$  and  $\mathbf{T}_r$  must be equal.

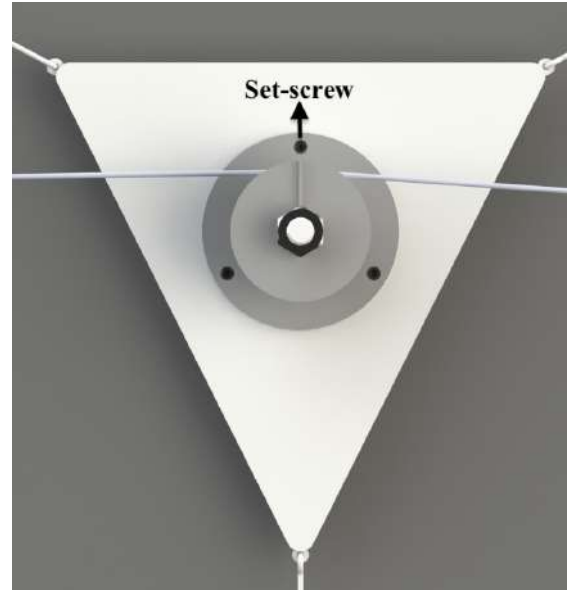
$$T_s = T_r = k(\Delta s) \quad (5.1)$$

$$\Delta s = \delta - r_p \phi + \sqrt{(y + r_p - y_s)^2 + (x - x_s)^2} - \sqrt{(r_p - y_s)^2 + (x_s)^2} \quad (5.2)$$

where  $\phi$  is the orientation of the spool (i.e., platform's orientation) and all other variables are the same as considered for Eqs. 4.1 and 4.2. Load vector  $\mathbf{f}$  is updated to  $\hat{\mathbf{f}}$  using Eqs. 4.3 – 4.5. Tension vector  $\mathbf{t}$  is obtained from static equilibrium equation given by Eq. 4.6. This is illustrated in Table 5.1 with the help of two examples.



(a) Top view of the set-up



(b) Spool is arrested to the platform

Figure 5.1: Platform's centroid is located at  $(0, 0)$  and its orientation is  $0^\circ$

Table 5.1: Cable forces of the three-cable robot when there is no moment load on the platform

No.	Variables	Configuration 1	Configuration 2
1	$(x_{fi}, y_{fi})$ where $(i = 1, 2, 3)$	$(30, 17.32)$ $(0, -34.64)$ $(-30, 17.32)$	$(30, 17.32)$ $(0, -34.64)$ $(-30, 17.32)$
2	$(P_{i0x}, P_{i0y})$	$(9, 6)$ $(0, -12)$ $(-9, 6)$	$(9, 6)$ $(0, -12)$ $(-9, 6)$
3	$(x, y)$	$(4, 3)$	$(-4, -3)$
4	$\phi$	$10^\circ$	$-10^\circ$
5	$\mathbf{f}$	$\begin{Bmatrix} 0 \\ -1 \\ 0 \end{Bmatrix}$	$\begin{Bmatrix} 0 \\ -1 \\ 0 \end{Bmatrix}$
6	$k$	3	3
7	$\delta$	10	10
8	$r_p$	2.13	2.13
9	$(x_s, y_s)$	$(-30, 0)$	$(-30, 0)$
10	$(x_r, y_r)$	$(30, 0)$	$(30, 0)$
11	$\Delta s$	13.94	6.31
12	$T_s$	41.81	18.93
13	$T_r$	41.81	18.93

Continued on the next page

Table 5.1 – continued from the previous page

No.	Variables	Configuration 1	Configuration 2
14	$\theta_s$	$-171.39^\circ$	$178.08^\circ$
15	$\theta_r$	$-11.22^\circ$	$1.47^\circ$
16	$\beta_1$	$3.58^\circ$	$-4.69^\circ$
17	$\beta_2$	$4.69^\circ$	$-3.58^\circ$
18	$\hat{\mathbf{f}}$	$\begin{Bmatrix} -0.33 \\ -15.39 \\ 0 \end{Bmatrix}$	$\begin{Bmatrix} 0 \\ 0.12 \\ 0 \end{Bmatrix}$
19	$\mathbf{L}$	$\begin{bmatrix} 0.94 & -0.23 & -0.92 \\ 0.35 & -0.97 & 0.38 \\ -4.23 & -4.74 & 0.23 \end{bmatrix}$	$\begin{bmatrix} 0.83 & 0.29 & -0.82 \\ 0.55 & -0.96 & 0.58 \\ 1.85 & 5.46 & 1.59 \end{bmatrix}$
20	$\mathbf{t}$	$\begin{Bmatrix} 9.50 \\ -7.95 \\ 11.24 \end{Bmatrix}$	$\begin{Bmatrix} -0.08 \\ 0.04 \\ -0.06 \end{Bmatrix}$

Negative values of cable forces indicate that the configurations are not in static equilibrium. Now, consider a case where moment load is applied on the platform. Note that  $T_s$  depends on spring stiffness and the elongation of the spring. For the application of a specific moment load ( $M$ ),  $T_r$  must be chosen appropriately. The relationship between  $M$ ,  $T_r$ ,  $T_s$ , and  $r_p$  is given as follows.

$$M = (T_s - T_r) r_p \quad (5.3)$$

The preceding equation can be rewritten as

$$T_r = T_s - \frac{M}{r_p} \quad (5.4)$$

If  $M$  is positive,  $T_r$  must satisfy the condition given below.

$$T_s > T_r \geq \frac{T_s}{e^{\mu'\theta_l}} \quad (5.5)$$

where  $\theta_l = 2\pi n_w + \beta_1 + \beta_2$ .  $\mu'$  is the coefficient of static friction between the cable and the spool.  $n_w$  is the number of windings of the cable on the spool. Condition given by Eq. 5.5 must be satisfied in order to prevent the cable from slipping on the surface of the spool because of lack of sufficient frictional force. For negative moment load, condition for  $T_r$  is given below.

$$T_s e^{\mu'\theta_l} \geq T_r > T_s \quad (5.6)$$

Eq. 5.6 serves the same purpose as Eq. 5.5 when a negative moment load is applied on the platform. After obtaining  $T_s$  and  $T_r$ , the load vector is updated using Eq. 4.3. From static equilibrium equations, the tension vector is calculated as per the Eq. 4.6. This procedure is illustrated with the help of two examples in Table 5.2.

Table 5.2: Cable forces of the robot when a moment load is applied on the platform

No.	Variables	Configuration 1	Configuration 2
1	$(x_{fi}, y_{fi})$ where $(i = 1, 2, 3)$	(30, 17.32) (0, -34.64) (-30, 17.32)	(30, 17.32) (0, -34.64) (-30, 17.32)

Continued on the next page

Table 5.2 – continued from the previous page

No.	Variables	Configuration 1	Configuration 2
2	$(P_{i0x}, P_{i0y})$	(9,6) (0, -12) (-9,6)	(9,6) (0, -12) (-9,6)
3	$(x, y)$	(3,5)	(3,-5)
4	$\phi$	20°	-2°
5	$\mathbf{f}$	$\begin{Bmatrix} 0 \\ 0 \\ 0 \end{Bmatrix}$	$\begin{Bmatrix} 0 \\ 0 \\ 0 \end{Bmatrix}$
6	$k$	3	3
7	$\delta$	10	10
8	$r_p$	2.13	2.13
9	$(x_s, y_s)$	(-30,0)	(-30,0)
10	$(x_r, y_r)$	(30,0)	(30,0)
11	$M$	3	-2
12	$n_w$	3	3
13	$\mu'$	0.1	0.1
14	$\Delta s$	12.94	13.12
15	$T_s$	38.83	39.37
16	$T_r$	37.42	40.31

Continued on the next page

Table 5.2 – continued from the previous page

No.	Variables	Configuration 1	Configuration 2
17	$\beta_1$	3.66°	−3.66°
18	$\beta_2$	4.45°	−4.45°
19	$\theta_l$	1088.10°	1071.9°
20	$\hat{\mathbf{f}}$	$\begin{Bmatrix} -1.78 \\ -17.83 \\ 3 \end{Bmatrix}$	$\begin{Bmatrix} 0.86 \\ 7.65 \\ -2 \end{Bmatrix}$
21	$\mathbf{L}$	$\begin{bmatrix} 0.99 & -0.24 & -0.92 \\ 0.17 & -0.97 & 0.40 \\ -7.48 & -6.72 & -1.84 \end{bmatrix}$	$\begin{bmatrix} 0.73 & -0.14 & -0.83 \\ 0.68 & -0.99 & 0.55 \\ 2.14 & -1.32 & 0.42 \end{bmatrix}$
22	$\mathbf{t}$	$\begin{Bmatrix} 8.85 \\ -12.36 \\ 10.84 \end{Bmatrix}$	$\begin{Bmatrix} 12.07 \\ 20.55 \\ 8.04 \end{Bmatrix}$

Positive cable forces in configuration 2 indicate that the platform is in static equilibrium. For a given moment load at a point, there may be multiple feasible orientations of the platform. To find these orientations,  $\phi$  is varied from  $-180^\circ$  to  $180^\circ$  similar to the procedure discussed in Section 3.2, with a slight modification:  $\hat{\mathbf{f}}$  is used instead of  $\mathbf{f}$ . Note that  $\hat{\mathbf{f}}$  varies with  $M$ . For the configuration 1 in Table 5.2, feasible orientations of the platform are  $-180^\circ$ ,  $-179^\circ$ ,  $0^\circ$ ,  $179^\circ$ , and  $180^\circ$ . For the configuration 2, they vary from  $-6^\circ$  to  $-1^\circ$  and then from  $178^\circ$  to  $179^\circ$ .

### 5.3 Platform tracing a prescribed trajectory with a specified moment load on it

Here, a path consisting of discrete waypoints to be traced by the moving platform is considered. Moment ( $M$ ) is applied on the platform while it is tracing the path. At every waypoint, for

every orientation, values of  $T_s$  and  $T_r$  are calculated. Load vector  $\mathbf{f}$  is updated to  $\hat{\mathbf{f}}$  using Eq. 4.3. Optimal  $\phi$  of the platform is obtained as per the procedure discussed in Section 3.5.1. To illustrate this, we consider an example where the platform of three-cable robot is required to trace a path along the  $x$ -axis. The path is made up of 15 equidistant points between the points  $(-5, -5)$  and  $(5, -5)$  including them. Parameters of the three-cable robot are provided in Table 5.3. For this example, we consider the minimum  $\|\mathbf{t}\|$  as the criteria for obtaining the optimal orientations. Figs. 5.2 – 5.5 present the simulated task at four-waypoints. Fig. 5.6 indicates minimum tensions in the cables and Fig. 5.7 presents the updated load vector at every waypoint. Optimal orientations of the platform chosen for minimum tensions in the cables are shown in Fig. 5.8.

Table 5.3: Parameters of the cable robot used for simulation

No.	Variables	Values
1	$(x_{fi}, y_{fi})$ where $(i = 1, 2, 3)$	$(30, 17.32)$ $(0, -34.64)$ $(-30, 17.32)$
2	$(P_{i0x}, P_{i0y})$	$(9, 6)$ $(0, -12)$ $(-9, 6)$
3	$\mathbf{f}$	$\begin{Bmatrix} 0 \\ 0 \\ 0 \end{Bmatrix}$
4	$k$	3
5	$\delta$	10
6	$r_p$	2.13
Continued on the next page		

Table 5.3 – continued from the previous page

No.	Variables	Values
7	$(x_s, y_s)$	$(-30,0)$
8	$(x_r, y_r)$	$(30,0)$
9	$M$	2
10	$n_w$	3
11	$\mu'$	0.1

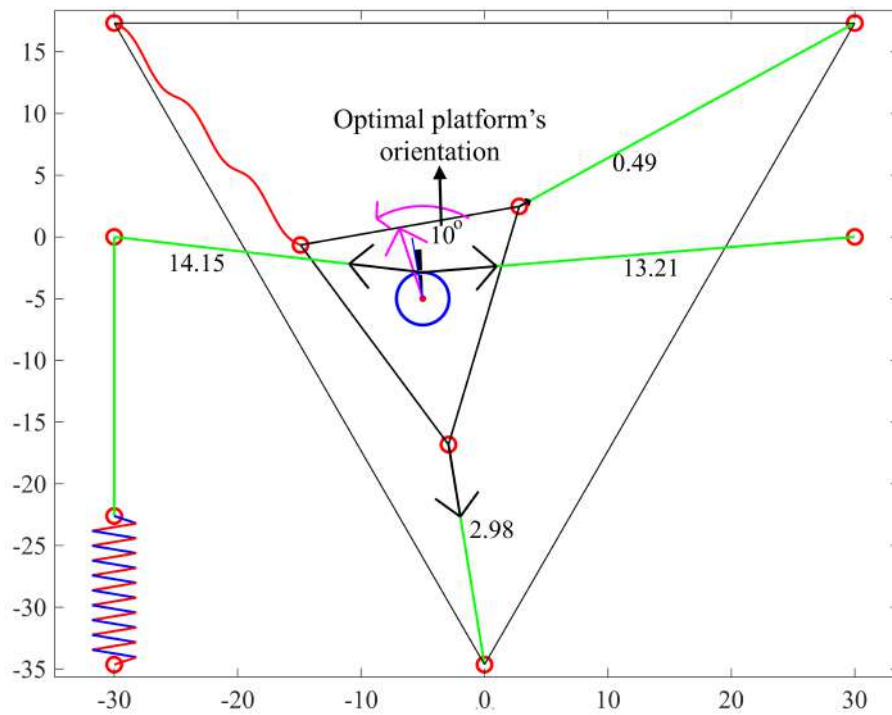


Figure 5.2: Platform's centroid is located at  $(-5,-5)$

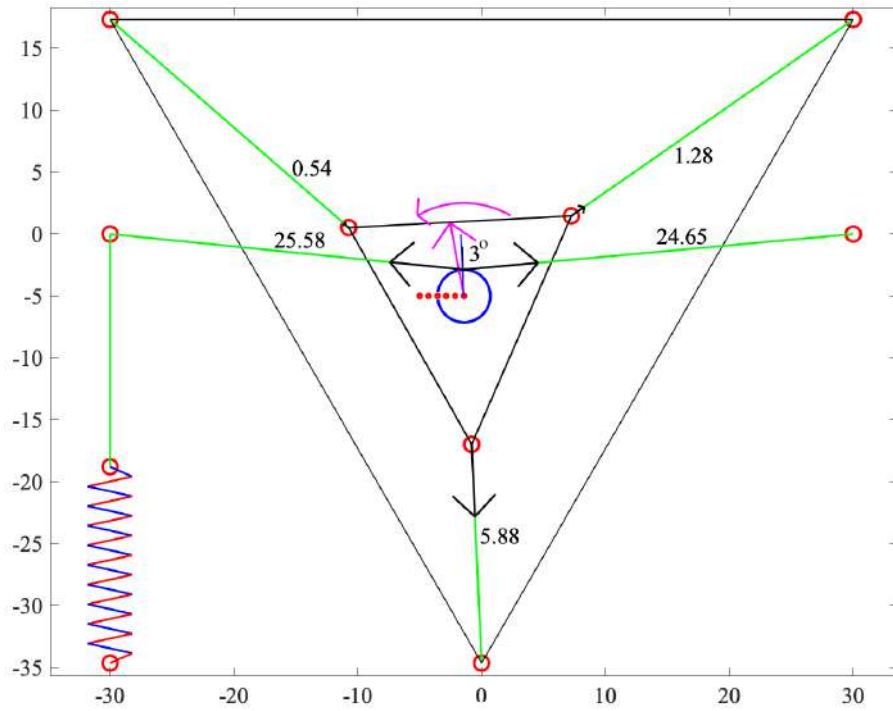


Figure 5.3: Platform's centroid is located at  $(-1.43, -5)$

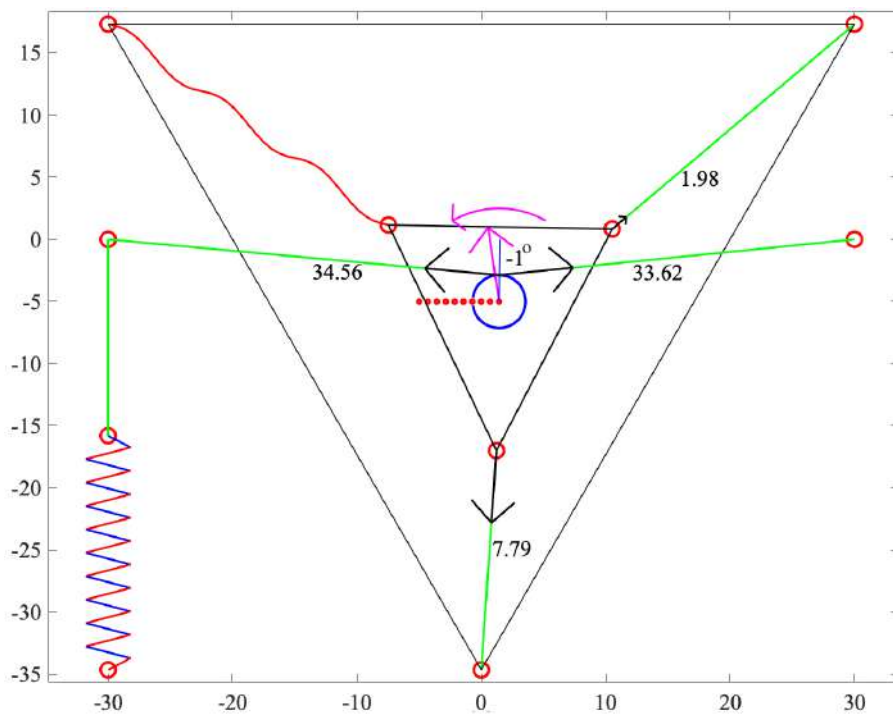


Figure 5.4: Platform's centroid is located at  $(1.43, -5)$

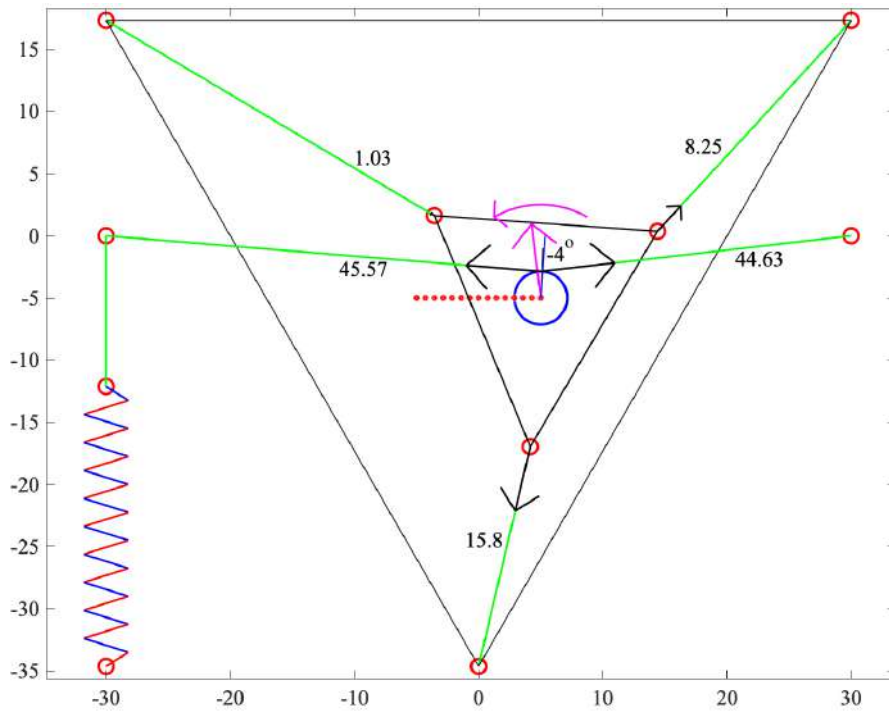


Figure 5.5: Platform's centroid is located at (5,-5)

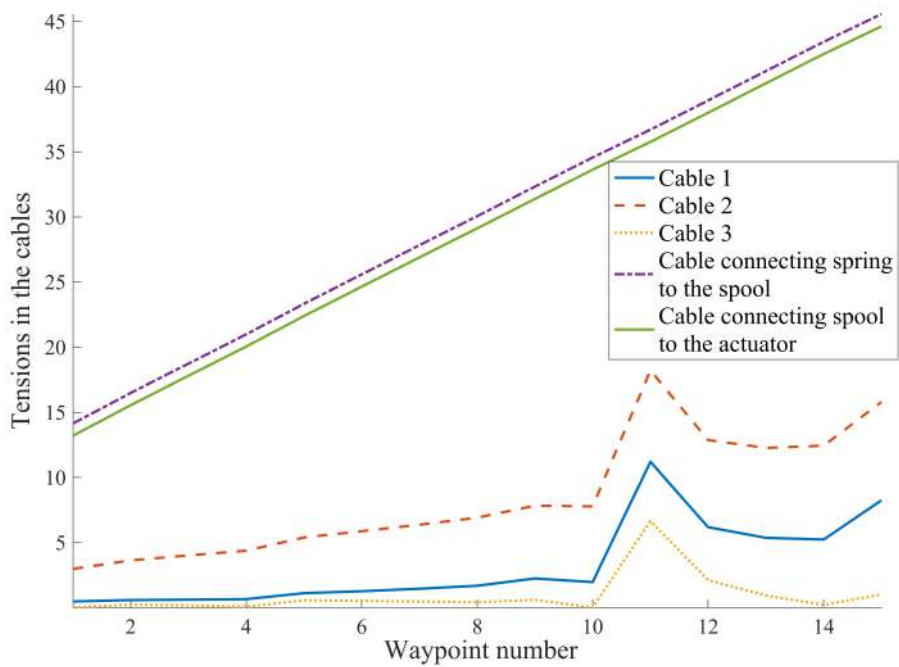


Figure 5.6: Minimum tensions in the cables

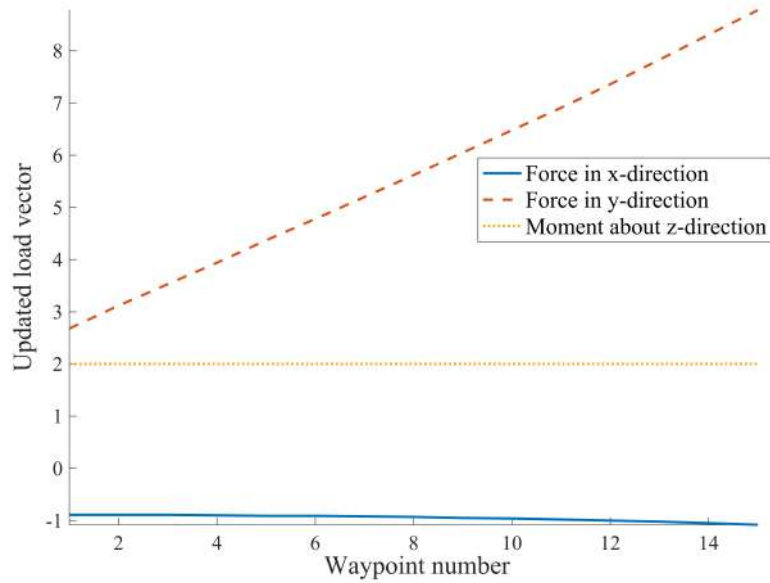


Figure 5.7: Updated load vector  $\hat{\mathbf{f}}$  at every waypoint

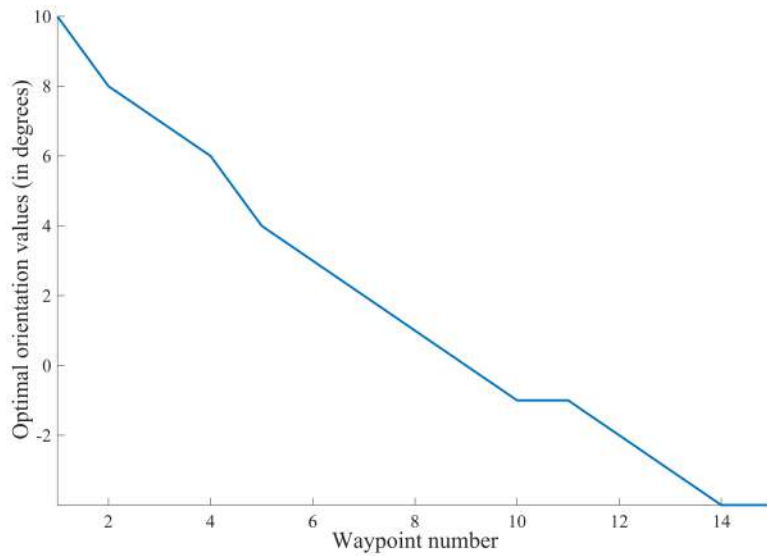


Figure 5.8: Optimal orientation of the platform for the minimum  $\|\mathbf{t}\|$  at every waypoint

## Closure

The set-up used for enhancing the orientability of the cable robot is modified for the application of moment load on the platform in this chapter. Equations relating the moment load to cable tensions are derived. The cases considered here are that of no moment load, a specific moment load, and a path with specified moment loads. Examples are provided for all cases.

# Chapter 6

## Prototyping

### Summary

In this chapter, we validate the mathematical models (presented in Chapters 3 and 4) by experimenting on the prototype of a three-cable robot. Orientability limits obtained from the MATLAB simulations are compared with those obtained from the experiments. Using the technique proposed in Chapter 4, we verify that the orientability of the three-cable robot can be improved significantly by modifying the set-up.

### 6.1 Prototype of the three-cable robot

Every physical system is influenced by its environment while it also influencing the environment. There can be arbitrarily large number of influences or inputs to a physical system and a large number of corresponding responses or outputs from the physical system. It might not be practical to store all possible combinations of inputs and outputs. In such cases, we cannot find inputs required for the desired outputs from lookup tables. We solve this problem by creating a mathematical model whose behavior is similar to the physical system. The model can predict the output for any input. It is often more practical to store the parameters of the mathematical model rather than the lookup tables. In the process of building a simple and efficient mathematical model, we select only the most important features and ignore the minor features. The model can fail for many reasons like misidentification of the underlying physics, ignoring important features, and so on. To prove that the mathematical model closely resembles the physical system, we compare both the responses to a wide variety of inputs. If the responses of the physical system closely resemble the responses of the model, we can go on to assume that for any combination of the given inputs, the mathematical model will have a response similar to the physical system. Physical systems of interest to us are the cable robots.

Validation of the mathematical models of the cable robots is done by experimenting with the actual prototype.

Fig. 6.1 shows the prototype of a three-cable robot built at M2D2 Lab for the purpose of validating the models presented in this thesis. A smartphone (iPhone 7) is attached to the platform for the purpose of measuring the orientation of the platform. Its weight is considered in the corresponding simulation. The robot has an open-loop position control system. Parameters of the robot are provided in Table 6.1. Details of the components used for building the prototype are provided in Table 6.2.

Table 6.1: Parameters of the three-cable robot

No.	$(x_{fi}, y_{fi})$	$(P_{i0x}, P_{i0y})$	$\mathbf{f}$
1	(30, 17.32)	(7, 4.67)	$\left\{ \begin{array}{c} 0 \\ -8.81 \\ 0 \end{array} \right\}$
	(0, -34.64)	(0, -9.33)	
	(-30, 17.32)	(-7, 4.67)	

Table 6.2: Components used for building the prototype

No.	Component/Part	Specifications
1	Microcontroller board	Arduino MEGA 2560
2	Micro-stepping motor driver	TB6560
3	DC stepper motor	NEMA-23, holding torque 1.89N-m at 2.8A/phase
4	Power supply	12V 5A 60W SMPS Unit
5	Base plate	Mild steel (1m x 1m x 2.2mm)
6	Triangular platform	Stainless steel (14cm x 14cm x 10.6mm)
7	Platform's weight	0.761kg

Continued on the next page

Table 6.2 – continued from the previous page

No.	Component/Part	Specifications
8	Cables used	Synthetic tennis gut (nylon), dia = 1.56mm
9	Pulley (winch) Aluminium alloy	OD = 42.60mm, pitch = 4mm number of threads = 8, and thread angle = 60°

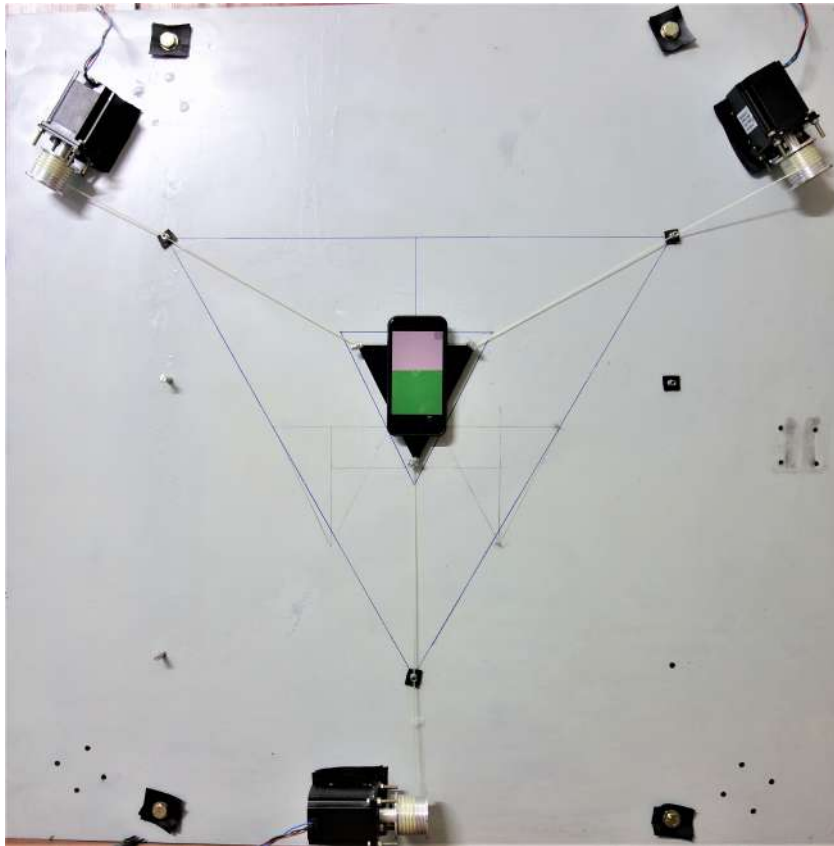


Figure 6.1: Prototype of the three-cable robot built at M2D2 Lab

## 6.2 Experimenting on the prototype

This section contains the comparison between the MATLAB simulations and actual experiments. Feasible orientations of the triangular platform are obtained at different points in the workspace. This is done in simulations as well as in the experiments. The procedure used to

obtain feasible orientations using simulations has been explained in Section 3.2. The procedure used for measuring the range of feasible orientations using the experiments is described next.

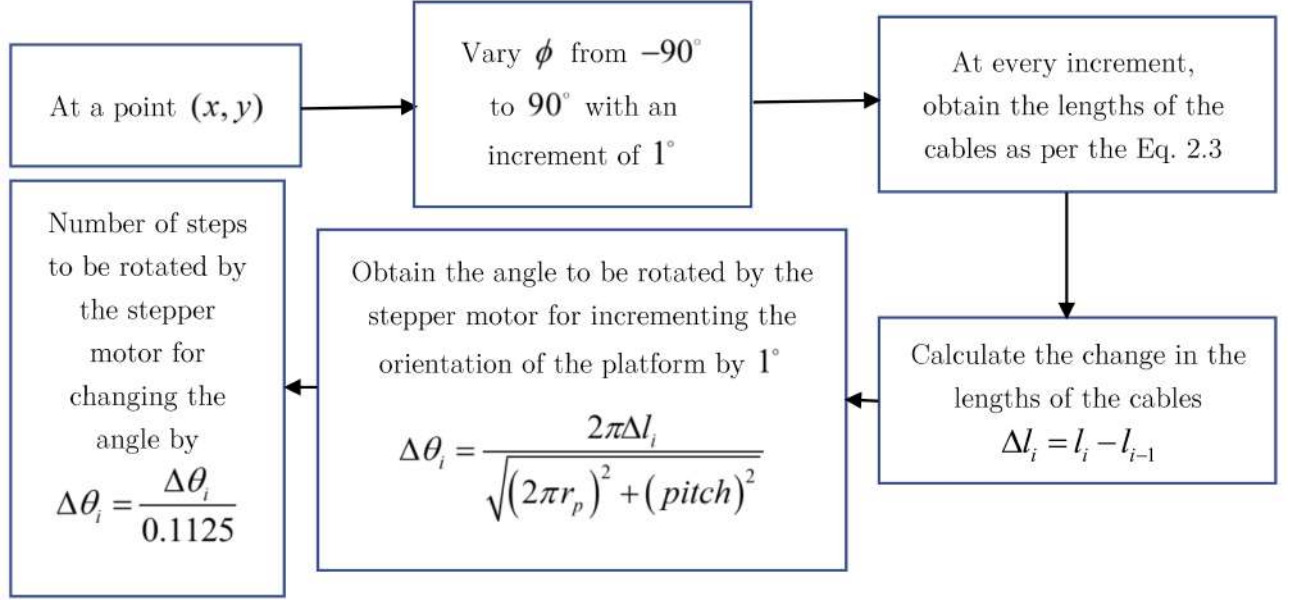


Figure 6.2: Procedure for obtaining the number of steps of the stepper motors for incrementing the orientation of the platform by 1°

The angle of rotation,  $\phi$  is varied from  $-90^\circ$  to  $90^\circ$  (instead of  $-180^\circ$  to  $180^\circ$ ) in order to avoid the interference of the cables with the platform and the other cables. It is not practical to orient the platform beyond  $-90^\circ$  to  $90^\circ$  range using the only cables. The value 0.1125 in Fig. 6.2 indicates the angle (in degrees) that the stepper motor rotates per step. The procedure shown in Fig. 6.2 is used for generation of a data file that contains the number of steps required by stepper motors for every  $1^\circ$  increment in the orientation of the platform. Fig. 6.3 shows the schematic of the experimental set-up. The data file generated in the computer is fed to the Arduino microcontroller, which regulates the stepper motors.

As discussed previously, there are limits to the orientability of the platform at every point in the workspace. It is observed during the experiment that when an attempt is made to orient the platform to an angle outside the permissible range at a point, the platform moves away from that point. This phenomena is used to identify the experimental limits of orientability. Experimental limits are obtained at three different points in the workspace. Table 6.3 contains the comparison of these experimental limits with the corresponding limits obtained from simulations. The discrepancy in the data could be attributed to various factors. Some of the observable factors

include inaccuracies in manufactured dimensions, bending stiffness of the cables, etc.

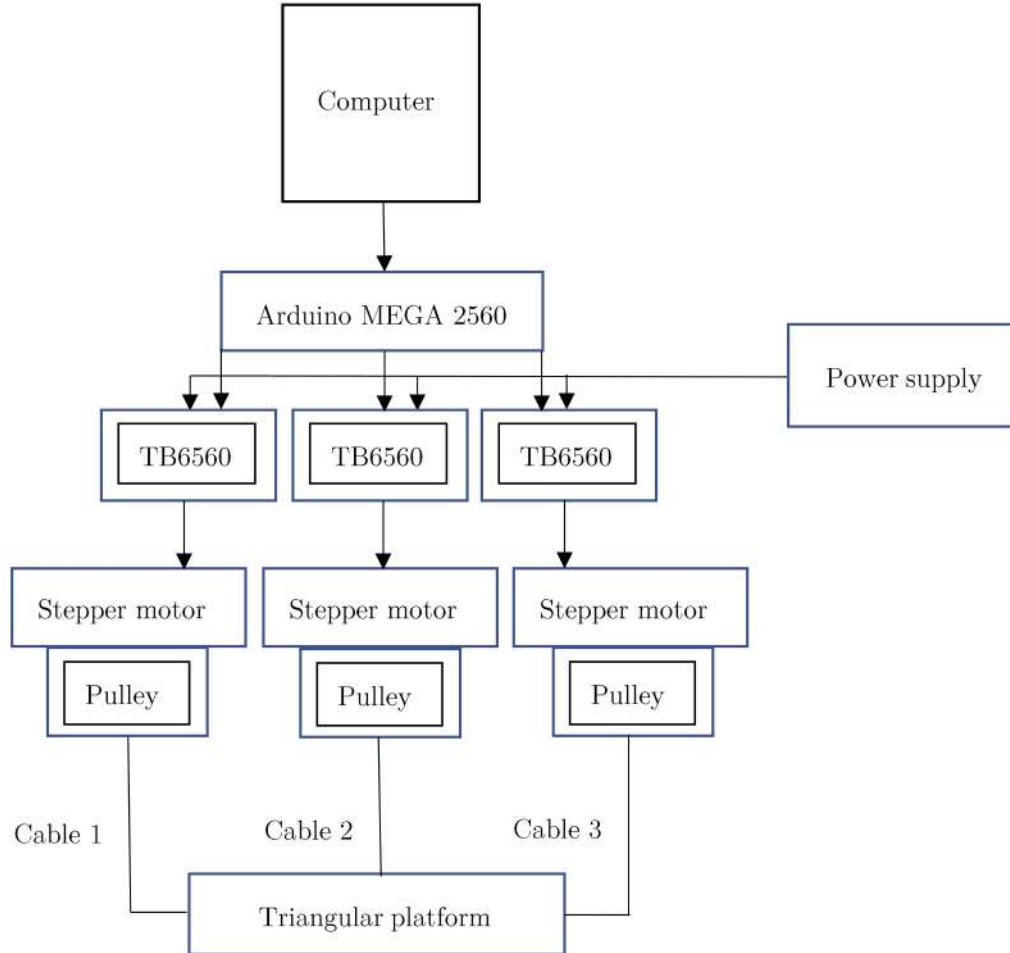


Figure 6.3: Schematic of the experimental set-up

Table 6.3: Comparison of the experimental orientability limits with the corresponding limits obtained from simulations at three different points

No.	$(x, y)$	Simulation	Experiment
1	(0,0)	0°	0°
2	(10,-10)	-2° to 12°	-1° to 8°
3	(-10,-10)	-12° to 2°	-9° to 1°

### 6.3 Prototype with additional rotary DoF

This section contains a comparison of the feasible orientations between simulations and experiments at four different points in the workspace. We demonstrate that the orientability of the cable robot can be enhanced by modifying the set-up using the technique proposed in Chapter 4. Parameters of the three-cable robot (used in this example) are provided in Table 6.4. Orientability limits from the experiments and simulations are juxtaposed in Table 6.5.

The modified set-up for enhanced orientability is shown in Fig. 6.4. It involves an appendage of a spool, a translational spring, an additional cable, and a rotary actuator to the existing set-up. The spool (OD = 42.60mm, pitch = 4mm, number of threads = 10, and thread angle = 60°) is attached to the center of the platform with a pin joint, allowing it to rotate freely w.r.t. the platform. A fourth cable is wound on the spool. Its one end is attached to an additional NEMA-23 stepper motor. Its other end is attached to a fixed point with a tension spring. Initial elongation ( $\delta$ ) of the spring is 16cm and its stiffness ( $k$ ) is 0.66N/cm.

Table 6.4: Parameters of the three-cable robot

No.	$(x_{fi}, y_{fi})$	$(P_{i0x}, P_{i0y})$	$\mathbf{f}$
1	(30, 17.32)	(9, 6)	$\left\{ \begin{array}{c} 0 \\ -3.43 \\ 0 \end{array} \right\}$
	(0, -34.64)	(0, -12)	
	(-30, 17.32)	(-9, 6)	

Table 6.5: Orientability limits from the experiments and simulations

No.	$(x, y)$	Simulation	Experiment
1	(5,6)	0° to 2°	0° to 1°
2	(-5,6)	-2° to 0°	-1° to 0°
3	(5,0)	0° to 3°	0° to 3°
Continued on the next page			

Table 6.5 – continued from the previous page

No.	$(x, y)$	Simulation	Experiment
4	$(-5, 0)$	$-3^\circ$ to $0^\circ$	$-2^\circ$ to $0^\circ$

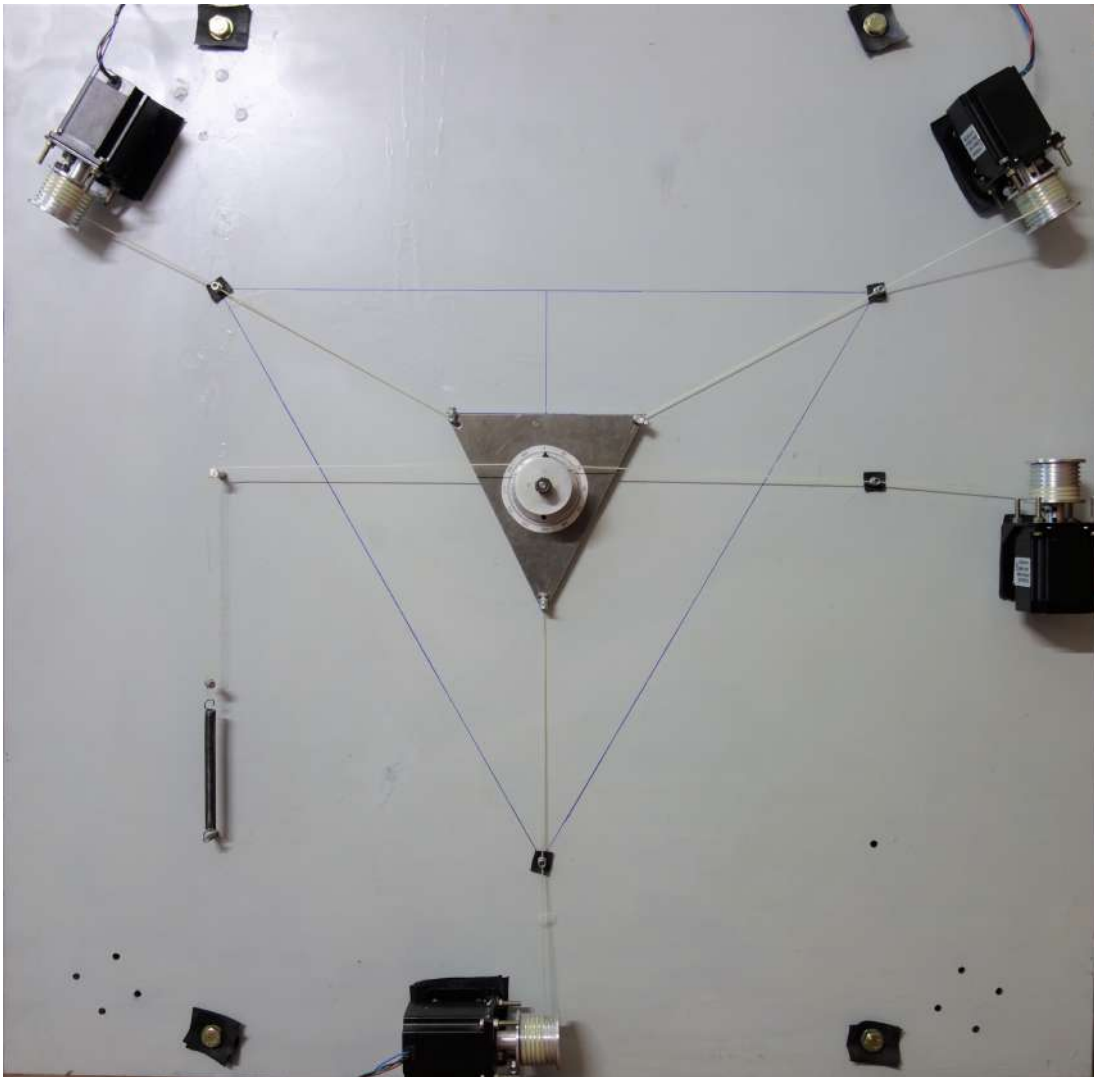


Figure 6.4: Prototype of the three-cable robot with additional rotary degree of freedom

The experimental procedure is as follows. Since  $0^\circ$  orientation of the platform is feasible at all the four points, the platform is placed at each point with  $0^\circ$  orientation. To find the range of orientability of the spool at these points, it is rotated to maximum possible angle in either directions. Fig. 6.5 shows the method for calculating the number of steps required

by the stepper motor for incrementing the orientation of the spool by  $1^\circ$ . It is observed that the spool can be rotated from  $-180^\circ$  to  $180^\circ$  at all the four points. This observation cannot be generalized to the entire workspace. Nonetheless, there is a significant improvement in the orientability of the cable robot in most of the workspace (after the modification of the set-up). This technique can also be applied for orientability enhancement of robots with more cables.

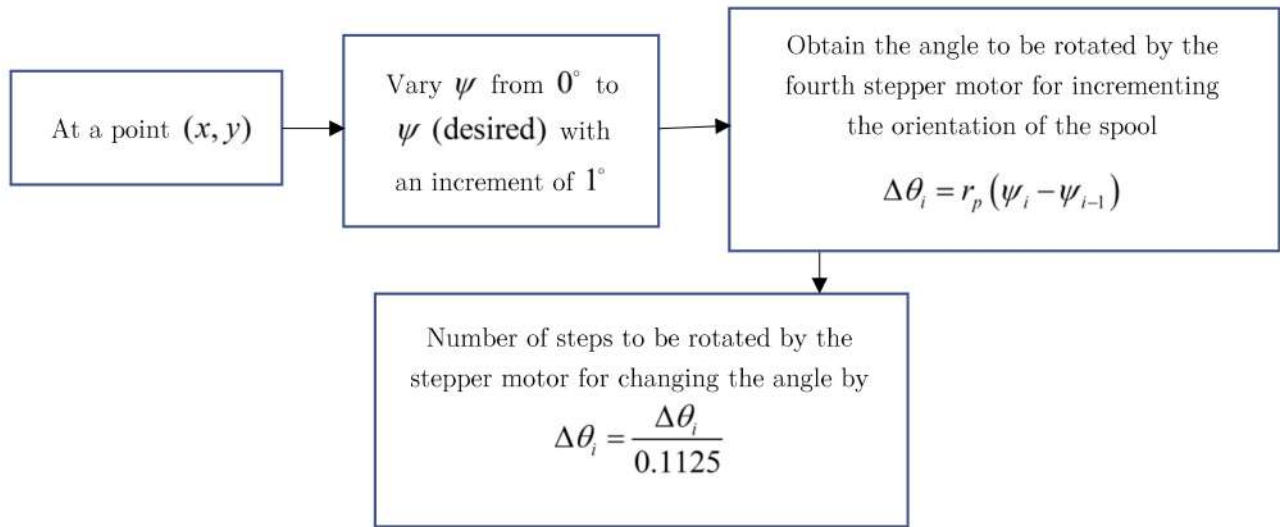


Figure 6.5: Procedure for obtaining the number of steps of the stepper motor for incrementing the orientation of the spool by  $1^\circ$

## Closure

Orientability limits of the triangular platform between the simulations and experiments are compared. It is shown that the orientability of the platform is limited with the aid of both the experiments and simulations. To overcome this, we modified the prototype using the proposed technique. It is confirmed that the orientability can be significantly improved by implementing the technique.

# Chapter 7

## Closure and Future perspectives

### 7.1 Summary of the work done

- The focus of this thesis is to reveal the limited orientability of cable robots and suggest a method to enhance it. Towards this, the following investigations were conducted.
- A procedure to obtain tension vectors for different cases of planar cable robots is discussed. To confirm the feasibility of the pose of the platform, one has to go through the tedious process of obtaining the tension vector with non-negative elements. To circumvent this, an alternate approach (i.e., the determinant approach) that confirms the feasibility of the pose of the platform (with the aid of nullspace) is discussed.
- The determinant approach is used for obtaining the feasible orientations of the moving platform that allows it to be in static equilibrium at a point in the workspace of the cable robot. Feasible orientations are obtained not only at a single point, but also at multiple points. For this purpose, a grid is defined with uniform step size along both  $x$  and  $y$  axes. It is confined to the rectangular region within the specified lower and upper limits of  $x$  and  $y$  values. At every point in the grid, the determinant approach is implemented to obtain the feasible orientations.
- Examples of three and four-cable robots are considered. Feasible orientations of the platforms are obtained at multiple points in a space of interest. With the example of the three-cable robot, it is shown that the nature of the load acting on the platform influences the orientability of the platform. And it is observed that feasible orientations always lie in the direction of the load acting on the platform. Furthermore, when a moment load is acting on the platform, feasible orientations are confined within the convex hull of the

fixed pivots.

- With the example of the four-cable robot, it is shown that as the number of cables increases, the orientability of the platform increases. Additionally, it is shown that the size and shape of the platform play an important role in the behaviour of the feasible orientations.
- A fully constrained configuration of the cable robot is explained in detail. Feasible orientations that fully constrain the cable robot are obtained at multiple points in a space of interest. Here, load (acting on the platform) does not have any role in the behaviour of the feasible orientations. It is revealed with the examples of four and five-cable robots that the feasible orientations that fully constrain the cable robot are confined within the convex hull of the fixed pivots. It is also observed that they are a subset of those that are required to keep the cable robot in static equilibrium. Furthermore, the size and shape of the platform play an important role in the behaviour of the feasible orientations that fully constrain the cable robot. It is noted that as the number of cables increases, the orientability of the platform increases as observed in the case of static equilibrium.
- A path comprising a finite number of waypoints is given to the moving platform of the cable robot. We have discussed the two ways of tracing the trajectory. The first case deals with obtaining an optimal orientation of the platform at every waypoint to achieve maximum or minimum tensions in the cables at that point. In the second case, we specified the desired orientation for the platform at every waypoint. Examples of five and six-cable robots are provided.
- At every point in the workspace, depending on the nature of the load and geometry of the cable robot, there is a limit to the range within which the platform can rotate. Although a cable robot with more cables increases the orientability of the platform, this enhanced range does not guarantee the full orientability of the platform i.e., the platform cannot be oriented with any angle between  $0^\circ$  and  $360^\circ$ . This problem of the limited range is solved by adding a rotary degree of freedom on the moving platform. It involves the addition of a motor, an extra cable, a spring, and a spool to the three-cable robot. Examples of a three-cable robot are considered. This is because a three-cable robot has highly restricted orientability as compared to a four-cable robot, a five-cable robot, and so on. It is shown that there is a significant improvement in the orientability of the three-cable robot after the modification.

- The set-up used for enhancing the orientability of the cable robot can also be used to apply or support a moment load on the moving platform with a slight modification. The modification of the set-up involves arresting the spool to the platform using set-screws. The equations governing for the application of a specific moment load and the corresponding examples are presented. Furthermore, a simulated task where the platform of the three-cable robot was made to trace a path with a moment load specified along the path.
- Mathematical models were validated by conducting experiments on the prototype of a three-cable robot. Orientability limits obtained from simulations are compared with those obtained from the experiments. It is verified that the orientability of the cable robot can be improved by modifying the set-up of the three-cable robot.

## 7.2 Contributions

- It was demonstrated that the orientability of the moving platform of cable robots is limited. The orientability of the platform is studied for different cases.
- A method is proposed to enhance the orientability of cable robots using an additional cable, a spring, a spool, and a motor.
- The method of enhancing the orientability is also used to create an external moment load on the moving platform.

## 7.3 Future perspectives

- In this thesis, an exhaustive numerical approach was implemented to find the extent of the orientability of the moving platform. It is beneficial if the limits of the orientability of the moving platform are obtained analytically or semi-analytically.
- It is useful if a design procedure is developed for a planar cable robot for specified limits of orientation in a given workspace.
- Extending the planar cable robot concepts developed in this thesis to spatial cable robots is the next natural step.

# Appendix

OneDrive links of the MATLAB scripts are provided here:

[https://indianinstituteofscience-my.sharepoint.com/:u:/g/personal/vikranthk\\_iisc\\_ac\\_in/EUttgR-cC0dBhWfsRRJrWzoBVx8IFDfQii4n1AxRDV9Z8A?e=SBZBmI](https://indianinstituteofscience-my.sharepoint.com/:u:/g/personal/vikranthk_iisc_ac_in/EUttgR-cC0dBhWfsRRJrWzoBVx8IFDfQii4n1AxRDV9Z8A?e=SBZBmI)

For obtaining the feasible range of  $\alpha$  (for the examples of four and five-cable robots provided in Section 3.1)

[https://indianinstituteofscience-my.sharepoint.com/:u:/g/personal/vikranthk\\_iisc\\_ac\\_in/EYzwiwA6PdNKvkEAl0IhwxBCEkXthiAs6q2j0Gv6BjVeg?e=ZNqFnA](https://indianinstituteofscience-my.sharepoint.com/:u:/g/personal/vikranthk_iisc_ac_in/EYzwiwA6PdNKvkEAl0IhwxBCEkXthiAs6q2j0Gv6BjVeg?e=ZNqFnA)

For obtaining feasible orientations at a point in the workspace of the planar cable robot (for the example of a three-cable robot provided in Section 3.2)

[https://indianinstituteofscience-my.sharepoint.com/:u:/g/personal/vikranthk\\_iisc\\_ac\\_in/EQFsLNU14WR0itsKyXE-DM4BwTv-7xQ0Gy0xv12kYU\\_h2Q?e=2TYkpn](https://indianinstituteofscience-my.sharepoint.com/:u:/g/personal/vikranthk_iisc_ac_in/EQFsLNU14WR0itsKyXE-DM4BwTv-7xQ0Gy0xv12kYU_h2Q?e=2TYkpn)

For obtaining feasible orientations at multiple points in a space of interest for both the cases i.e., static equilibrium and fully constrained configuration of the cable robot (for the examples provided in Sections 3.3 and 3.4)

[https://indianinstituteofscience-my.sharepoint.com/:u:/g/personal/vikranthk\\_iisc\\_ac\\_in/EeHBj4lq3QdHlf2I6NB8zfsB-zsjfX4EiksvtLG7l9ec-A?e=kXTLFG](https://indianinstituteofscience-my.sharepoint.com/:u:/g/personal/vikranthk_iisc_ac_in/EeHBj4lq3QdHlf2I6NB8zfsB-zsjfX4EiksvtLG7l9ec-A?e=kXTLFG)

Platform tracing a path with an optimal orientation at every waypoint (for the example provided in Section 3.5.1)

[https://indianinstituteofscience-my.sharepoint.com/:u:/g/personal/vikranthk\\_iisc\\_ac\\_in/EShnYY-8lkJI1v\\_Lmc2uQ2MB4JW2AHdGNh7tfC00vHFg0g?e=YOQwbN](https://indianinstituteofscience-my.sharepoint.com/:u:/g/personal/vikranthk_iisc_ac_in/EShnYY-8lkJI1v_Lmc2uQ2MB4JW2AHdGNh7tfC00vHFg0g?e=YOQwbN)

Platform tracing a path with a desired orientation at every waypoint (for the example provided in Section 3.5.2)

## Appendix

[https://indianinstituteofscience-my.sharepoint.com/:u:/g/personal/vikranthk\\_iisc\\_ac\\_in/EVeiHm2F9kFHoH37\\_efPZnsBeU-DL99LqrbizODGgAA8xQ?e=W0A1Rg](https://indianinstituteofscience-my.sharepoint.com/:u:/g/personal/vikranthk_iisc_ac_in/EVeiHm2F9kFHoH37_efPZnsBeU-DL99LqrbizODGgAA8xQ?e=W0A1Rg)

For the examples provided in Chapter 4

[https://indianinstituteofscience-my.sharepoint.com/:u:/g/personal/vikranthk\\_iisc\\_ac\\_in/ESu8xZfqfDxIgAZ-kLF4370BqwxQZP\\_XUJFCXsWZ576GVg?e=ZVTg1T](https://indianinstituteofscience-my.sharepoint.com/:u:/g/personal/vikranthk_iisc_ac_in/ESu8xZfqfDxIgAZ-kLF4370BqwxQZP_XUJFCXsWZ576GVg?e=ZVTg1T)

For the examples provided in Chapter 5

[https://indianinstituteofscience-my.sharepoint.com/:u:/g/personal/vikranthk\\_iisc\\_ac\\_in/ET7zvrN7G\\_JLrd\\_YW9R8W4ABqIo5XXXng-wSud4jjWKLRA?e=wg7nB](https://indianinstituteofscience-my.sharepoint.com/:u:/g/personal/vikranthk_iisc_ac_in/ET7zvrN7G_JLrd_YW9R8W4ABqIo5XXXng-wSud4jjWKLRA?e=wg7nB)

Arduino code for controlling three stepper motors

[https://indianinstituteofscience-my.sharepoint.com/:u:/g/personal/vikranthk\\_iisc\\_ac\\_in/EVx0ARRjL81MkF3PGm5nPh8BYnoTAeudxn5Q--4RWUualg?e=JrqJe9](https://indianinstituteofscience-my.sharepoint.com/:u:/g/personal/vikranthk_iisc_ac_in/EVx0ARRjL81MkF3PGm5nPh8BYnoTAeudxn5Q--4RWUualg?e=JrqJe9)

Arduino code for controlling four stepper motors

[https://indianinstituteofscience-my.sharepoint.com/:f:/g/personal/vikranthk\\_iisc\\_ac\\_in/EtWb9N2La0RNr49XUQH7pUoBjkNHQTPRvSu2nzXC7S5PA?e=ayiSy2](https://indianinstituteofscience-my.sharepoint.com/:f:/g/personal/vikranthk_iisc_ac_in/EtWb9N2La0RNr49XUQH7pUoBjkNHQTPRvSu2nzXC7S5PA?e=ayiSy2)

Experimental videos

# Bibliography

- [1] So-Ryeok Oh and Sunil Kumar Agrawal. Cable suspended planar robots with redundant cables: Controllers with positive tensions. *IEEE Transactions on Robotics*, 21(3):457–465, 2005. [1](#), [26](#), [31](#)
- [2] Jason Pusey, Abbas Fattah, Sunil Agrawal, and Elena Messina. Design and workspace analysis of a 6–6 cable-suspended parallel robot. *Mechanism and machine theory*, 39(7):761–778, 2004. [1](#), [28](#)
- [3] Abbas Fattah and Sunil K Agrawal. On the design of cable-suspended planar parallel robots. *Journal of mechanical design*, 127(5):1021–1028, 2005. [1](#), [25](#)
- [4] Abdullah B Alp and Sunil K Agrawal. Cable suspended robots: design, planning and control. 4:4275–4280, 2002.
- [5] Abbas Fattah and Sunil K Agrawal. Workspace and design analysis of cable-suspended planar parallel robots. In *ASME 2002 International Design Engineering Technical Conferences and Computers and Information in Engineering Conference*, pages 1095–1103. American Society of Mechanical Engineers, 2002. [25](#)
- [6] AB Alp and Sunil K Agrawal. Cable suspended robots: Feedback controllers with positive inputs. In *Proceedings of the 2002 American Control Conference (IEEE Cat. No. CH37301)*, volume 1, pages 815–820. IEEE, 2002. [1](#)
- [7] Nicholas G Dagalakis, James S Albus, B-L Wang, Joseph Unger, and James D Lee. Stiffness study of a parallel link robot crane for shipbuilding applications. *Journal of Offshore Mechanics and Arctic Engineering*, 111(3):183–193, 1989. [1](#), [2](#)
- [8] Sadao Kawamura et al. <sup>a</sup>development of an ultrahigh speed robot falcon using wire drive system<sup>o</sup>. *Robotics and Automation*, pages 215–220, 1995. [2](#), [5](#), [29](#)

## BIBLIOGRAPHY

- [9] T Higuchi. Application of multi-dimensional wire crane in construction. In *Proc. 5th Int. Symp. on Robotics in Construction*, volume 661, 1988. [2](#)
- [10] Wei-Jung Shiang, David Cannon, and Jason Gorman. Optimal force distribution applied to a robotic crane with flexible cables. In *Proceedings 2000 ICRA. Millennium Conference. IEEE International Conference on Robotics and Automation. Symposia Proceedings (Cat. No. 00CH37065)*, volume 2, pages 1948–1954. IEEE, 2000. [7](#)
- [11] Li-Farn Yang and MARTIN MIKULAS, JR. Mechanism synthesis and 2-d control designs of an active three cablecrane. In *33rd Structures, Structural Dynamics and Materials Conference*, page 2342, 1992. [2](#)
- [12] James Albus, Roger Bostelman, and Nicholas Dagalakis. The NIST robocrane. *Journal of Robotic Systems*, 1993. [2](#), [21](#), [28](#)
- [13] Roger Bostelman, James Albus, Nicholas Dagalakis, Adam Jacoff, and John Gross. Applications of the nist robocrane. In *Proceedings of the 5th International Symposium on Robotics and Manufacturing*, pages 14–18, 1994. [2](#)
- [14] Perry D Campbell, Patrick L Swaim, and Clark J Thompson. Charlotte™ robot technology for space and terrestrial applications. *SAE transactions*, pages 641–648, 1995. [2](#), [7](#), [49](#)
- [15] Frank Eichstadt, Perry Campbell, and Tim Haskins. Tendon suspended robots: Virtual reality and terrestrial applications. Technical report, SAE Technical Paper, 1995.
- [16] Lawrence L Cone. Skycam-an aerial robotic camera system. *Byte*, 10(10):122, 1985.
- [17] Kiyoshi Maeda, Satoshi Tadokoro, Toshi Takamori, Manfred Hiller, and Richard Verhoeven. On design of a redundant wire-driven parallel robot warp manipulator. In *Proceedings 1999 IEEE International Conference on Robotics and Automation (Cat. No. 99CH36288C)*, volume 2, pages 895–900. IEEE, 1999.
- [18] Tamio Aria, Hiroaki Yamaguchi, and Hisashi Osumi. *Assembly robot suspended by three wires with seven degrees of freedom*. Society of Manufacturing Engineers, 1990. [2](#), [7](#)
- [19] Bin Zi, BY Duan, JL Du, and Hong Bao. Dynamic modeling and active control of a cable-suspended parallel robot. *Mechatronics*, 18(1):1–12, 2008. [2](#), [31](#), [32](#)

## BIBLIOGRAPHY

- [20] Hui Li, Xinyu Zhang, Rui Yao, Jinghai Sun, Gaofeng Pan, and Wenbai Zhu. Optimal force distribution based on slack rope model in the incompletely constrained cable-driven parallel mechanism of fast telescope. In *Cable-driven parallel robots*, pages 87–102. Springer, 2013. [31](#)
- [21] BY Duan, YY Qiu, FS Zhang, and B Zi. On design and experiment of the feed cable-suspended structure for super antenna. *Mechatronics*, 19(4):503–509, 2009. [32](#)
- [22] Wenbai Zhu, Rendong Nan, and Gexue Ren. Modeling of a feed support system for fast. *Experimental Astronomy*, 17(1-3):177–184, 2004.
- [23] Rendong Nan. Five hundred meter aperture spherical radio telescope (fast). *Science in China series G*, 49(2):129–148, 2006.
- [24] Xiaoqiang Tang and Rui Yao. Dimensional design on the six-cable driven parallel manipulator of fast. *Journal of Mechanical Design*, 133(11):111012, 2011. [2](#)
- [25] Samuel Bouchard and Clément M Gosselin. Workspace optimization of a very large cable-driven parallel mechanism for a radiotelescope application. In *ASME 2007 International Design Engineering Technical Conferences and Computers and Information in Engineering Conference*, pages 963–970. American Society of Mechanical Engineers, 2007. [2](#)
- [26] Gabriel Meunier, Benoit Boulet, and Meyer Nahon. Control of an overactuated cable-driven parallel mechanism for a radio telescope application. *IEEE transactions on control systems technology*, 17(5):1043–1054, 2009. [31](#)
- [27] Meyer Nahon, Gabriele Gilardi, and Casey Lambert. Dynamics/control of a radio telescope receiver supported by a tethered aerostat. *Journal of Guidance, Control, and Dynamics*, 25(6):1107–1115, 2002. [32](#)
- [28] Brent Carlson, Luc Bauwens, Leonid Belostotski, Elizabeth Cannon, Ya-Ying Chang, Xiaohui Deng, Peter E Dewdney, Joe Jeff T Fitzsimmons, David J Halliday, Kai Kuerschner, et al. The large adaptive reflector: a 200-m diameter wideband centimeter-to meter-wave radio telescope. In *Radio Telescopes*, volume 4015, pages 33–44. International Society for Optics and Photonics, 2000.
- [29] Peter Dewdney, Meyer Nahon, and Bruce Veidt. The large adaptive reflector: A giant radio telescope with an aero twist. *Canadian aeronautics and space journal*, 48(4):239–250, 2002.

## BIBLIOGRAPHY

- [30] Casey Lambert, Meyer Nahon, and Dean Chalmers. Implementation of an aerostat positioning system with cable control. *IEEE/ASME Transactions on Mechatronics*, 12(1):32–40, 2007. [2](#)
- [31] Clément Gosselin. Cable-driven parallel mechanisms: state of the art and perspectives. *Mechanical Engineering Reviews*, 1(1):DSM0004–DSM0004, 2014. [5](#), [21](#), [22](#)
- [32] Blake Hannaford and Allison M Okamura. Haptics. *Springer Handbook of Robotics*, pages 719–739, 2008. [5](#)
- [33] Makoto Sato. Development of string-based force display: Spidar. In *8th international conference on virtual systems and multimedia*. Citeseer, 2002. [5](#)
- [34] Tetsuya Morizono, Kazuhiro Kurahashi, and Sadao Kawamura. Realization of a virtual sports training system with parallel wire mechanism. In *Proceedings of International Conference on Robotics and Automation*, volume 4, pages 3025–3030. IEEE, 1997. [21](#)
- [35] Vincent Duchaine, Samuel Bouchard, and Clément M Gosselin. Computationally efficient predictive robot control. *IEEE/ASME Transactions On Mechatronics*, 12(5):570–578, 2007. [31](#)
- [36] Masahiro Ishii and Makoto Sato. A 3d spatial interface device using tensed strings. *Presence: Teleoperators & Virtual Environments*, 3(1):81–86, 1994.
- [37] Y Takeda and H Funabashi. Kinematic synthesis of spatial in-parallel wire-driven mechanism with six degrees of freedom with high force transmissibility. In *Proceedings of the ASME International Design Engineering Technical Conference*, pages 1–9, 2000.
- [38] Claudio Melchiorri and Gabriele Vassura. Development and application of wire-actuated haptic interfaces. *Journal of Robotic Systems*, 18(12):755–768, 2001.
- [39] Paolo Gallina, Giulio Rosati, and Aldo Rossi. 3-dof wire driven planar haptic interface. *Journal of Intelligent and Robotic Systems*, 32(1):23–36, 2001.
- [40] Seahak Kim, Masahiro Ishii, Yasuharu Koike, and Makoto Sato. Development of tension based haptic interface and possibility of its application to virtual reality. In *Proceedings of the ACM symposium on Virtual reality software and technology*, pages 199–205. ACM, 2000.

## BIBLIOGRAPHY

- [41] Hitoshi Kino and Sadao Kawamura. Development of a serial link structure/parallel wire system for a force display. In *Proceedings 2002 IEEE International Conference on Robotics and Automation (Cat. No. 02CH37292)*, volume 1, pages 829–834. IEEE, 2002.
- [42] Nicolas Tarrin, Sabine Coquillart, Shoichi Hasegawa, Laroussi Bouguila, and Makoto Sato. The stringed haptic workbench: a new haptic workbench solution. In *Computer graphics forum*, volume 22, pages 583–589. Wiley Online Library, 2003.
- [43] Jun Murayama, Laroussi Bougrila, YanLin Luo, Katsuhito Akahane, Shoichi Hasegawa, Béat Hirsbrunner, and Makoto Sato. Spidar g&g: a two-handed haptic interface for bimanual vr interaction. In *Proceedings of EuroHaptics*, volume 2004, pages 138–146. Citeseer, 2004.
- [44] II Williams and V Jigar. Planar translational cable-direct-driven robots: hardware implementation. In *CD proceedings of ASME design technical conferences, 29th design automation conference, Chicago, IL*, pages 2–6, 2003.
- [45] Robert L Williams, Venkat Chadaram, and Federica Giacometti. Three-cable haptic interface. In *CD Proceedings of the ASME International Design Technical Conferences, 30th Mechanisms and Robotics Conference, Paper# DETC2006-99177, Philadelphia PA, September*, pages 10–13, 2006.
- [46] Robert L Williams II. Cable-suspended haptic interface. *International Journal of Virtual Reality*, 3(3):13–21, 1998.
- [47] Clément Gosselin, Régis Poulin, and Denis Laurendeau. A planar parallel 3-dof cable-driven haptic interface. In *12th World Multi-Conference on Systemics, Cybernetics and Informatics, Orlando, FL, USA*, pages 266–271, 2008.
- [48] Hossein S Farahani and Jeha Ryu. Design and control of a wire-driven haptic device: Hapticpen. pages 1662–1667, 2005.
- [49] Greg Billette and Clément Gosselin. Producing rigid contacts in cable-driven haptic interfaces using impact generating reels. In *2009 IEEE International Conference on Robotics and Automation*, pages 307–312. IEEE, 2009. 5
- [50] Simon Perreault and Clément M Gosselin. Cable-driven parallel mechanisms: Application to a locomotion interface. *Journal of Mechanical Design*, 130(10):102301, 2008. 5, 29

## BIBLIOGRAPHY

- [51] Martin J-D Otis, Marielle Mokhtari, Charles du Tremblay, Denis Laurendeau, François-Michel De Rainville, and Clément M Gosselin. Hybrid control with multi-contact interactions for 6dof haptic foot platform on a cable-driven locomotion interface. In *2008 Symposium on Haptic Interfaces for Virtual Environment and Teleoperator Systems*, pages 161–168. IEEE, 2008.
- [52] Martin J-D Otis, Sylvain Comtois, Denis Laurendeau, and Clément Gosselin. Human safety algorithms for a parallel cable-driven haptic interface. In *Brain, Body and Machine*, pages 187–200. Springer, 2010. 5
- [53] Sadao Kawamura and Ken Ito. A new type of master robot for teleoperation using a radial wire drive system. In *Proceedings of 1993 IEEE/RSJ International Conference on Intelligent Robots and Systems (IROS'93)*, volume 1, pages 55–60. IEEE, 1993. 5
- [54] Giulio Rosati, Mattia Andreolli, Andrea Biondi, and Paolo Gallina. Performance of cable suspended robots for upper limb rehabilitation. In *2007 IEEE 10th International Conference on Rehabilitation Robotics*, pages 385–392. IEEE, 2007. 5
- [55] Stephen J Ball, Ian E Brown, and Stephen H Scott. A planar 3dof robotic exoskeleton for rehabilitation and assessment. In *2007 29th Annual International Conference of the IEEE Engineering in Medicine and Biology Society*, pages 4024–4027. IEEE, 2007. 5
- [56] Sai K Banala, Seok Hun Kim, Sunil K Agrawal, and John P Scholz. Robot assisted gait training with active leg exoskeleton (alex). In *2008 2nd IEEE RAS & EMBS International Conference on Biomedical Robotics and Biomechatronics*, pages 653–658. IEEE, 2008. 5
- [57] Elizabeth A Brackbill, Ying Mao, Sunil K Agrawal, Madhu Annapragada, and Venkatesh N Dubey. Dynamics and control of a 4-dof wearable cable-driven upper arm exoskeleton. In *2009 IEEE International Conference on Robotics and Automation*, pages 2300–2305. IEEE, 2009. 5
- [58] Ying Mao and Sunil K Agrawal. Wearable cable-driven upper arm exoskeleton-motion with transmitted joint force and moment minimization. In *2010 IEEE International Conference on Robotics and Automation*, pages 4334–4339. IEEE, 2010.
- [59] Ying Mao and Sunil Kumar Agrawal. Design of a cable-driven arm exoskeleton (carex) for neural rehabilitation. *IEEE Transactions on Robotics*, 28(4):922–931, 2012. 5

## BIBLIOGRAPHY

- [60] Dragoljub Surdilovic and Rolf Bernhardt. String-man: a new wire robot for gait rehabilitation. In *IEEE International Conference on Robotics and Automation, 2004. Proceedings. ICRA '04. 2004*, volume 2, pages 2031–2036. IEEE, 2004. 5
- [61] Sadao Kawamura, Hitoshi Kino, and Choe Won. High-speed manipulation by using parallel wire-driven robots. *Robotica*, 18(1):13–21, 2000. 5
- [62] Jean-Pierre Merlet. Kinematics of the wire-driven parallel robot marionet using linear actuators. In *2008 IEEE International Conference on Robotics and Automation*, pages 3857–3862. IEEE, 2008. 5
- [63] Johann Lamaury and Marc Gouttefarde. Control of a large redundantly actuated cable-suspended parallel robot. In *2013 IEEE International Conference on Robotics and Automation*, pages 4659–4664. IEEE, 2013. 5
- [64] Tej Dallej, Marc Gouttefarde, Nicolas Andreff, Redwan Dahmouche, and Philippe Martinet. Vision-based modeling and control of large-dimension cable-driven parallel robots. In *2012 IEEE/RSJ International Conference on Intelligent Robots and Systems*, pages 1581–1586. IEEE, 2012.
- [65] Dinh Quan Nguyen, Marc Gouttefarde, Olivier Company, and François Pierrot. On the simplifications of cable model in static analysis of large-dimension cable-driven parallel robots. In *2013 IEEE/RSJ International Conference on Intelligent Robots and Systems*, pages 928–934. IEEE, 2013.
- [66] Andreas Pott, Christian Meyer, and Alexander Verl. Large-scale assembly of solar power plants with parallel cable robots. In *ISR 2010 (41st International Symposium on Robotics) and ROBOTIK 2010 (6th German Conference on Robotics)*, pages 1–6. VDE, 2010.
- [67] Philipp Miermeister and Andreas Pott. Modelling and real-time dynamic simulation of the cable-driven parallel robot ipanema. In *New Trends in Mechanism Science*, pages 353–360. Springer, 2010.
- [68] Andreas Pott, Hendrick Mütterich, Werner Kraus, Valentine Schmidt, Philipp Miermeister, and Alexander Verl. Ipanema: a family of cable-driven parallel robots for industrial applications. In *Cable-Driven Parallel Robots*, pages 119–134. Springer, 2013. 5
- [69] T Maier and C Woernle. Inverse kinematics for an underconstrained cable suspension manipulator. In *Advances in Robot Kinematics: Analysis and Control*, pages 97–104. Springer, 1998. 5

## BIBLIOGRAPHY

- [70] Christoph Woernle. Trajectory tracking for a three-cable suspension manipulator by nonlinear feedforward and linear feedback control. In *Cable-Driven Parallel Robots*, pages 371–386. Springer, 2013. [5](#)
- [71] Eric Barnett and Clément Gosselin. Time-optimal trajectory planning of cable-driven parallel mechanisms for fully specified paths with g1-discontinuities. *Journal of Dynamic Systems, Measurement, and Control*, 137(7):071007, 2015. [5](#)
- [72] Nathan Michael, Jonathan Fink, and Vijay Kumar. Cooperative manipulation and transportation with aerial robots. *Autonomous Robots*, 30(1):73–86, 2011. [6](#)
- [73] Clement Gosselin, Ping Ren, and Simon Foucault. Dynamic trajectory planning of a two-dof cable-suspended parallel robot. In *2012 IEEE International conference on Robotics and Automation*, pages 1476–1481. IEEE, 2012. [6](#), [31](#)
- [74] Clément Gosselin. Global planning of dynamically feasible trajectories for three-dof spatial cable-suspended parallel robots. In *Cable-Driven Parallel Robots*, pages 3–22. Springer, 2013. [6](#), [31](#)
- [75] Simon Perreault, Philippe Cardou, and Clément Gosselin. Towards parallel cable-driven pantographs. In *ASME 2011 International Design Engineering Technical Conferences and Computers and Information in Engineering Conference*, pages 1263–1272. American Society of Mechanical Engineers, 2011. [6](#)
- [76] Jean-Pierre Merlet. Wire-driven parallel robot: open issues. In *Romansy 19–Robot Design, Dynamics and Control*, pages 3–10. Springer, 2013. [6](#), [22](#)
- [77] Satoshi Tadokoro, Richard Verhoeven, Manfred Hiller, and Toshi Takamori. A portable parallel manipulator for search and rescue at large-scale urban earthquakes and an identification algorithm for the installation in unstructured environments. In *Proceedings 1999 IEEE/RSJ International Conference on Intelligent Robots and Systems. Human and Environment Friendly Robots with High Intelligence and Emotional Quotients (Cat. No. 99CH36289)*, volume 2, pages 1222–1227. IEEE, 1999. [33](#)
- [78] Paul Bosscher, Robert L Williams, and Melissa Tummino. A concept for rapidly-deployable cable robot search and rescue systems. In *ASME 2005 International Design Engineering Technical Conferences and Computers and Information in Engineering Conference*, pages 589–598. American Society of Mechanical Engineers, 2005.

## BIBLIOGRAPHY

- [79] Fumiaki Takemura, Masaya Enomoto, Kazuya Denou, Kemalettin Erbatur, Ulrike Zweirs, and Satoshi Tadokoro. Proposition of a human body searching strategy using a cable-driven robot at major disaster. In *2004 IEEE/RSJ International Conference on Intelligent Robots and Systems (IROS)(IEEE Cat. No. 04CH37566)*, volume 2, pages 1456–1461. IEEE, 2004.
- [80] Jean-Pierre Merlet. On the accuracy of n-1 wire-driven parallel robots. In *Romansy 19–Robot Design, Dynamics and Control*, pages 19–26. Springer, 2013. [6](#)
- [81] Pascal Lafourcade, Ya-Qing Zheng, and Xi-W Liu. Stiffness analysis of wire-driven parallel kinematic manipulators. In *Proceedings of the 11th World Congress on Theory of Machines and Mechanisms (IFTOMM'04)*, 2004. [6](#)
- [82] Clément M Gosselin, Imme Ebert-Uphoff, Pascal Lafourcade, Michel Llibre, and Claude Reboulet. Design of a parallel wire-driven manipulator for wind tunnels.
- [83] Tobias Bruckmann, Christian Sturm, and Wildan Lalo. Wire robot suspension systems for wind tunnels. *Wind tunnels and experimental fluid dynamics research*, 2010. [6](#)
- [84] Clément Gosselin and Samuel Bouchard. A gravity-powered mechanism for extending the workspace of a cable-driven parallel mechanism: Application to the appearance modelling of objects. *International Journal of Automation Technology*, 4(4):372–379, 2010. [6](#), [28](#)
- [85] J-D Deschênes, Philippe Lambert, Simon Perreault, Nicolas Martel-Brisson, Nathaniel Zoso, André Zaccarin, Patrick Hébert, Samuel Bouchard, and Clément M Gosselin. A cable-driven parallel mechanism for capturing object appearance from multiple viewpoints. In *Sixth International Conference on 3-D Digital Imaging and Modeling (3DIM 2007)*, pages 367–374. IEEE, 2007. [6](#)
- [86] Jean-Baptiste Izard, Marc Gouttefarde, Cédric Baradat, David Culla, and Damien Sallé. Integration of a parallel cable-driven robot on an existing building façade. In *Cable-driven parallel robots*, pages 149–164. Springer, 2013. [6](#)
- [87] Shiqing Fang, Daniel Franitza, Marc Torlo, Frank Bekes, and Manfred Hiller. Motion control of a tendon-based parallel manipulator using optimal tension distribution. *IEEE/ASME Transactions On Mechatronics*, 9(3):561–568, 2004. [6](#), [30](#)
- [88] Tobias Bruckmann, Andreas Pott, and Manfred Hiller. Calculating force distributions for redundantly actuated tendon-based stewart platforms. In *Advances in Robot Kinematics*, pages 403–412. Springer, 2006. [30](#)

## BIBLIOGRAPHY

- [89] Richard Verhoeven, Manfred Hiller, and Satoshi Tadokoro. Workspace, stiffness, singularities and classification of tendon-driven stewart platforms. In *Advances in robot kinematics: Analysis and Control*, pages 105–114. Springer, 1998.
- [90] Manfred Hiller, Shiqing Fang, Sonja Mielczarek, Richard Verhoeven, and Daniel Franitz. Design, analysis and realization of tendon-based parallel manipulators. *Mechanism and Machine Theory*, 40(4):429–445, 2005.
- [91] Richard Verhoeven and Manfred Hiller. Tension distribution in tendon-based stewart platforms. In *Advances in Robot Kinematics*, pages 117–124. Springer, 2002.
- [92] Joachim v Zitzewitz, Georg Rauter, Reto Steiner, Andreas Brunschweiler, and Robert Riener. A versatile wire robot concept as a haptic interface for sport simulation. In *2009 IEEE International Conference on Robotics and Automation*, pages 313–318. IEEE, 2009. [6](#)
- [93] Rodney G Roberts, Todd Graham, and Thomas Lippitt. On the inverse kinematics, statics, and fault tolerance of cable-suspended robots. *Journal of Robotic Systems*, 15(10):581–597, 1998. [7](#), [23](#), [56](#)
- [94] Jean-Pierre Merlet. *Parallel robots*, volume 128. Springer Science & Business Media, 2006. [14](#)
- [95] Jean-Pierre Merlet and Clément Gosselin. Parallel mechanisms and robots. *Springer Handbook of Robotics*, pages 269–285, 2008. [14](#)
- [96] VE Gough. Universal tyre test machine. *Proc. FISITA 9th Int. Technical Congr., London, 1962*, pages 117–137, 1962. [14](#)
- [97] Doug Stewart. A platform with six degrees of freedom. *Proceedings of the institution of mechanical engineers*, 180(1):371–386, 1965.
- [98] Ilian Bonev. The true origins of parallel robots. *ParalleMIC*, 2003. [14](#)
- [99] Samuel Ernest Landsberger. A new design for parallel link manipulators. In *Proc. of the IEEE International Conference on Systems*, pages 812–814, 1985. [15](#)
- [100] Koryo Miura, Hiroshi Furuya, and Kenichi Suzuki. Variable geometry truss and its application to deployable truss and space crane arm. *Acta Astronautica*, 12(7-8):599–607, 1985. [15](#)

## BIBLIOGRAPHY

- [101] H. Max. Irvine. *Cable structures*. Dover Publications, 1992. [15](#)
- [102] Kiyoshi Maeda, Satoshi Tadokoro, Toshi Takamori, Manfred Hiller, and Richard Verhoeven. On design of a redundant wire-driven parallel robot warp manipulator. In *Proceedings 1999 IEEE International Conference on Robotics and Automation (Cat. No. 99CH36288C)*, volume 2, pages 895–900. IEEE, 1999. [21](#)
- [103] Marc Gouttefarde and Clément M Gosselin. Wrench-closure workspace of six-dof parallel mechanisms driven by 7 cables. *Transactions of the canadian society for mechanical engineering*, 29(4):541–552, 2005. [22](#)
- [104] Marc Gouttefarde and Clément M Gosselin. Analysis of the wrench-closure workspace of planar parallel cable-driven mechanisms. *IEEE Transactions on Robotics*, 22(3):434–445, 2006. [22](#)
- [105] Ethan Stump and Vijay Kumar. Workspaces of cable-actuated parallel manipulators. *Journal of Mechanical Design*, 128(1):159–167, 2006. [22](#)
- [106] Kaveh Azizian, Philippe Cardou, and Brian Moore. Classifying the boundaries of the wrench-closure workspace of planar parallel cable-driven mechanisms by visual inspection. *Journal of Mechanisms and Robotics*, 4(2):024503, 2012. [22](#)
- [107] Andrew T Riechel and Imme Ebert-Uphoff. Force-feasible workspace analysis for under-constrained, point-mass cable robots. In *IEEE International Conference on Robotics and Automation, 2004. Proceedings. ICRA '04. 2004*, volume 5, pages 4956–4962. IEEE, 2004. [22](#), [23](#)
- [108] Paul Bosscher and Imme Ebert-Uphoff. Wrench-based analysis of cable-driven robots. In *IEEE International Conference on Robotics and Automation, 2004. Proceedings. ICRA '04. 2004*, volume 5, pages 4950–4955. IEEE, 2004. [23](#), [27](#)
- [109] Marc Gouttefarde, David Daney, and Jean-Pierre Merlet. Interval-analysis-based determination of the wrench-feasible workspace of parallel cable-driven robots. *IEEE Transactions on Robotics*, 27(1):1–13, 2010. [23](#)
- [110] Marc Gouttefarde, Jean-Pierre Merlet, and David Daney. Wrench-feasible workspace of parallel cable-driven mechanisms. In *Proceedings 2007 IEEE International Conference on Robotics and Automation*, pages 1492–1497. IEEE, 2007. [23](#)

## BIBLIOGRAPHY

- [111] Richard Verhoeven. *Analysis of the workspace of tendon based Stewart platforms*. PhD thesis, Verlag nicht ermittelbar, 2004. [22](#)
- [112] Guillaume Barrette and Clément M Gosselin. Determination of the dynamic workspace of cable-driven planar parallel mechanisms. *Journal of mechanical design*, 127(2):242–248, 2005. [23](#)
- [113] Clément M Gosselin Guillaume Barrette. Kinematic analysis of planar parallel mechanisms actuated with cables. [23](#)
- [114] Cong Bang Pham, Song Huat Yeo, Guilin Yang, Mustafa Shabbir Kurbanhusen, and I-Ming Chen. Force-closure workspace analysis of cable-driven parallel mechanisms. *Mechanism and Machine Theory*, 41(1):53–69, 2006. [23](#)
- [115] Samuel Bouchard, Clément Gosselin, and Brian Moore. On the ability of a cable-driven robot to generate a prescribed set of wrenches. *Journal of Mechanisms and Robotics*, 2(1):011010, 2010. [27](#)
- [116] Venus Garg, Scott B Nokleby, and Juan A Carretero. Wrench capability analysis of redundantly actuated spatial parallel manipulators. *Mechanism and machine theory*, 44(5):1070–1081, 2009. [27](#)
- [117] Daniel Cunningham and H Harry Asada. The winch-bot: A cable-suspended, underactuated robot utilizing parametric self-excitation. In *2009 IEEE International Conference on Robotics and Automation*, pages 1844–1850. IEEE, 2009. [28](#), [31](#)
- [118] Simon Lefrançois and Clément Gosselin. Point-to-point motion control of a pendulum-like 3-dof underactuated cable-driven robot. In *2010 IEEE International Conference on Robotics and Automation*, pages 5187–5193. IEEE, 2010. [28](#), [32](#)
- [119] Clément Gosselin, Simon Lefrançois, and Nathaniel Zoso. Underactuated cable-driven robots: machine, control and suspended bodies. In *Brain, Body and Machine*, pages 311–323. Springer, 2010. [28](#)
- [120] Damiano Zanotto, Giulio Rosati, and Sunil K Agrawal. Modeling and control of a 3-dof pendulum-like manipulator. In *2011 IEEE International Conference on Robotics and Automation*, pages 3964–3969. IEEE, 2011. [32](#)

## BIBLIOGRAPHY

- [121] Nathaniel Zoso and Clément Gosselin. Point-to-point motion planning of a parallel 3-dof underactuated cable-suspended robot. In *2012 IEEE International Conference on Robotics and Automation*, pages 2325–2330. IEEE, 2012. [28](#), [32](#)
- [122] Qimi Jiang and Vijay Kumar. The direct kinematics of objects suspended from cables. In *ASME 2010 international design engineering technical conferences and computers and information in engineering conference*, pages 193–202. American Society of Mechanical Engineers, 2010. [28](#)
- [123] Marco Carricato and Ghasem Abbasnejad. Direct geometrico-static analysis of under-constrained cable-driven parallel robots with 4 cables. In *Cable-Driven Parallel Robots*, pages 269–285. Springer, 2013. [28](#)
- [124] Marco Carricato and Jean-Pierre Merlet. Direct geometrico-static problem of under-constrained cable-driven parallel robots with three cables. In *2011 IEEE International Conference on Robotics and Automation*, pages 3011–3017. IEEE, 2011. [28](#)
- [125] Alessandro Berti, Jean-Pierre Merlet, and Marco Carricato. Solving the direct geometrico-static problem of 3-3 cable-driven parallel robots by interval analysis: Preliminary results. In *Cable-Driven Parallel Robots*, pages 251–268. Springer, 2013. [28](#)
- [126] Jean-François Collard and Philippe Cardou. Computing the lowest equilibrium pose of a cable-suspended rigid body. *Optimization and Engineering*, 14(3):457–476, 2013. [28](#)
- [127] K Azizian and P Cardou. The dimensional synthesis of planar parallel cable-driven mechanisms through convex relaxations. *Journal of Mechanisms and Robotics*, 4(3):031011, 2012. [29](#)
- [128] Kaveh Azizian and Philippe Cardou. The constant-orientation dimensional synthesis of planar cable-driven parallel mechanisms through convex relaxations. In *Cable-Driven Parallel Robots*, pages 215–230. Springer, 2013. [29](#)
- [129] Jean-Pierre Merlet. Analysis of the influence of wires interference on the workspace of wire robots. In *On Advances in Robot Kinematics*, pages 211–218. Springer, 2004. [29](#)
- [130] Simon Perreault, Philippe Cardou, Clément M Gosselin, and Martin J-D Otis. Geometric determination of the interference-free constant-orientation workspace of parallel cable-driven mechanisms. *Journal of Mechanisms and Robotics*, 2(3):031016, 2010. [29](#)

## BIBLIOGRAPHY

- [131] Martin J-D Otis, Simon Perreault, Thien-Ly Nguyen-Dang, Patrice Lambert, Marc Gouttefarde, Denis Laurendeau, and Clément Gosselin. Determination and management of cable interferences between two 6-dof foot platforms in a cable-driven locomotion interface. *IEEE Transactions on Systems, Man, and Cybernetics-Part A: Systems and Humans*, 39(3):528–544, 2009. [29](#)
- [132] Per Henrik Borgstrom, Nils Peter Borgstrom, Michael J Stealey, Brett Jordan, Gaurav S Sukhatme, Maxim A Batalin, and William J Kaiser. Design and implementation of nims3d, a 3-d cabled robot for actuated sensing applications. *IEEE Transactions on Robotics*, 25(2):325–339, 2009. [30](#)
- [133] Saeed Behzadipour and Amir Khajepour. Design of reduced dof parallel cable-based robots. *Mechanism and Machine Theory*, 39(10):1051–1065, 2004. [30](#)
- [134] Mahir Hassan and Amir Khajepour. Minimization of bounded cable tensions in cable-based parallel manipulators. In *ASME 2007 International Design Engineering Technical Conferences and Computers and Information in Engineering Conference*, pages 991–999. American Society of Mechanical Engineers, 2007. [30](#)
- [135] Lars Mikelsons, Tobias Bruckmann, Manfred Hiller, and Dieter Schramm. A real-time capable force calculation algorithm for redundant tendon-based parallel manipulators. In *2008 IEEE International Conference on Robotics and Automation*, pages 3869–3874. IEEE, 2008. [30](#)
- [136] Andreas Pott. An improved force distribution algorithm for over-constrained cable-driven parallel robots. In *Computational Kinematics*, pages 139–146. Springer, 2014. [31](#)
- [137] Johann Lamaury and Marc Gouttefarde. A tension distribution method with improved computational efficiency. In *Cable-driven parallel robots*, pages 71–85. Springer, 2013. [31](#)
- [138] Satoshi Tadokoro, Yoshio Murao, Manfred Hiller, Rie Murata, Hideaki Kohkawa, and Toshiyuki Matsushima. A motion base with 6-dof by parallel cable drive architecture. *IEEE/ASME transactions on mechatronics*, 7(2):115–123, 2002. [31](#)
- [139] Aiguo Ming. Study on multiple degree-of-freedom positioning mechanism using wires (part i)-concept, design and control. *International Journal of the Japan Society for Precision Engineering*, 28(2):131–138, 1994. [31](#)

## BIBLIOGRAPHY

- [140] Xianqiang You, Weihai Chen, Shouqian Yu, and Xingming Wu. Dynamic control of a 3-dof cable-driven robot based on backstepping technique. In *2011 6th IEEE Conference on Industrial Electronics and Applications*, pages 1302–1307. IEEE, 2011. 31
- [141] Alireza Alikhani and Mehdi Vali. Modeling and robust control of a new large scale suspended cable-driven robot under input constraint. In *2011 8th International Conference on Ubiquitous Robots and Ambient Intelligence (URAI)*, pages 238–243. IEEE, 2011. 31
- [142] Jason J Gorman, Kathryn W Jablokow, and David J Cannon. The cable array robot: Theory and experiment. In *Proceedings 2001 ICRA. IEEE International Conference on Robotics and Automation (Cat. No. 01CH37164)*, volume 3, pages 2804–2810. IEEE, 2001. 31
- [143] Ou Ma and Xiumin Diao. Dynamics analysis of a cable-driven parallel manipulator for hardware-in-the-loop dynamic simulation. In *Proceedings, 2005 IEEE/ASME International Conference on Advanced Intelligent Mechatronics.*, pages 837–842. IEEE, 2005. 31
- [144] Cong Bang Pham, Song Huat Yeo, and Guilin Yang. Tension analysis of cable-driven parallel mechanisms. In *2005 IEEE/RSJ International Conference on Intelligent Robots and Systems*, pages 257–262. IEEE, 2005. 31
- [145] Edouard Laroche, Ryad Chellal, Loïc Cuvillon, and Jacques Gangloff. A preliminary study for  $H_\infty$  control of parallel cable-driven manipulators. In *Cable-Driven Parallel Robots*, pages 353–369. Springer, 2013. 31
- [146] So-Ryeok Oh and Sunil K Agrawal. Guaranteed reachable domain and control design for a cable robot subject to input constraints. In *Proceedings of the 2005, American Control Conference, 2005.*, pages 3379–3384. IEEE, 2005. 31
- [147] Mojtaba Azadi, Saeed Behzadipour, and Garry Faulkner. Antagonistic variable stiffness elements. *Mechanism and Machine Theory*, 44(9):1746–1758, 2009. 31
- [148] Juan Ramón Sanmartín Losada. La physique de l’encensoir. *Pour la science*, 155:96–104, 1990. 32
- [149] Kris Kozak, Qian Zhou, and Jinsong Wang. Static analysis of cable-driven manipulators with non-negligible cable mass. *IEEE Transactions on Robotics*, 22(3):425–433, 2006. 32

## BIBLIOGRAPHY

- [150] Marc Arsenault. Stiffness analysis of a planar 2-dof cable-suspended mechanism while considering cable mass. In *Cable-Driven Parallel Robots*, pages 405–421. Springer, 2013. [32](#)
- [151] Nicolas Riehl, Marc Gouttefarde, Sébastien Krut, Cédric Baradat, and François Pierrot. Effects of non-negligible cable mass on the static behavior of large workspace cable-driven parallel mechanisms. In *2009 IEEE international conference on robotics and automation*, pages 2193–2198. IEEE, 2009. [32](#)
- [152] Shabbir Kurbanhusen Mustafa, Guilin Yang, Song Huat Yeo, Wei Lin, and I-Ming Chen. Self-calibration of a biologically-inspired cable-driven robotic arm. In *2007 IEEE/ASME international conference on advanced intelligent mechatronics*, pages 1–6. IEEE, 2007. [32](#)
- [153] Per Henrik Borgstrom, Brett L Jordan, Bengt J Borgstrom, Michael J Stealey, Gaurav S Sukhatme, Maxim A Batalin, and William J Kaiser. Nims-pl: A cable-driven robot with self-calibration capabilities. *IEEE Transactions on Robotics*, 25(5):1005–1015, 2009. [32](#)
- [154] M Saeed Varziri and Leila Notash. Kinematic calibration of a wire-actuated parallel robot. *Mechanism and Machine Theory*, 42(8):960–976, 2007. [32](#)
- [155] Yuanying Qiu, Baoyan Duan, and Ying Sheng. Indirect calibration of initial cable lengths of a huge parallel cable robot. *Chinese Journal of Mechanical Engineering(English Edition)*, 17:79–81, 2004.
- [156] SA Joshi and A Surianarayan. Calibration of a 6-dof cable robot using two inclinometers. *Performance metrics for intelligent systems*, pages 3660–3665, 2003.
- [157] Julien Alexandre Dit Sandretto, David Daney, and Marc Gouttefarde. Calibration of a Fully-Constrained Parallel Cable-Driven Robot. Technical report. [32](#)
- [158] Valentin Schmidt and Andreas Pott. Implementing extended kinematics of a cable-driven parallel robot in real-time. In *Cable-driven parallel robots*, pages 287–298. Springer, 2013. [32](#)
- [159] Ryad Chellal, Edouard Laroche, Loïc Cuvillon, and Jacques Gangloff. An identification methodology for 6-dof cable-driven parallel robots parameters application to the inca 6d robot. In *Cable-Driven Parallel Robots*, pages 301–317. Springer, 2013. [33](#)

## BIBLIOGRAPHY

- [160] Thomas Reichenbach, Philipp Tempel, Alexander Verl, and Andreas Pott. Static analysis of a two-platform planar cable-driven parallel robot with unlimited rotation. In *International Conference on Cable-Driven Parallel Robots*, pages 121–133. Springer, 2019. [70](#)